



Optical methods for ultrafast screening of microorganisms

Carme Català García

ADVERTIMENT. L'accés als continguts d'aquesta tesi doctoral i la seva utilització ha de respectar els drets de la persona autora. Pot ser utilitzada per a consulta o estudi personal, així com en activitats o materials d'investigació i docència en els termes establerts a l'art. 32 del Text Refós de la Llei de Propietat Intel·lectual (RDL 1/1996). Per altres utilitzacions es requereix l'autorització prèvia i expressa de la persona autora. En qualsevol cas, en la utilització dels seus continguts caldrà indicar de forma clara el nom i cognoms de la persona autora i el títol de la tesi doctoral. No s'autoritza la seva reproducció o altres formes d'explotació efectuades amb finalitats de lucre ni la seva comunicació pública des d'un lloc aliè al servei TDX. Tampoc s'autoritza la presentació del seu contingut en una finestra o marc aliè a TDX (framing). Aquesta reserva de drets afecta tant als continguts de la tesi com als seus resums i índexs.

ADVERTENCIA. El acceso a los contenidos de esta tesis doctoral y su utilización debe respetar los derechos de la persona autora. Puede ser utilizada para consulta o estudio personal, así como en actividades o materiales de investigación y docencia en los términos establecidos en el art. 32 del Texto Refundido de la Ley de Propiedad Intelectual (RDL 1/1996). Para otros usos se requiere la autorización previa y expresa de la persona autora. En cualquier caso, en la utilización de sus contenidos se deberá indicar de forma clara el nombre y apellidos de la persona autora y el título de la tesis doctoral. No se autoriza su reproducción u otras formas de explotación efectuadas con fines lucrativos ni su comunicación pública desde un sitio ajeno al servicio TDR. Tampoco se autoriza la presentación de su contenido en una ventana o marco ajeno a TDR (framing). Esta reserva de derechos afecta tanto al contenido de la tesis como a sus resúmenes e índices.

WARNING. Access to the contents of this doctoral thesis and its use must respect the rights of the author. It can be used for reference or private study, as well as research and learning activities or materials in the terms established by the 32nd article of the Spanish Consolidated Copyright Act (RDL 1/1996). Express and previous authorization of the author is required for any other uses. In any case, when using its content, full name of the author and title of the thesis must be clearly indicated. Reproduction or other forms of for profit use or public communication from outside TDX service is not allowed. Presentation of its content in a window or frame external to TDX (framing) is not authorized either. These rights affect both the content of the thesis and its abstracts and indexes.

Carme Català García

Optical methods for ultrafast screening of microorganisms

DOCTORAL THESIS

Supervised by

Prof. Ramón Álvarez Puebla

Dr. Nicolás Pazos Pérez

Doctoral program in nanoscience, materials and chemical engineering,

Department of Chemical Engineering,

Escola Tècnica Superior d'Enginyeria Química (ETSEQ).



**UNIVERSITAT
ROVIRA I VIRGILI**

Tarragona, April 2017



Department of Physical and Inorganic Chemistry
C/ Marcel·li Domingo s/n, Edifici N4
Campus Sescelades
43007 Tarragona, Spain
secqfqui@urv.cat
Tel. +34 977 55 81 37
Fax. 977 55 95 63

I STATE that the present study, entitled “**Optical methods for ultrafast screening of microorganisms**”, presented by **Carme Català García** for the award of the degree of Doctor, has been carried out under my supervision at the Department Physical and Inorganic Chemistry Department (DQFI) of this university.

Tarragona, April 2017

Doctoral Thesis Supervisor/s



Prof. Ramón Álvarez Puebla



Dr. Nicolás Pazos Pérez

Als meus pares,

Agraïments

Al Prof. Ramón per moltes coses, doncs més de tres anys donen per viure molt! Gràcies per brindar-me la oportunitat de fer un PhD, hores de laboratori compartides, etc. i fins i tot algun Pont de la Constitució treballant braç a braç. Els teus singulars mètodes d'ensenyança, que encara avui em segueixen sorprenent, han contribuït a convertir-me en una científica de pensament crític, perseverant i metòdica. Gràcies especialment, per fer-me costat en el darrer tram del camí, doncs sense el teu suport avui no seria aquí.

Al Dr. Nicolás per ser el meu company de camí des de el primer dia, per donar-me aire quant em feia falta, respostes quan no les trobava, explicacions breus i completes que em van permetre endinsar-me en el món de les nanopartícules, i asseure'ns junts a buscar respostes als problemes que anaven apareixen, etc. gràcies per la teva passió i no deixar mai de fer camí amb mi.

Als meus companys de PhD... podria escriure una altra tesis de tot el viscut i compartit, però en manquen forces. Gràcies per les mil i una experiències viscudes i compartides, reunions de grup, barbacoes, nits de farres, nous coneixements, móns descoberts, secrets, pors, il·lusions i bombolles de sabó! Sense vosaltres aquest temps no hagués sigut el mateix.

A les Dr. Elena Pazos Chantrero i Dr. Sara Gómez de Pedro, per els seus coneixements i consells científics, sense oblidar els cafès compartits. Al Dr. Luca Guerrini per la seva visió ordenada i estricta de la ciència, sempre amb un toc del seu humor tant característic.

A la gent del Centre tecnològic de la Química de Catalunya, CTQC, que han fet dia a dia amb mi: administratius, investigadors, seguretat consergeria i neteja; citar particularment a la Isabel de Lucas i a la Carmen Claver.

Al Servei de recursos científics i tècnics, SRCT, de la URV per no deixar d'estar allí, especialment a Martí Yebras i al servei de microscòpia.

Al equip del Dr. Álex Soriano de l'Hospital Clínic de Barcelona. A Ignacio Moriyón per estar sempre disposat a escoltar-me, mentre mengem una hamburguesa i regalar-me la teva crítica opinió. En gran part la meva passió pel món del micro es deu a la teva presència en la meva vida. A Jaume Almacelles per les nostres converses i partides d'escacs mentals.

Als meus companys del Nort, Iruña i Gasteiz, per estar sempre disposats a fer un *vinillo*, cantar una cançó, etc. Alenades d'aire fresc! Sempre recolzar-me i animar-me al llarg del camí. Sense oblidar als meus companys de les terres catalanes per escoltar-me hores parlant de "bitxos", nanopartícules, etc. i haver estat al meu costat, arrancant-me un somriure i fent-me oblidar els moments difícils. Gràcies: Jordi, Rafa, David, Ximo, Lourdes, Marta Galofré, Marta Llord, Sonia, Bea i Alex i a tots aquells que feu camí amb mi.

A les meves àvies, Cèlia, Maria i Lluïsa i especialment al Joan per cuidar-me, consentir-me i recolzar-me, i per les carmanyoles de lasanya i macarrons i truites de patates.

A tu Oriol, per recordar-me mil i un cops que hi ha vida fora el laboratori, per ser tu, fer-me riure i no deixar-me mai de fer-me costat.

Als meus Pares, Carme i Josep, pels seus esforços per donar-me educació, suport incondicional en tots els projectes que vull construir i escoltar-me; malgrat que de vegades... no enteneu del que us parlo.

La gratitud és una vacuna, antitoxina i antisèptic.

John Henry Jowett

*El que coneix totes les respostes,
no s'ha fet totes les preguntes.*

Confucio

Table of contents

Chapter 1	Thesis Scope.....	1
Chapter 2	Introduction.....	7
2.1	PREFACE.....	9
2.1.1	PLASMONIC MATERIALS FOR DIAGNOSIS OF INFECTIOUS DISEASES	14
2.1.2	FABRICATION AND LABELLING OF SERS-ENCODED NANOPARTICLES.....	17
2.1.3	DIRECT SERS ANALYSIS OF BACTERIA	20
2.1.4	INTEGRATED SERS-MICROFLUIDIC DEVICES AND SERS-ENCODED NANOPARTICLES.....	22
2.2	THEORETICAL BACKGROUND	27
2.2.1	OPTICAL BACKGROUND	27
2.2.1.1	Laser and waves	27
2.2.1.2	Optical properties of metals.....	28
2.2.1.3	Localized surface plasmon resonances (LSPR).....	28
2.2.2	RAMAN SPESCTROSCOPY	30
2.2.2.1	Raman effect.....	30
2.2.2.2	Raman selection rules	32
2.2.3	SERS	33
2.2.3.1	Hot Spot.....	34
2.2.3.2	SERS substrates.....	35
2.2.3.3	Colloidal silver nanoparticles.....	36
2.2.3.4	SERS instrumentation.....	38
2.2.3.5	Biomedical applications and SERS sensing.....	39
2.2.4	MICROORGANISMS.....	40
2.2.4.1	Bacteria pathogens.....	42
2.2.4.2	Isolation of pathogens from clinical specimens.....	43

2.2.4.3	Gram positive /Gram negative.....	45
2.2.5	ANTIBIOTICS	46
2.2.5.1	Antimicrobial resistance	48
2.2.6	SEPSIS	48
2.2.7	CHARACTERISTICS OF THE BACTERIA USED IN THIS THESIS	49
2.2.7.1	<i>Streptococcus agalactiae</i>	50
2.2.7.2	<i>Staphylococcus aureus</i>	51
2.2.7.3	<i>Escherichia coli</i>	52
2.2.7.4	<i>Pseudomona aeruginosa</i>	53
2.2.8	BIOLOGICAL TARGETS.....	54
2.2.8.1	Antibody.....	55
2.2.8.2	Antibody-antigen-interaction.....	56
2.2.8.3	Aptamer.....	57
2.2.8.4	Identification of aptamers by SELEX.....	58
2.2.8.5	Aptamer vs Antibody.....	58
Chapter 3	Multiplex bacteria quantification in blood samples.....	61
3.1	INTRODUCTION	63
3.2	EXPERIMENTAL SECTION.....	65
3.2.1	MATERIALS.....	65
3.2.2	ANTIBODIES AND BACTERIA	65
3.2.3	SYNTHESIS OF CITRATE-STABILIZED SPHERICAL Ag NPs.....	66
3.2.4	MUA FUNCTIONALIZATION AND CODIFICATION OF Ag NPs.....	66
3.2.5	ANTIBODY CONJUGATION TO Ag NPs	67
3.2.6	CHARACTERIZATION OF THE NANOPARTICLES	68
3.2.7	MICROFLUIDIC DEVICE MANUFACTURING	68
3.2.8	BACTERIAL SAMPLES	69
3.2.9	MEASUREMENT SYSTEM SETUP	70
3.2.10	ELECTROMAGNETIC SIMULATIONS	71

3.3 RESULTS AND DISCUSSION	71
3.3.1 DIMMERS ELECTROMAGNETIC SIMULATIONS.....	71
3.3.2 SIMULATION OF PARTICLE ATTACHMENT	73
3.3.3 SIMULATION OF SERS ENHANCEMENT PRODUCED BY PARTICLE ATTACHMENT.....	76
3.3.4 SIMULATION OF THE EFFECTIVE PERMITTIVITY OF THE NP COATING DESCRIBED AS A METAMATERIAL.....	77
3.3.5 MICROORGANISM OPTICAL DETECTION SYSTEM (MODS)	78
3.3.6 MODS DEMONSTRATION IN SERUM.....	81
3.3.7 MODS DEMONSTRATION IN BLOOD.....	91
3.3.8 NANOPARTICLE AGGREGATION ON BACTERIA.....	92
3.3.9 OPTICAL EFFECTS OF THE NANOPARTICLE AGGREGATION ON BACTERIA.....	94
Chapter 4 Ab vs Apt for SERS detection in human fluids: The case of <i>S. aureus</i>	95
4.1 INTRODUCTION.....	97
4.2 EXPERIMENTAL SECTION	100
4.2.1 MATERIALS	100
4.2.2 SYNTHESIS OF CITRATE-STABILIZED SPHERICAL Ag NPs	100
4.2.3 Ag NPs CODIFICATION AND ANTIBODY CONJUGATION.....	101
4.2.4 Ag NPs CODIFICATION AND APTAMER CONJUGATION.....	102
4.2.5 NANOPARTICLE CHARACTERIZATION	102
4.2.6 MICROFLUIDIC DEVICE MANUFACTURING.....	103
4.2.7 BACTERIAL SAMPLES.....	103
4.2.8 MEASUREMENT SYSTEM SETUP	103
4.3 RESULTS AND DISCUSSION	105
4.3.1 DESIGN AND PREPARATION OF AB /APT- FUNCTIONALIZED Ag NPs.....	105
4.3.2 Ag NPs -APT VS Ag NPs -AB FOR <i>S. aureus</i> QUANTIFICATION.....	108
4.3.3 <i>S. aureus</i> QUANTIFICATION IN HUMAN FLUIDS.....	115

Chapter 5	Conclusions.....	117
	References.....	123
	Appendices.....	139
APPENDIX I	LIST OF FIGURES.....	A
APPENDIX II	LIST OF TABLES.....	I
APPENDIX III	CURRICULUM VITAE.....	K

List of Abbreviations

2MBA	2-mercaptobenzoic acid
4MBA	4-mercaptobenzoic acid
Ab	Antibody
AC	Altern corrent
AMR	antimicrobial resistance
Apt	Aptamer
BBL	Enriched thioglycollate medium
BEM	boundary-element method
BSA	Boviene serum albumin
C	Cosntant fragment of Ig
CCD	charge-coupled device
CFU	colony forming unit
COIN	composite organic-inorganic nanopaticles
DDA	discret dipole approximation
DEP	dielectrophoresis
DFBT	3,4-difluorobenzenethiol
DNA	Desoxiribonucleic acid
DPBS	Dulbecco's phosphate buffered saline
ECDC	European Centre for Disease prevention and Control
EDC	<i>N</i> -(3-dimethylaminopropyl)- <i>N</i> '-ethylcarbodiimide hydrochloride
EDTA	Ethylenediaminetetraacetic acid
EF	enhancement factors
ELISA	enzyme-linked immune sorbent assay
EPPS	European Prevalence Survey of Healthcare-Associated Ingections an Antimicrobial Use
ESEM	environmental scannig electron microscopy
Fab	fragment antigen binding
Fc	fragment crystallizable
FIA	fluorescence immune assay
GRAM -	Gram negative
GRAM +	Gram positive
H	Heavy fragment of Ig

List of Abbreviations

HIV-1	lentivirus, specie Human immunodeficiency virus 1
HPTZT	1-(4-hydroxyphenyl)-1H-tetrazole-5-thiol
HS-PEG-CO ₂ H	heptaethylene glycol
Ig	Immunoglobulins
IR	Infrared
Kd	disassociation constant
L	Light fragment of Ig
LOD	Limit of detection
LSPRs	Localized surface plasmon resonances
LTA	lipoteichoid acid
MALDI-TOF	matrix-assisted laser desorption/ionization-time-of-flight
MESME	multiple elastic scattering of multipolar expansions
MODS	microorganism optical detection system
MRSA	methicillin-resisntant <i>Staphylococcus aureus</i>
MS	mas spectrometry
MSA test	Mannitol salt agar
MUA	11-mercaptoundecanoic acid
NIR	near-infrared
NP	nanoparticles
PBS	Phosphate-buffered saline
PCA PLOT	Principal component analysis plot
PCR	polymerase chain reaction
PDMS	polydimethylsiloxane
PEG	Polyethylene glycol
PLLA-b	polymer mats
PMMA	poly(methyl methacrylate)
PTFE	polytetrafluoroethylene
QDs	Quantum dots
RIA	radioimmunoassay
RNA	Ribonucleic acid
RS	Raman Scattering
SDS	sodium docecyl sulfate
SELEX	systematic evolution of ligands by exponential enrichment
SEM	Scanning electron microscopy

SERS	Surface-enhanced Raman scattering
ssDNA	single-stranded DNA
TBE Buffer	buffer solution containing a mixture of Tris base, boric acid and EDTA
TEM	transmission electronic microscopy
TFMBT	2-(trifluoromethyl)benzenethiol
TGA test	Tellurite Glycine Agar
UV-vis	ultraviolet-visible
V	Variable fragment of Ig
Van	Vancomycin
Vis	visible

1

Thesis Scope

Thesis Scope

Infectious diseases are currently responsible for over eight million deaths per year. Efficient treatments require accurate recognition of pathogens at low concentrations, which in the case of blood infection (septicemia) can go as low as one per milliliter. Detecting and quantifying bacteria at such low concentrations is challenging and typically demands cultures of large samples of blood (~1 milliliter) extending over 24-72 hours. This delay seriously compromises the health of patients and is largely responsible for the death toll of bacterial infections. Recent advances in nanoscience, spectroscopy, plasmonics, and microfluidics allow for the development of optical devices capable of monitoring minute amounts of analytes in liquid samples. Among all of them, surface-enhanced Raman scattering (SERS) offer several advantages over other optical probes with respect to versatility, sensitivity, selectivity and biocompatibility. Future challenges to achieve this, include the development of multifunctional SERS probes with optimized plasmonic nanostructures as basic building blocks. Plasmonic structures as key components of SERS probes can offer high local optical fields for sensitive diagnostic with much lower acquisition times. This later parameter is of paramount importance due to the sample volumes commonly screened in the actual medical practice. Utilizing the progress that has been made in the design of SERS-encoded particles, the application of SERS probes is about to revolutionize bioanalysis. In this thesis we will show the proof-of-principle for enabling the multiplex identification and quantification of microorganisms directly on their biological matrix with unprecedented speed, low cost and sensitivity using SERS. These studies are very promising and will pave the way for further development of a new generation of medical devices.

Based on the precedents indicated previously described, the **general objective** of this work is the design of a system able to detect microorganisms faster and in a more efficient way than those used in the clinical practice. This doctoral thesis intended to **develop and optimize a method for multiplex detection and quantification of the most common microorganisms causing bacterial infections**. The design of this system will be based on a variation in the SERS intensity. This will be accomplished using encoded plasmonic nanoparticles (NP) functionalized with bio-recognition elements. In this case, when a sample (biological fluid) containing the biological target to be identified interacts with the recognition elements on the NP surface, will induce an accumulation of them at the targeted microorganism surface generating thus, an enhancement of the SERS signal.

After an exhaustive bibliographical revision of the, to date, detection methods; It can be summarized that the application of nanostructured materials to the development of new detection techniques is a fact. Among them, SERS is a powerful analytical technique that has proven to be particularly effective in environmental monitoring and detection applications. The field of microbiological determination requires an imminent advance in the detection time with respect to the identification and quantification of the microorganism. Therefore we can define the following **specific objectives** for this thesis:

1. **Synthesis and functionalization of plasmonic nanostructures with different Raman codes**. Importantly, each batch of nanoparticles should be functionalized with a concrete Raman code while keeping its colloidal stability to assure a homogeneous SERS signal. Moreover, the multiplex capability of the system will relay in the production of as many codes as possible keeping the colloidal stability of the encoded nanoparticles.

2. **Bio-functionalization of the encoded nanoparticles with different bio-recognition elements (antibodies or aptamers)** each one targeting a specific microorganism. A very important fact is that these structures will be designed to be colloidal stable in saline aqueous media, after being bio-functionalized and subsequently will be capable of keeping their colloidal stability in biological fluids. This a crucial factor, in order to induce differences in the SERS intensity depending on the presence or absence of the targeted microorganisms. Optimization of the different functionalization protocols and quantities of recognizing element to functionalize will be studied. As well as the parameters of specificity, cost, reproducibility, variability of the produced signal or the loss of its biological function.

3. **System design and development of the microfluidic platform.** In order to carry out the system tuning, different components have to be optimized. I) Design of the microfluidic system including the channel pattern, diameter and flow rate. II) Volume and concentration of the functionalized plasmonic nanostructures in relation to the volume of the sample to be measured. III) Selection of wavelength and power of the laser. IV) Position of the microfluidic system during the measurement in order to minimize background / instrumental noise and thus obtain an accurate quantification in the shortest time possible.

4. **Assays in saline medium and biological samples using the bio-functionalized encoded plasmonic nanostructures and the microorganisms** to be quantified. In order to achieve this, several steps will be taken: I) Detection and quantification of a single microorganism in saline medium, checking that the recognition element works properly and that the SERS signal increment is sufficient to carry out both the identification and the quantification of the microorganisms. II) Detection and quantification of a mixture of microorganisms in saline medium.

Testing that the recognition elements are specific for each microorganism and interactions between them or with other components of the sample do not occur. III) After testing the microorganism optical detection system (MODS) in saline medium, different biological fluids will be used to check its performance in real samples. IV) All the obtained results previously mentioned in the steps above, will be corroborated in parallel with traditional methods for microorganism quantification like bacteria culture in blood agar plates.

5. **Comparison between the different available recognition elements** studying their efficiency. This will be checked by means of their affinity to the microorganisms and the intensity of the SERS signal obtained. Time dependent studies will be performed monitoring how the SERS intensity increases and which is the highest value when screening a sample.

6. **Optimization of the method** to achieve the lowest sensitivity as possible meanwhile the acquisition times are also maintained very short. For this, it is important to make variations of the different parts of the system, in order to obtain the best result in the final gear. The influence of various parameters in the synthesis and functionalization of the nanoparticles will be studied; As well as composition material, shape or size, looking for greater efficiency in the signal of the hot spots generated. Such as stability of NPs in different media, cross reactivity or loss of specificity, among others. It will also be necessary to optimize the orders of magnitude in the final mixes analyzed for NPs and bacteria, as well as the design of the microchips with variations of the channel size and the flow rate.

2

Introduction

Introduction

2.1. PREFACE

Despite the progress in modern medicine, infection continues to represent one of the greatest challenges facing humanity. Such type of infections can be broadly divided into two main categories according to the location of the patient at the time the infection developed: (i) community-acquired and (ii) nosocomial (hospital-acquired) infections. Nosocomial infections occur worldwide and affect both developed and resource-poor countries, and they are mostly related to infections of surgical wounds, as well as the urinary and lower respiratory tracts.¹

Infections acquired in health care settings are among the major causes of death and increased morbidity among hospitalized patients leading, consequently, to a remarkable increase in health care costs (only in Europe the estimated costs are €7 billion/year, including direct costs only and reflecting 16 million extra days of hospital stay²). The European Centre for Disease Prevention and Control, ECDC, estimates that nosocomial infections contributes to 50,000 deaths only in Europe in 2011 and that an average of 7.7% of hospital patients had nosocomial infections in Europe (>2 million individuals annually) and almost 9% worldwide.¹ The increased length of stay for infected patients is the greatest contributor to costs. One study showed that the overall increase in the duration of hospitalization for patients with surgical wound infections was 8.2 days, ranging from 3 days for gynaecology to 9.9 for general surgery and up to 19.8 for orthopaedic surgery. Prolonged stay not only increases direct costs to patients or payers but also indirect costs due to lost work. The advancing age and the greater prevalence of chronic diseases among admitted patients as well as the increased use of diagnostic and therapeutic procedures which affect the host defences will provide continuing pressure on nosocomial infections in the future. The increased use of

drugs, the need for isolation, and the use of additional laboratory and other diagnostic studies also contribute to costs.

Additionally, rapid and long range human mobility is now responsible for the fast geographical spread of infectious disease, making the fight against infections to be tackled globally. Nowadays, mobility and traffic have reached a complexity and volume of unprecedented degree. More than 60 million people travel billions of miles on more than 2 million international flights each week.³ Hundreds of millions of people commute on a complex web of highways and railroads most of which operate at their maximum capacity. Despite this increasing connectivity and our ability to visit virtually every place on this planet in a matter of days, the magnitude and intensity of modern human traffic has made human society more susceptible to threats intimately connected to human travel.

Notably, although both community-acquired and nosocomial infections can be due to many agents, 95% of the infections can be ascribed to around 30 microorganisms (Figure 2.1).

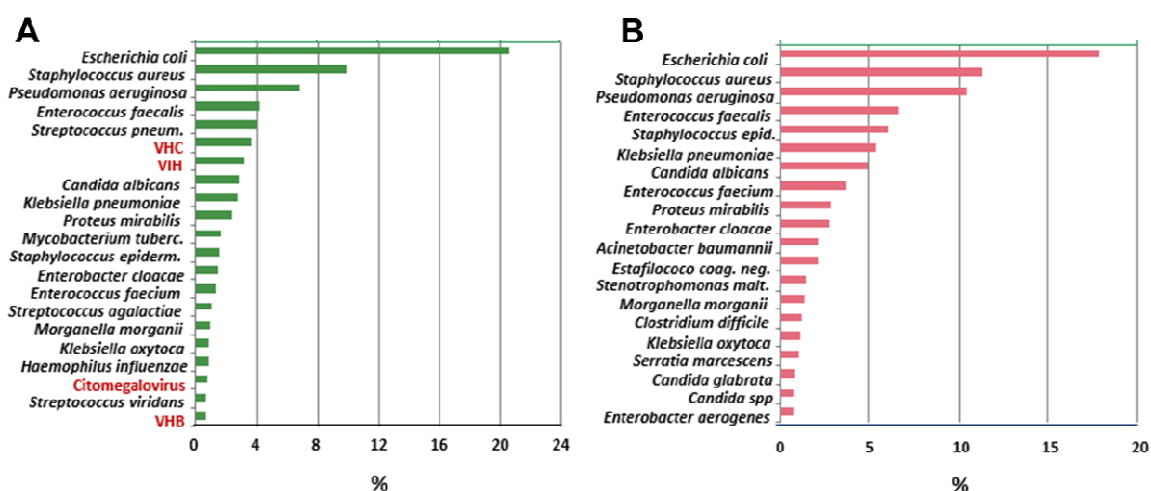


Figure 2.1. Most prevalent pathogens in (A) community-acquired and (B) nosocomial infections. Viral agent in red. Data obtained from European Prevalence Survey of Healthcare-Associated Infections and Antimicrobial Use (EPPS) 2012.

The time to initiation of effective antimicrobial therapy is known to be the single strongest predictor of outcome, as every hour delay in its administration increases by 8% the risk of death.^{4,5} Besides the obvious economic benefits, the development of fast, accurate, and inexpensive diagnostic methods appears as a major goal for alleviating human pain. Conventional microbial typing methods are reliable but suffer from inherent time-consuming complexities. Among these methods, the most common one remains the culture of the microorganism in different media to isolate the species and identify its nature (**Figure 2.2 A**). Sequential cultures can be avoided by implementing mass spectrometry (MS) techniques to the identification of isolated pure colonies (**Figure 2.2 B**). These methods, including the identification by MS, require of time for the agent to grow (24-72 h). On the other hand, immunological test to identify microorganism are also popular. Immunological techniques such as enzyme-linked immune sorbent assay (ELISA, **Figure 2.2 C**), fluorescence immune assay (FIA) or radioimmunoassay (RIA) offer faster results but cannot be considered multiplex. Further, they require a considerable amount of sample and are expensive (100 € for each analytical kit or 100.000 € for an automatized system). To increment portability, a new FIA-like technique known as lateral flow immunochromatography has been recently developed (**Figure 2.2 D**). This method is simple, the chemicals can be stored for certain time, and offers results that can be easily interpreted with the naked eye (i.e., it does not require extensively trained personnel). However, each reactive strip, necessary to identify a single given agent in a single given sample, is about 200 €. Furthermore, this method suffers from poor sensitivity and, thus, accumulation of microorganisms in the sample is a necessary step to allow the positive detection of the target. Alternatively, some labs are introducing the polymerase chain reaction (PCR) to identify microorganisms through the profiling of their genetic code (**Figure 2.2 E**). This technique is quantitative and semi-multiplex, but also laborious, slow and expensive (250 € each analysis of sample). Overall, it can be concluded that the current methods for detection of

microorganisms are flawed of problems related to sensitivity, selectivity, speed, price and technological restrictions. In this scenario, surface-enhanced Raman scattering (SERS) spectroscopy offers an exceptional opportunity for the development of new sensing devices amenable to implementation quantitative multiplex analysis in real time.⁶

The application of nanostructured materials toward the development of novel detection techniques with improved sensitivity and/or simplified and faster applicability has rapidly become an appealing alternative to other technologies. Among them, SERS is a powerful analytical technique which has already proven to be particularly effective in environmental detection and monitoring applications.

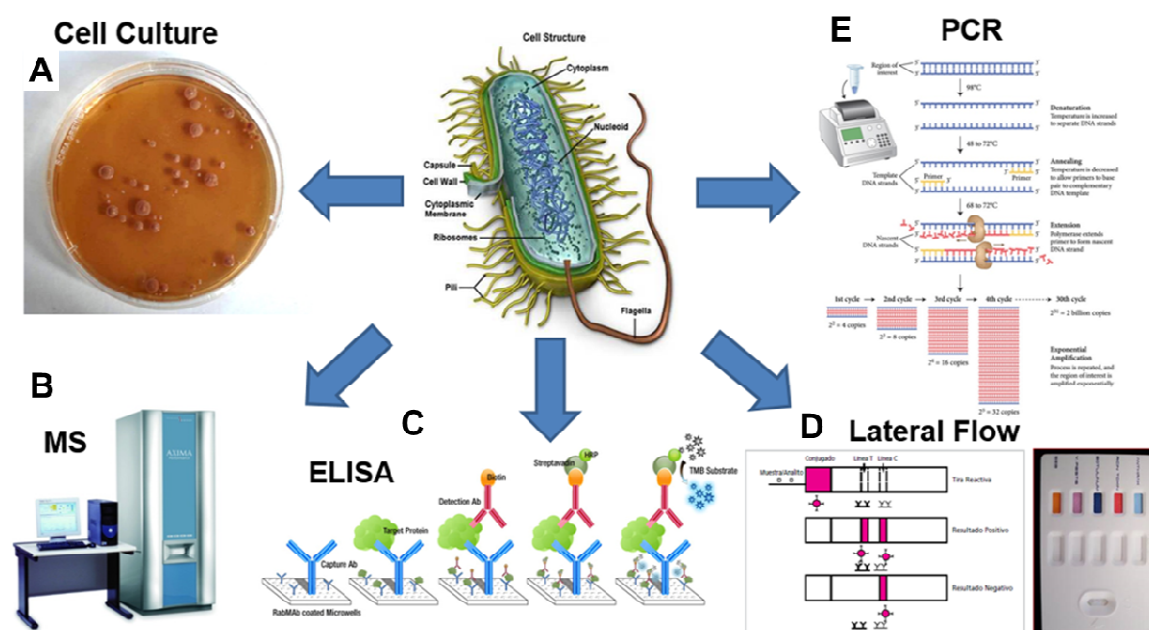


Figure 2.2. Some examples for the actual detection of microorganism in clinical diagnosis. (A) Cell culture, (B) Mass spectrometry of isolated pure colonies, (C) ELISA, (D) Lateral flow immunochromatography, and (E) PCR.

Essentially, SERS can be described as the Raman scattering amplified by the presence of a plasmonic structure in the close vicinity to the target analyte. In such

a case, the main cause of the excitation of the vibrational levels of the molecule is the collective oscillation of the conduction electrons of the metal, upon excitation with the appropriate light. This generates an ultra-strong electromagnetic near-field in the proximity of the nanostructure surface (known as localized surface plasmon resonances, LSPRs). As Raman scattering, SERS provides a complex spectral pattern that contains all the compositional and structural characteristics of the molecule under study.⁷ SERS, as Raman, is also characterized by an extreme experimental flexibility since Raman measurements can be carried out over a wide spectral range, are insensitive to air and water and require no sample preparation.

Recent spectacular advances in nanofabrication techniques fuelled the development of a large variety of rationally designed SERS substrates with an optimized, uniform and reproducible response. This successfully translated the spectacular analytical potential of SERS to reliable, widely accepted and commercially viable sensing applications. The dependence of LSPRs with parameters such as size, shape, composition and surrounding medium provides multiple possibilities for tuning the optical response and, thus, optimizing the SERS performance of the plasmonic nanostructure for a specific application. In conjunction with the control of the signal amplification provided by the optical enhancer, a key step in the practical implementation of sensing applications (including SERS) is the appropriate chemical functionalization of the “bare” metallic surface. This step is necessary to impart the required selectivity and/or sensitivity towards the target analyte, especially in complex mediums. Two design approaches are commonly used to devise plasmonic nanostructures as SERS sensing platforms: (i) direct SERS and (ii) encoded particles. In direct SERS, the detection is achieved by directly acquiring the SERS spectrum of the analyte. However, when performing direct SERS, several other species besides the target molecules can be detected simultaneously thus hampering the application of this strategy when complex analytical matrixes are involved, such as those in bio- or environmental

applications. In fact, when the number of targets and background species is high, the overlapping of vibrational modes of different molecules is very likely then making the interpretation of the overall vibrational spectrum extremely difficult or nearly impossible. On the other hand, SERS-encoded particles can be typically prepared by using an efficient plasmonic substrate which is labelled with a SERS molecule, protected with an external inert layer and functionalized with the appropriate selective chemoreceptor (such as an antibody, *Ab*, or an aptamer, *Apt*,). In this case, the identification and quantification of the analyte are indirectly correlated to the presence and intensity of the specific SERS label.

2.1.1. PLASMONIC MATERIALS FOR DIAGNOSIS OF INFECTIOUS DISEASES

A critical aspect in the implementation of a SERS-based sensing strategy for microorganism detection relies on the preparation of the appropriate plasmonic materials. In general, the format and functionalization of the plasmonic materials are dictated by the selected strategy (i.e., either direct SERS or by using encoded nanoparticles). The task of finding ‘the universal SERS substrate’ is not trivial and may not even be the right approach for implementing SERS as an analytical tool. For practical quantitative analytical applications, SERS must fulfil the typical requirements of an analytical technique: reproducibility of the results, linearity of the response, standardization, molecular selectivity and clear methodology for sample preparation. Unfortunately, these requirements are not easily met in the case of SERS experiments. Chemical and electronic effects must be carefully controlled to bring SERS as close as possible to the basic analytical requirements. SERS can be maximized mainly through control of two main factors: (i) careful design of the optical substrate and (ii) its appropriate functionalization.

Regarding the optical substrate, SERS has been mainly obtained in nanostructured thin films and colloidal nanoparticles.⁸⁻¹⁰ Colloidal nanoparticles are advantageous for many reasons. Their versatility and easy synthesis with a high degree of control

over the composition, shape and size, make them by far, the most commonly used substrates in SERS. Through careful control of these three key factors (composition, size and shape), the optical and plasmonic properties can be tuned to maximize the SERS enhancement.¹¹ The composition of the metallic nanoparticles deeply affects the intensity of the SERS signal. In this respect, the most important SERS platforms so far have been made of silver and gold,¹² while research using other materials (Cu, Pd, Pt, Rh, CuTe, Si, etc.)¹³ is still marginal. In general, it can be stated that silver is a much more efficient optical material than gold, giving rise to SERS signals over two orders of magnitude higher than those of gold, as silver scattering contribution is larger than that of gold. Additionally, silver can be excited from the UV to the IR while gold is restricted to the red or IR owing to damping by the interband transitions. As a consequence, silver nanoparticles are preferred when dealing with practical applications. However, it is worth noting that gold nanoparticles not only permit a better control of particle size and shape but they are also significantly more stable and biocompatible.^{14,15 16}

Nowadays, many methods are available to obtain colloids with high SERS activity, but this topic continues to be a booming research field. Within the limits of wet chemistry, colloidal methods can be divided in a variety of processes, including chemical reduction, laser ablation or photo-reduction, being the first one the most commonly used.^{11,17} The chemical reduction usually comprises a metallic salt (precursor), which is reduced by a chemical agent to produce colloidal dispersions that containing particles of different size and variable shapes. Regarding the synthesis of silver nanoparticles, the control over size and shape is much more difficult than in the case of gold due to its higher reactivity. However, many synthetic processes have been described to obtain different sized and shaped nanoparticles including seed-mediated, polyol, biological, hydro/solvothermal, galvanic replacement, photochemical, electrochemical or template-mediated synthesis,¹⁸⁻²¹ which give rise to highly monodisperse colloids in shape and size.

Among these methods, the seed-mediated growth process is the most widely used when dealing with shape controlled nanoparticle synthesis. This protocol includes a two-step process in which the first step consists in the generation of very small spherical particles. In the second step, the particles grow anisotropically in a different direction due to the reduction of metal salts on the surface of the initial seed nanoparticles. The presence of preformed seeds is highly advantageous since the particle size distribution becomes significantly narrower. The control of experimental variables such as the concentration of the metal salt, the reducing agent, the growth speed, the temperature, the capping agent or the chosen solvent provides a broad range of different sized and shaped nanoparticles (Figure 2.3).^{17,22}

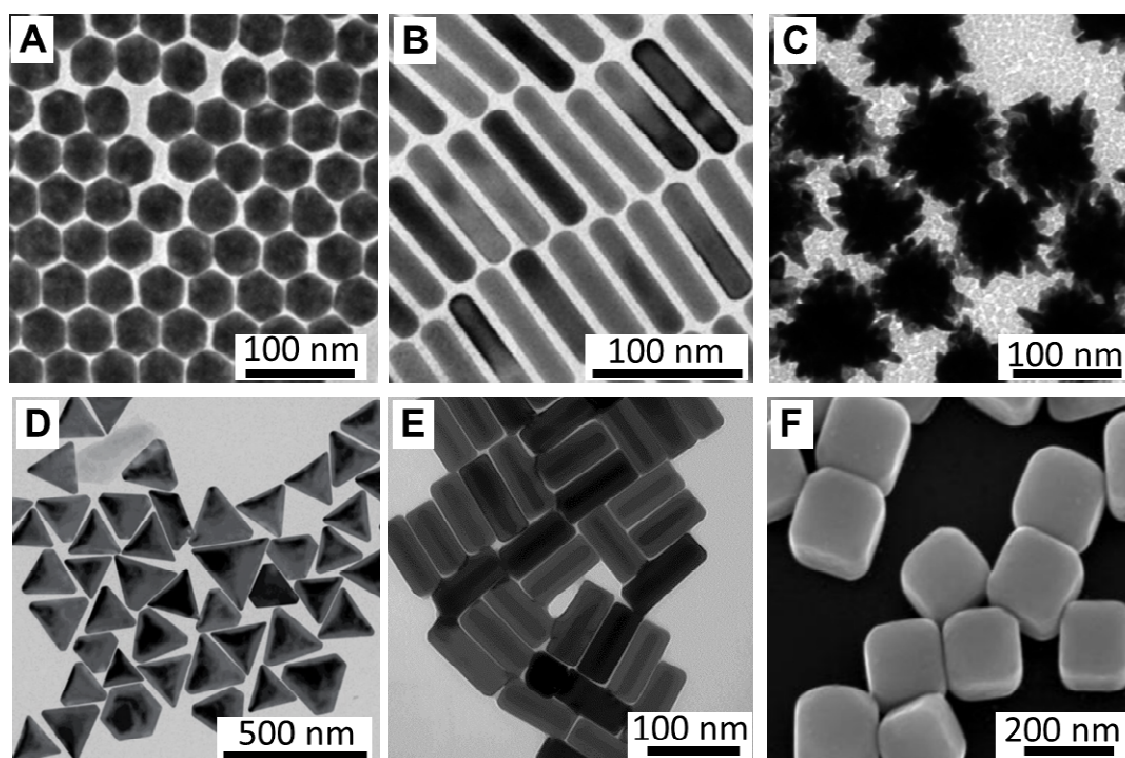


Figure 2.3. Transmission electron microscopy (TEM) images of nanoparticles with different shapes, sizes and composition; (A) gold nanospheres; (B) gold nanorods; (C) silver nanoplates; (D) gold nanostars; (E) Ag nanobars; (F) Ag nanocubes. Figures adapted with permission from ref. ^{17,22-25} and ²⁶.

Besides the simplicity of the synthetic methods, 'as prepared' metal nanoparticles present remarkable advantages when dealing with diagnostic systems in biofluids as permit direct SERS analysis within the analyte natural solution medium; present a large surface area and good dispersion in liquids that allows for a close adsorbent–adsorbate interaction, so that the analyte can be naturally retained onto the nanoparticles' surface; the Brownian motion of the analyte-particle complexes minimize the damage to the sample, even when using more energetic laser lines and higher power at the sample for excitation; and, fundamentally allows for the screening of large volumes of fluids, as required in the modern clinical practice for diagnosing infectious diseases.

2.1.2. FABRICATION AND LABELLING OF SERS-ENCODED NANOPARTICLES

Despite all the advantages mentioned above, bare plasmonic nanoparticles are usually not enough for the appropriate recognition of complex analytes such as microorganisms. Direct SERS spectra of microorganism usually show common spectral patterns, especially when studying close related species. Additionally, if the goal of the method is the determination of the microorganism directly in the biological matrix, the chemical species present will overlap the microorganism SERS spectra making impossible the interpretation of the result. Thus, as an alternative, SERS can be used to identify as a labelling method in a similar to the way as fluorophores are used in immunology bioassays.²⁷ Although fluorescence is powerful and convenient, the lack of features in the obtained spectra (usually composed of just one broad feature) limits the number of analytes that can be recognized without uncertainty. Thus, the use of SERS as encoding alternative is rapidly gaining relevance not only because of its unprecedented detection limits that dramatically decrease the detection times, but also owing to the practically unlimited number of barcodes that can be used for simultaneous detection.

The fabrication and characteristics (material, size, biocompatibility, and others) of the desired SERS-encoded particles strongly depend on each specific application. However, all of them share some common requirements: a) the presence of an optical enhancer; b) the addition of the SERS code; and c) the protection with a silica or polymer layer to prevent leaching of the SERS reporter while providing a suitable surface for biofunctionalization²⁸ and colloidal stability (**Figure 2.4 A,B**). The first reported works using SERS-encoded particles for multiplex determination relied either on the addition of a SERS tag directly onto the plasmonic particles or on the pre-coupling of the tag to the biomolecular interface.²⁹ Nowadays, the preparation of SERS-encoded particles is becoming more exotic. The simplest way to produce SERS-encoded nanoparticles comprises the SERS codification of single spherical plasmonic colloids and encapsulation within silica or polymer shells.³⁰⁻³² On the other hand, silica coating of nanoparticles is also a mature technology.³³ Thus, the key step for the codification of single nanoparticles relies on the incorporation of the Raman label to give rise to a signal as strong as possible without compromising colloidal stability (**Figure 2.4 C**). The formation of the protective shell around the single colloidal particles inhibits plasmon coupling and, in turn, the generation of hot spots (specific gaps between particles where the electromagnetic field is extremely high due to coupling between their plasmon resonances^{34,35}). Even though the recent demonstration of the heterogeneous distribution of plasmon modes within anisotropic particles^{36,37} is leading to the development of highly active nanoparticles such as nanostars or lace^{38,39} (**Figure 2.3**), still the most popular approach for the fabrication of nanometer-sized SERS-encoded particles is the use of nanoparticle aggregates as plasmonic cores. Particle aggregation can be easily promoted by changing the solvent, increasing the ionic strength of the suspension,⁴⁰ or just spontaneously due to the adsorption of the Raman label.⁴¹ Notwithstanding, these uncontrollable aggregation processes are usually undesired because they lead to a random distribution of hot spots with the subsequent signal heterogeneity from cluster to cluster. Thus, several

approaches were developed toward controlling aggregation (**Figure 2.4 D**). One of the oldest and probably most successful approaches comprises the so-called composite organic-inorganic nanoparticles (COIN).⁴²⁻⁴⁴ The COIN approach consists in the controlled label-induced aggregation of silver particles. An external shell of bovine serum albumin (BSA) is spontaneously retained onto the COIN and not only protects the code but also allows for further functionalization with biomolecules such as proteins (antibodies). Other strategies for the generation of aggregated encoded particles relies on inducing aggregation by increasing the ionic strength followed by silica coating of silver or gold colloids.^{45,46} In fact, these particles have recently been demonstrated to give rise to a sufficiently intense signal to be individually identified in a Raman flow-cytometer.⁴⁷ Nevertheless, both methods still yield uncontrollable aggregates with the ensuing fluctuations in their SERS intensity. For this reason, an increasing activity is observed toward the development of controlled methods for the fabrication of SERS active dimers including spheres, cages, pyramids, or even rods.^{13,48-54}

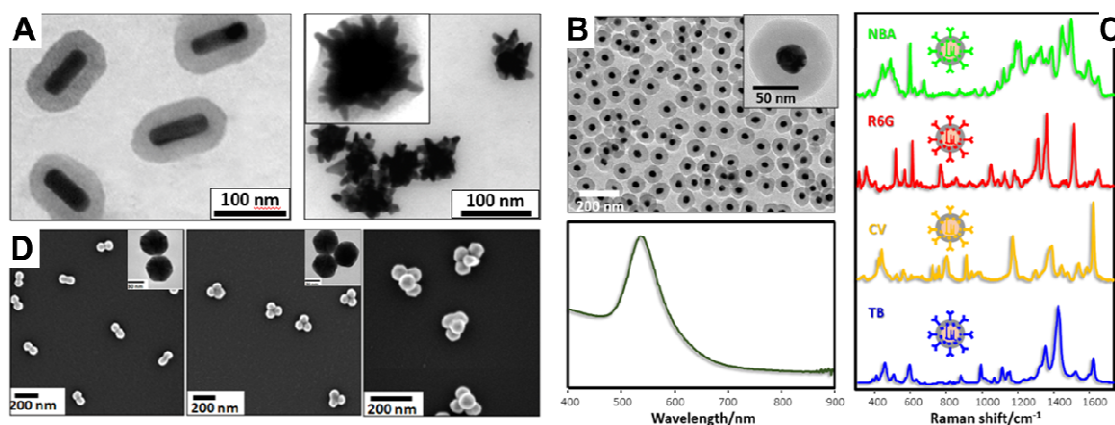


Figure 2.4. (A) Some examples of encoded plasmonic nanostructures including single particle rods or stars and dimers, trimers and tetramers of spheres. (B) Encoded gold spheres and their plasmonic response. (C) SERS response of encoded (gold spheres) with four different SERS labels. Figures adapted with permission from ref. ^{30,55} and ^{30,55,56}

2.1.3. DIRECT SERS ANALYSIS OF BACTERIA

The most common approach for the SERS analysis of bacteria relies on the acquisition of the intrinsic SERS spectra of the microorganisms placed in direct contact with the SERS substrate. Traditionally, this was achieved by simply drying a mixture of unfunctionalized “naked” silver nanoparticles and highly concentrated bacteria onto an appropriate Raman spectroscopy substrate, prior to spectral acquisition (**Figure 2.5 A**).⁵⁷⁻⁶⁰ A large number of SERS spectra is then collected over different points to improve the statistical reliability and reproducibility of the final bacterial fingerprint (**Figure 2.5 B**). Chemometrics is finally applied for positive identification and discrimination between bacteria (**Figure 2.5 C**).

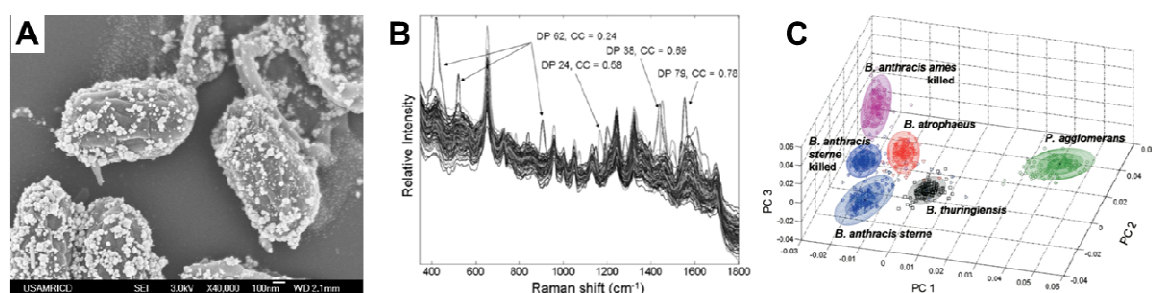


Figure 2.5. (A) SEM image showing coverage of silver nanoparticles on *Bacillus atrophaeus* spores. (B) 110 *Bacillus atrophaeus* spore spectra overlaid showing good signal reproducibility (DP = data point, CC = cross-correlation value). (C) PCA plot showing discrimination between five *Bacillus* spore samples and *Pantoea agglomerans*. Figure adapted with permission from ref. ⁵⁷.

Under this scenario, the SERS spectra are the sole result of the contributions from the components of the bacterial membrane. Nonetheless, the final spectral profile has shown to be extremely sensitive to several experimental factors such as colloidal properties and sample preparation.⁵⁹ In particular, the rather inhomogeneous distribution of the nanoparticles onto the bacterial walls significantly limits the spectral reproducibility and hampers any quantitative

estimation of the target concentration. Several new approaches were developed for solving this problem while reducing the bacteria concentration required to achieve a detectable signal. For instance, magnetic-plasmonic core-shell nanoparticles were used in place of traditional colloids to enable the fast concentration of bacteria by applying an external point magnetic field. As a result, a large number of microorganisms and nanoparticles can be effectively condensed into a highly compact dot (**Figure 2.6 A**).⁶¹ On the other hand, Szymborski et al.⁶² combined periodic structures of nanosized fibers with nanostructured gold layers to be used as a dual efficient SERS-filter for the immobilization of bacteria from solutions such as blood, urine, water, or milk (**Figure 2.6 B**).

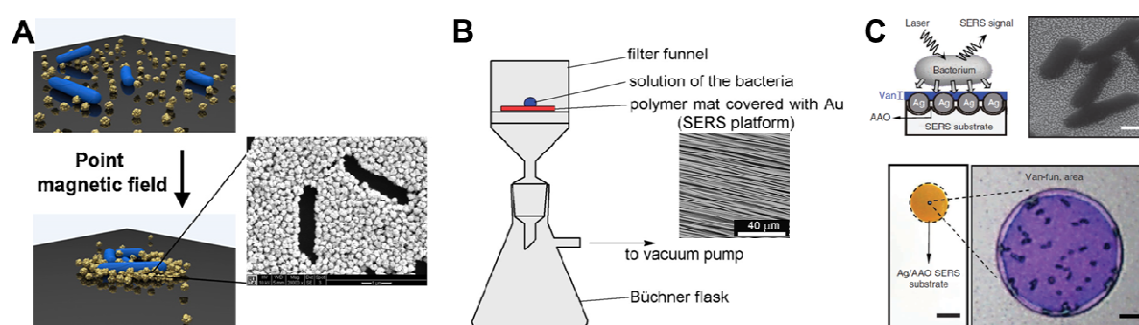


Figure 2.6. (A) Schematics of the condensation process of magnetic gold nanoparticles and bacteria, together with a SEM image of the area of analysis (bacteria are shown in dark contrast, the scale bars is 1 μm). Figure adapted with permission from ref. ⁶¹. (B) Scheme of embedding bacteria on the SERS platform directly from the solution and SEM image of the polymer mats (PLLA-b) covered with 90 nm of gold. Figure adapted with permission from ref. ⁶². (C) Schematic diagram showing the cross-sectional view of a bacterium on a Van-coated substrate. SEM images of bacteria on the substrate (scale bar 500 nm) plus an optical image of the Van-coated region with the captured *E. coli* (scale bar 5 μm). Figure adapted with permission from ref. ⁶³.

In addition to mechanical forces, other strategies exploiting biochemical interactions have been developed to this purpose. A paradigmatic example is

represented by the work of Wang and co-workers.⁶³ Here, SERS active silver nanoparticle arrays were coated with vancomycin (Van), an antibiotic used to treat a number of bacterial infections. Profiting from the high binding affinity of bacteria towards Van, a thousand-fold increase in bacteria capture from biofluids (saliva, phlegm or blood) was achieved without introducing significant spectral interference (**Figure 2.6 C**). Van-coated SERS substrates acted both as a bacterial capturing tool and an efficient sensing platform for the identification of the SERS fingerprints of the targeted bacteria. The authors reported the concentration of 30% of *Enterococcus* contained in 1 mL of water (10^2 cfu/mL) onto a microscopic Van-coated area of 30 μm in diameter. This microscopic localization helps to reduce the laborious procedure required to locate the bacteria on the substrate and therefore facilitate their subsequent sensing by SERS.

2.1.4 INTEGRATED SERS-MICROFLUIDIC DEVICES AND SERS-ENCODED NANOPARTICLES

Despite all the improvements regarding sample manipulation and concentration, the traditional approach to the direct SERS analysis of bacteria dried on a solid substrate retains major issues in terms of spectral fluctuations, extremely long measuring time to acquire statistically reliable datasets, and lack of quantitative response.^{48,64,65} These limitations can be potentially addressed by combining SERS with microfluidics.

Recent advances in the microfabrication have led to the development of novel microflowing systems for bio-particle separation and analysis. Implementation of microfluidics and biosensor technologies provides the ability to manage and integrate chemical and biological components into a single platform, offering the opportunity for developing portable, autonomous and disposable devices capable of performing real-time detection, unprecedented accuracies, and simultaneous analysis of different analytes in a single device.⁶⁶ Microsystems are already

revolutionising the way we do science and have led to the development of a number of ultrasensitive bioanalytical devices capable of analysing complex biological samples.^{67,68}

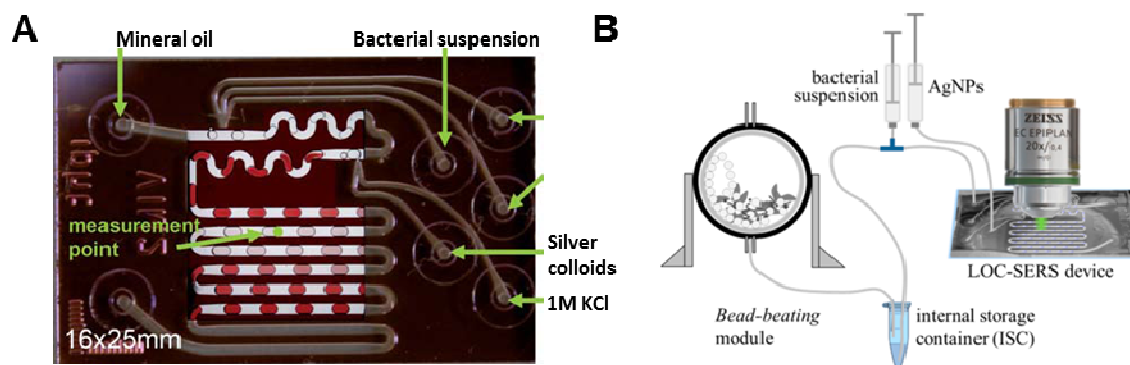


Figure 2.7. (A) Application of two-phase liquid/liquid segmented flow in a microfluidic chip for the acquisition of Raman spectra of the separation medium oil and SERS spectra within the droplets at the measurement point in the second channel. Figure adapted with permission from ref. ⁶⁴. (B) Scheme of sample preparation, including the sample lysing module (bead-beating system) for the bacterial cell disruption, the internal storage container, the syringe pump system, and the droplet-based microfluidic device mounted to the microscope stage.

Popp and co-workers^{64,69} provided the first example of flow-through SERS measurements of bacterial samples in a microfluidic device (Figure 2.7 A). Such approach drastically reduced the acquisition time while improving the spectral reproducibility by analysing the sample in suspension. Initially, the authors demonstrated the efficiency of this SERS-microfluidic device in the classification of 9 different pre-cultivated *E. Coli* strains (buffered solutions, ca. 8×10^7 cells/ml).⁶⁴ Subsequently, 6 different species of pre-cultivated mycobacteria (buffered solutions, concentration range from ca. 4 to 40×10^7 cells/ml) were successfully identified.⁶⁹ In this latter work, a bead-beating module for the disruption of the bacterial cells was combined with the microfluidic device (Figure 2.7 B), leading to an automated closed system for sample preparation and measurement. Disruption of the bacterial membrane allows the colloidal silver nanoparticles to interact with

all cell components rather than the sole bacterial walls. As a result, richer spectral information is available in the SERS spectra, thus improving the overall discrimination capabilities via chemometric methods.

As the ultimate goal for bacterial identification is the complete bypassing of the cultivation step, concentration procedures were then implemented into SERS-microfluidics biosensors, mostly based on microfluidic dielectrophoresis.⁷⁰⁻⁷³ In dielectrophoresis (DEP), non-uniform electric fields are exerted on dielectric particles, including cells and microorganisms, to control their location.⁷⁴ Cheng et al.⁷⁰ combined a short-range DEP and long-range AC electroosmosis flows to rapidly and selectively concentrate pathogens in the diluted human blood sample at the stagnation area on a SERS-active roughened electrode. The high density of bacteria aggregates at the measuring spot allowed obtaining intense SERS fingerprints of *S. aureus*, *E. coli*, and *P. aeruginosa* spiked into blood down to ca. 10^3 cfu/mL. Typically, 50 μ L of 20 times diluted human whole blood spiked with pathogens (dilution was necessary to avoid blood cell coagulation) were dropped onto the chips and subjected to AC excitation for 3 minutes (ca. 40–50% capture efficiency onto the stagnation area was achieved) before being investigated by SERS during 5 minutes.

Microfluidic DEP devices were also integrated with SERS using encoded nanoparticles for the detection of bacteria. Madiyar et al.⁷² captured and concentrated *E. coli* DH α 5 cells coated with SERS tags on a nanoelectrode array placed at the bottom of a microfluidic chip (**Figure 2.8 A**). The SERS signal was successfully measured during DEP capture with single bacterium sensitivity and a quantitative response in the 5 to 1×10^9 cfu/ml range (buffered solutions, **Figure 2.8 B**). The SERS-encoded nanoparticles consisted of iron oxide–gold core–shell nanoparticles initially coated with thiolated-PEG, then infused with a Raman reporter and finally conjugated with a selective Ab. Typically, the bacteria and antibody-conjugated SERS-encoded nanoparticle solutions were mixed together

and incubated overnight at 4 °C. Then several centrifugation/washing cycles were applied to remove the excess of unbound particles, before the analysis. Bacteria detection was also successfully performed in more complex media spiked with 5×10^5 cfu/mL *E. coli* cells.

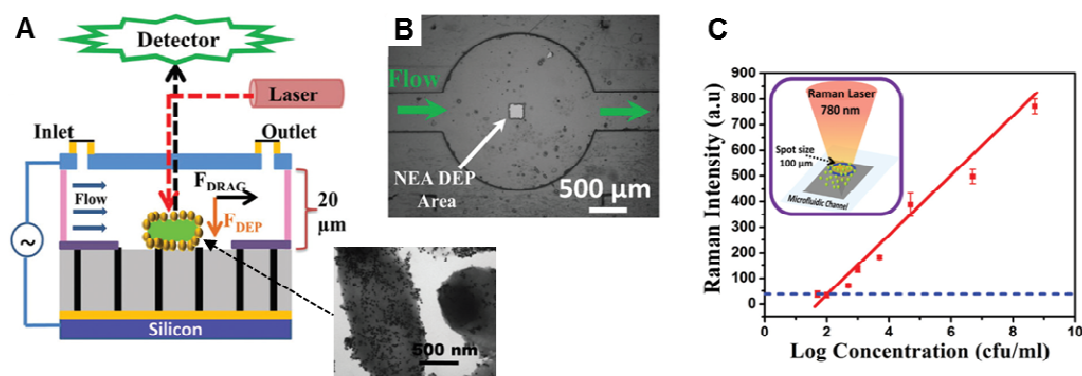


Figure 2.8. (A) Outline of the DEP capture of the bacteria coated with SERS-encoded nanoparticles for the Raman detection. A representative TEM of *E. coli* DHα5 bacterial cells attached with SERS-encoded nanoparticles is also included. (B) Optical microscope image taken under 4× magnification showing the microfluidic channel and the active square at the center. (C) SERS intensity from the samples with the bacterial concentrations in the 5 to 1.0×10^9 cfu/mL range (DEP capture time = 50 s). The inset shows that a 100 μm diameter laser focal spot aligned with a 200 μm × 200 μm active DEP area. Figure adapted with permission from ref. ⁷².

Lin et al.⁷¹ exploited a DEP microfluidic device for trapping individual microorganisms in a defined location in space for their *in situ* interrogation with a confocal micro-Raman system. Clusters of gold nanoparticles aggregated in the presence of dye molecules where silica-coated and bioconjugated with Ab to be used as SERS-encoded nanoparticles. Buffered suspensions of two bacteria (*Salmonella enterica serotype Choleraesuis* and *Neisseria lactamica*) were mixed with SERS-encoded particles and incubated for 1 h at room temperature before being submitted to multiple centrifugation/washing cycles to eliminate unbound nanoparticles prior to DEP–Raman analysis. The practical detection limit with a 10

min measurement time was estimated to be 70 cfu/mL while the total assay time including sample pre-treatment was less than 2 h (no quantitative response was reported).

With the aim of improving the detection specificity and signal enhancement by reducing the miss-binding, Wang et al.⁷³ recently developed a biosensor using a three-epitope detection scheme to avoid the antibody-antigen binding failures which may occur in the one-epitope setup. Here, different SERS-encoded nanoparticles were conjugated with three monoclonal antibodies binding to three different membrane receptors. Buffered suspensions of *E. Coli* O157:H7 pre-concentrated via a DEP-microfluidic device were then incubated with the mixture of SERS-encoded nanoparticles. SERS analysis was performed on droplets of sample solutions placed on a gold-coated microscope slide. Under this set-up, only SERS signals consisting of the superimposed contributions of the different SERS tags were associated with positive recognition events. LOD down to 1 CFU/mL were reported.

Unfortunately, while the sensitivity issue has been addressed by some of these methods, only small volumes (~microliters) of samples, which are normally not relevant for clinical diagnosis, can actually be investigated. Further, additional steps to record a suitable signal for identification are often required.

2.2. THEORETICAL BACKGROUND

2.2.1. OPTICAL BACKGROUND

2.2.1.1. Laser and waves

The laser has revolutionized the world of Science and Technology in multiple fields as, for instance, that of Spectroscopy, which is a scientific area of great relevance for the study of molecular structure and dynamics as well as for chemical analysis.^{75,76} Spectroscopy^{77,78} is based on the interaction of light with matter. Light is an electromagnetic radiation, which is the combination of an oscillating electric and magnetic field, mutually perpendicular, which propagates through space carrying energy from one location to another (see **Figure 2.9**). Nearly all types of electromagnetic radiation can be used to study and characterize matter by means of spectroscopic technics.⁷⁹

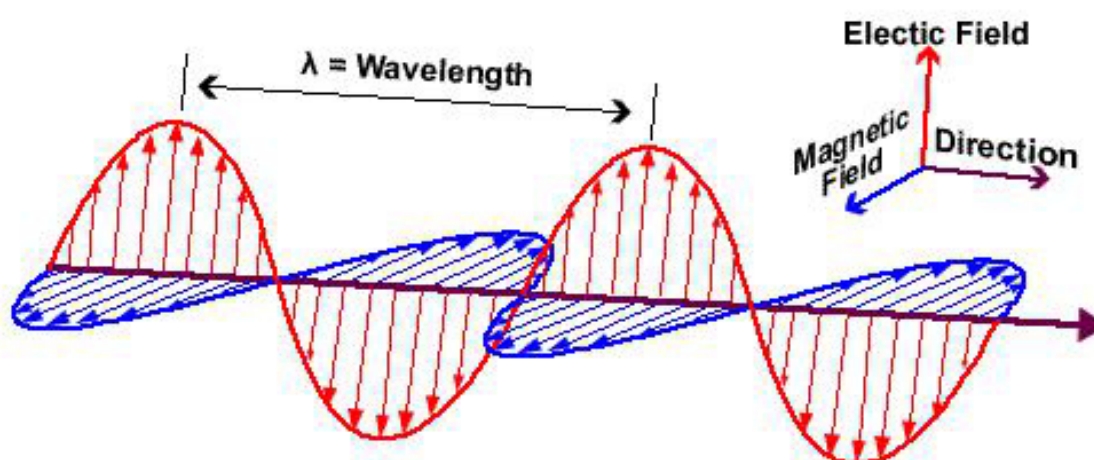


Figure 2.9 Diagram showing the propagation of an electromagnetic wave. Adapted from <http://www.google.es/search?q=electromagnetic+radiation>

2.2.1.2. Optical properties of metals

Metals such as gold (Au), silver (Ag), copper (Cu), or aluminum (Al), have long been known to have different optical properties from standard dielectrics. They, for example, reflect light very efficiently in the visible, making them good materials for mirrors of various types. These particular optical properties, along with many other physical properties, such as heat or electrical conductivity, all have the same physical origin: the presence of free conduction electrons. It seems fairly intuitive that these free electrons result in large heat or electrical conductivity. Their connection with the optical response of metals may however appear less obvious at first sight.

The free electrons of a metal move in a background of fixed positive ions (the vibrations of ions, or phonons, are ignored here in a first approximation), which ensures overall neutrality. This forms, by definition, a plasma and can be called a free-electron plasma, or solid-state plasma.⁸⁰ The study of a solid-state plasma is different from that of a gaseous plasma, since the emphasis is on equilibrium phenomena in the first case, while it is more on instabilities or steady state properties in the latter.^{80,81} The optical response of this free-electron plasma will govern all the optical properties of metals, at least in the visible part of the spectrum where its characteristic resonant energies reside.

2.2.1.3. Localized surface plasmon resonances (LSPR)

In metallic nanoparticles, the localized surface plasmon resonances (LSPR) appears because the electric field of an incoming light wave induces a polarization of the "free electrons with respect to the much heavier ionic core. The net charge difference occurs at the nanoparticle boundaries (the surface) which in turn act as a restoring force (see **Figure 2.10**). The surface plasmon absorption metallic nanoparticles can be shifted depending on the size, shape and nature of the

surrounding medium.⁸²⁻⁸⁵ For gold and silver particles, the surface plasmon resonance occurs within the visible region, (see **Figure 2.11**).

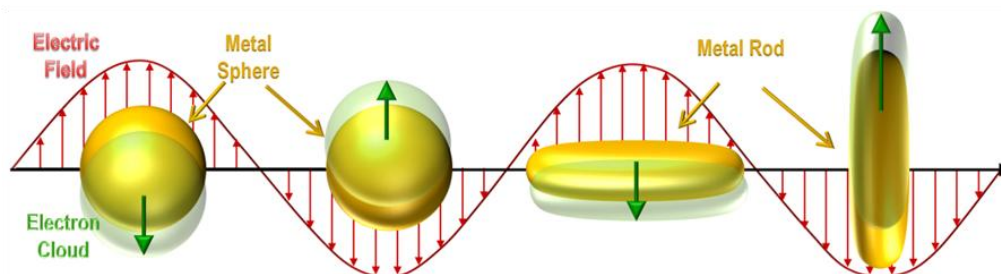


Figure 2.10. In this figure illustrating the excitation of dipole surface plasmon oscillations. The electric field of an incoming electromagnetic radiation induces a polarization of the "free" electrons with respect to the much heavier ionic core of a (gold) nanoparticle. A net charge difference is only felt at the nanoparticle boundaries (surface) which in turn acts as a restoring force. In this way, a dipolar oscillation of the electrons is created. This is known as the surface plasmon resonance. In the case of rods or ellipsoids, the oscillation can take place in two different directions, so that longitudinal and transverse surface plasmon resonances can be excited.

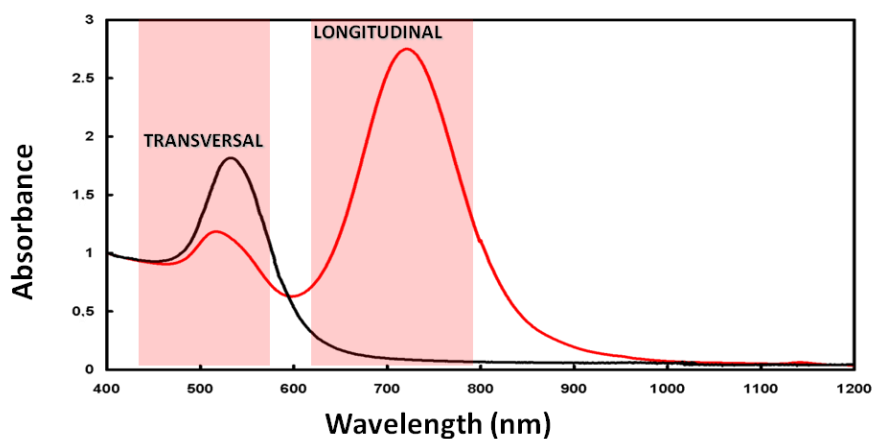


Figure 2.11. Characteristic extinction spectra (absorption + scattering) corresponding to spherical and rod shaped gold nanoparticles. The spherical gold nanoparticles only display one plasmonic band (at 536 nm for this particular sample), while rod shaped gold nanocrystals exhibit two plasmon bands, transverse and longitudinal (with corresponding maxima at 517 and 722 nm, respectively, for this particular example).

2.2.2. RAMAN SPECTROSCOPY

In 1928 the Indian scientist Sir Chandrasekhara Venkata Raman, together with K. S. Krishnan and independently by Grigory Landsberg and Leonid Mandelstam in the former Soviet Union⁸⁶, were the first to experimentally demonstrate the phenomenon named after him as Raman scattering (RS) or Raman effect which led him a couple of years later to be awarded with the Nobel Prize in physics (1930) for his work on the scattering of light and the discovery of the Raman effect⁸⁷. It must be recalled though, that the theoretical principle of this effect was predicted by the Austrian scientist Adolf Smekal in 1923.⁸⁸ Raman spectroscopy is based on the Raman effect which lies in the inelastic light scattering by any particular substance upon illumination. In the original experiment a simple hardware setup, consisted of sunlight as the light source focused onto the sample, passing through a telescope.⁸⁹ The sample could be either a liquid or its dust-free vapour.

At first, the phenomenon was measured on a number of different common liquids with the observer's eye to be the proof of the existence of a modified scattered radiation. However, the Raman scattering is a very weak effect. Only one in ten millions of the scattered light particles, or photons, actually exhibit a change in wavelength. Because of this, advances in Raman spectroscopy were delayed for several decades, until the discovery of intense light sources to amplify the effect and consequently the observed scattered light. The laser as an intense and efficient light source from one hand, along with the development of more effective detection systems on the other hand, brought breakthrough changes later on, in the field of Raman spectroscopy.

2.2.2.1. Raman effect

Absorption or scattering are among the major phenomena that may occur when light interacts with matter. Absorption occurs when the energy of the incident photon, which the light is composed of, corresponds to the energy gap between

the ground state of an atom or a molecule and an excited state. The photon may be absorbed and the molecule will be promoted to an excited state of higher energy. In the case when the energy of the incident photon does not correspond to a specific energy level of an excited state of an atom or a molecule upon illumination, scattering may occur. The predominant part of the photons are elastically scattered in a process called Rayleigh scattering. During this process the scattered photons have the same frequency as the incident photons (ν_0). A very small fraction of the scattered light, one in a 10^6 - 10^8 photons, undergoes inelastic scattering in the process known as Raman scattering, resulting in a scattered photon with different frequency than the incident photon. In this case, the energy of the scattered photon is different from that of the incident photon by one vibrational unit. For example if the energy of incident photon is $h\nu_0$, the difference between the two energy states (V_0 and V_1) is $h\Delta\nu$.

The Raman scattering effect comes from the fact that the light interacts with the molecule and distorts, polarizes, the cloud of electrons surrounding the nuclei to form a short-lived state known as "virtual state". This state is not a stable stage and the photon is re-radiated. This occurs when the light and the electrons interact and the nuclei begin to move at the same time. Since the nuclei are much heavier than the electrons, there is a change in energy of the molecule. Transfer of energy will occur either from the incident photon to the atom or molecule or from the atom or molecule to the scattered photon. Depending on whether the process starts with a molecule in the ground state or from an atom in a vibrationally excited state, the scattering process may be classified as Stokes or anti-Stokes scattering. Stokes scattering occurs from the ground vibrational state (V_0) to an excited vibrational state (V_1) due to the energy absorption by the molecules ($h\Delta\nu$). However, some molecules due to thermal energy may be already in an excited state (V_1) as shown in **Figure 2.12**. Therefore anti-Stokes scattering occurs from the excited state (V_1) to the ground state (V_0) a process that involves energy transfer to the scattered

photon ($h\Delta\nu$). The relative intensities of these two processes depend on the population of the various states of the molecules. The fact that the majority of the molecules are in room temperature, very small number of atoms are expected to be found to an excited state.

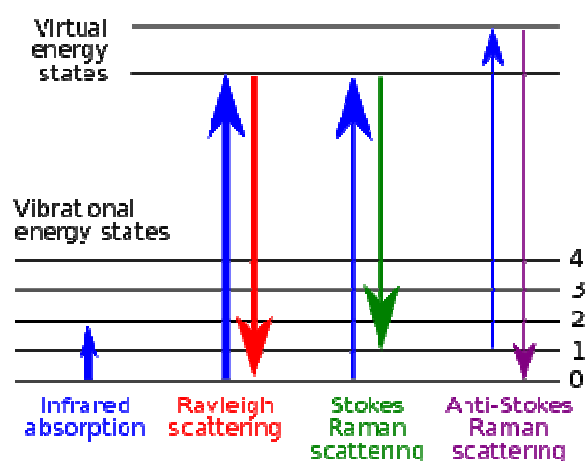


Figure 2.12. Schematic representation of the Rayleigh and Raman scattering.

2.2.2.2. Raman selection rules

The infrared (IR) spectroscopy and the Raman spectroscopy are the two types of spectroscopy that involve vibrational transitions. The fundamental vibrational transitions can be studied by both IR and Raman spectroscopy because they have different selection rules. Whether a transition is allowed or not, is defined by the selection rules. For Raman scattering the fundamental selection rule is the one that occurs from the change in polarizability in a molecule. The polarizability is a molecular property and measures the deformability of a bond under the influence of an external electric field, inducing a temporary dipole. Symmetric vibrations will give the most intense Raman scattering (Raman-active). Unlike to Raman spectroscopy, in IR spectroscopy, an asymmetric vibration (IR-active) will be more intense when a net change in the permanent dipole moment occurs during the vibrations.



Figure 2.13. Raman active (left) and IR active (right) vibrations of carbon dioxide.

Figure 2.13 shows the C-O symmetric (left) and asymmetric (right) stretch in carbon dioxide. The symmetric one is not IR-active because no net change occurs in the dipole moment, while the asymmetric one is IR-active due to a change in dipole moment.

On the other hand the symmetric stretch in carbon dioxide is Raman-active due to the change of the polarizability of the molecule **Figure 2.14** illustrates the different shapes of the electron cloud which can be found during the equilibrium, the extended and compressed symmetric motions.

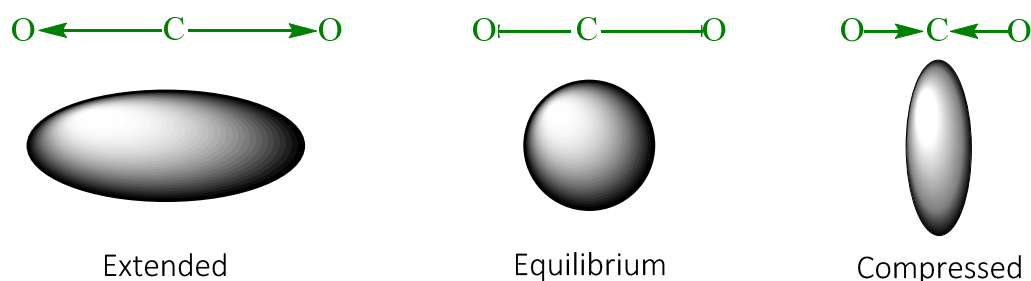


Figure 2.14. Changes in the polarizability of the carbon dioxide molecule. In green are represent the molecular movement and with black tones shown polarizability ellipsoid.

2.2.3. SERS

Surface-enhanced Raman scattering (SERS) spectroscopy is a surface-sensitive technique that enhances the Raman scattering of molecules that are in the close vicinity or directly attached to plasmonic materials such nanostructures metal surfaces or metallic nanoparticles.⁹⁰ The amplification of the Raman signal is so

efficient that can be increased by several orders of magnitude reaching enhancement factors (EF) higher than 10^{13} being even able to detect single molecules.^{73,91-93}

2.2.3.1. Hot Spots

The maximum SERS EF may be of the order of $\sim 10^6$ on a spherical nanoparticle and under certain conditions can be as high as $\sim 10^{10}$ - 10^{11} . As an example of such cases is the apex of a metallic.^{34,92}

Additional signal amplification arises from the interaction of two or more neighbouring plasmonic nanoobjects. The maximum SERS EF typically occurs at some specific regions on the substrate surface where the localized surface plasmon resonances (LSPRs) between individual nanostructures are coupled resulting in a significantly higher electromagnetic field and therefore, molecules adsorbed on these points can profit from it.^{34,92} Shalaev et al developed a theoretical approach that predicts extremely large electromagnetic field enhancement on fractal surfaces⁹⁴⁻⁹⁶ combining the discrete dipole approximation (DDA) method and the fractal features from the aggregated colloids or rough surfaces.^{97,98} It is in these special regions “hot spots” that the resonance of the electromagnetic radiation is concentrated. The locations of the hot areas depend strongly on the geometry of the fractal, the excitation wavelength and the polarization of the incident laser. In addition, it has been demonstrated that the same area could be a hot spot or a cold zone depending on the excitation wavelength used.

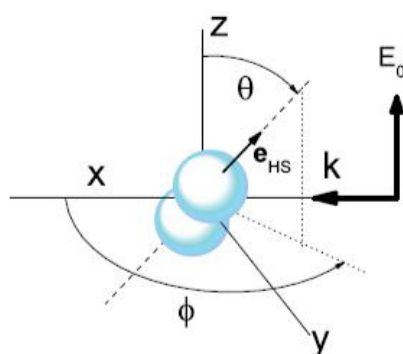


Figure 2.15. Schematic configuration of a hot spot. The incoming wave is incident along the x-axis with polarization along z, and the signal is analyzed in the backscattered direction with polarization either parallel \parallel (z) or perpendicular \perp (y) to the incoming polarization. The main axis joining the two particles, which defines the direction of the main axis of the hot spot, e_{HS} is defined by angles θ (co-latitude) and ϕ (longitude) in spherical coordinates.

In **Figure 2.15** we can see a geometrical scheme of a hot spot. The excitation beam is considered to be incident along x and perpendicular to the dimer axis along z and we consider excitation occurring only with incident polarization along the dimer axis, for which maximum coupling to the main LSPR is obtained.⁹⁹

2.2.3.2. SERS substrates

The success condition for the SERS studies is highly dependent on the interaction between the absorbed probe molecule and the surface of the plasmonic nanostructure. The synthesis of metal nanoparticles is an expanding research area due to the potential applications for the development of novel technologies. The most used substrates in SERS are made mostly of silver (Ag), gold (Au), which are good candidates due to their stability and biocompatibility of the Au, and much less of copper (Cu) due to its high reactivity. Most Raman measurements occur in the visible and near infrared wavelength range where all the three metals mentioned above hold LSPRs.¹⁰⁰ In **Figure 2.16** are shown the approximate wavelength ranges for SERS of Ag, Au, and Cu.

Nevertheless SERS experiments have been also performed in other metals like rhodium (Rh),¹⁰¹ platinum (Pt),¹⁰² ruthenium (Ru),¹⁰³ and aluminium (Al).¹⁰⁴ Novel materials such as graphene,^{105,106} semiconductors such as TiO₂,¹⁰⁷ and quantum dots (QDs)^{108,109} have recently been reported to show SERS, although they do not fit traditional definitions of SERS substrates.

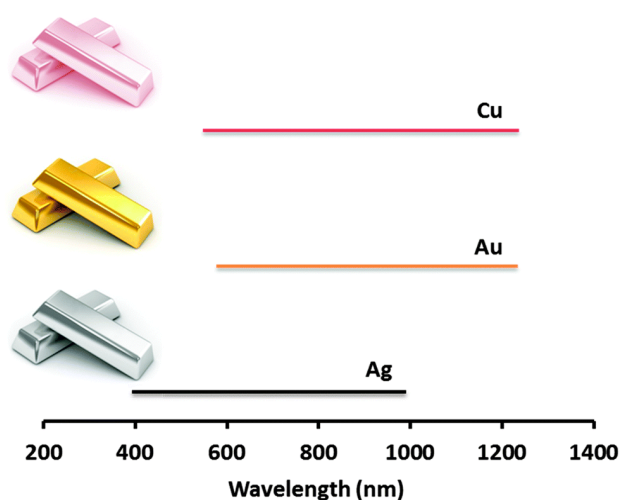


Figure 2.16. Approximate wavelength ranges where Ag, Au, and Cu have been well characterized and are established to support SERS.

2.2.3.3. Colloidal silver nanoparticles (AgNPs)

Among the previously mentioned materials, Ag is probably the most important one in plasmonics. And, since SERS is derived from the LSPRs in nanostructured metals, Ag outperforms the other materials due to its higher extinction coefficients, sharper extinction bands, higher ratio of scattering to absorption, and extremely high field enhancements. Moreover, silver is able to support strong surface plasmons in the visible (vis) and near-infrared (NIR) regions of the spectrum by tuning its size and shape.¹⁷

Nowadays, advances in synthetical methods allow the generation of Ag nanostructures with varied morphological properties which overcome the difficulties of the precise control of the Ag due to its lower chemical stability when

compared to gold.^{26,110,111} In **Figure 2.17** are presented briefly some of the synthetic methods used to generate certain morphologies.

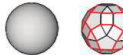












Shape	Illustration	LSPR ^a	Applications ^b	Method of Synthesis
Sphere and quasi-sphere		320 - 450	SERS; LSPR sensing; assembly	Polyol process (single-crystal); Citrate reduction (quasi-sphere)
Cube and truncated cube		400 - 480	SERS; LSPR sensing; assembly	Polyol process; Seed-mediated growth
Tetrahedron and truncated tetrahedron		350 - 450	SERS	Polyol process; Light-mediated Growth
Octahedron and truncated octahedron		400 - 500	Assembly	Polyol process; seed-mediated growth; light-mediated growth
Bar		350 - 900	SERS	Polyol process
Spheroid		350 - 900	SERS	Polyol process
Right bipyramid		500 - 700	-	Polyol process
Beam		-	Electron transport	Polyol process
Decahedron		350 - 450	-	Seed-mediated growth; light-mediated growth; citrate reduction
Wire and rod		380 - 460	Wave guiding; electronics; SERS; assembly	Seed-mediated growth
Polygonal plates and disc		350 - 1000	SERS; LSPR sensing	Light-mediated growth; polyol process
Branched structures		400 - 1100	SERS	Seed-mediated growth
Hollow structures		380 - 800	SERS; LSPR sensing	Template-directed growth

Figure 2.17. Summary of the Shapes, LSPR Absorption Peaks, Demonstrated Applications, and Methods for Synthesis of AgNPs. **a** The main absorption peak (nm). **b** Assembly means the nanostructure has been assembled into larger structures for plasmonic applications or studies.

2.2.3.4. SERS instrumentation

Current dispersive Raman instruments are coupled with microscopes and several laser beam lines as excitation sources. The choice of the excitation wavelength (mainly from the visible to NIR) depends strictly on the application. An important factor to take into account when performing a SERS measurement, is the Raman scattering efficiency since it depends on the fourth power of the frequency.¹¹² Therefore, shorter wavelengths improve the Raman sensitivity although the risk of fluorescence or sample degradation also increases and has to be considered.¹¹³

Figure 2.18, shows a basic Raman spectrophotometer set-up attached to a confocal microscope. In this particular set-up and in most modern Raman spectrophotometers, the inelastically scattered light is collected at 180° geometry. In the confocal unit, the light from the laser initially passes through a pinhole aperture. This light is then delivered through the notch filters (interference filters) where it is completely reflected into the microscope and reaches the sample through the beam splitter. Then, the inelastically scattered light passes back through the same optics, a monochromator and finally reaches the CCD detector.

113,114

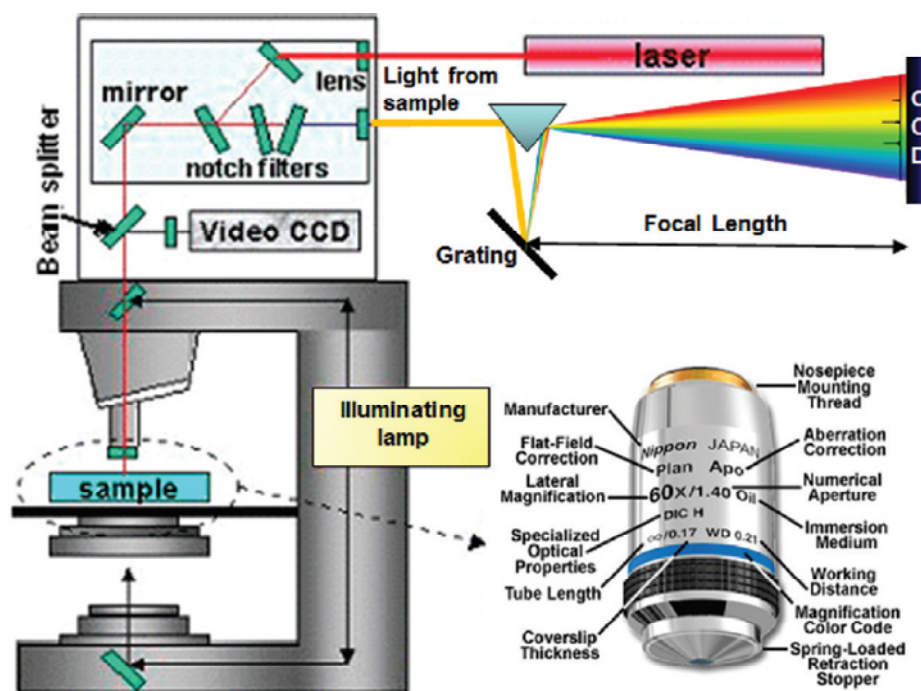


Figure 2.18. Schematic representation of a dispersive Raman instrument coupled with a confocal microscope with a detailed description of a microscope objective ¹¹³

2.2.3.5. Biomedical applications and SERS sensing

SERS as a powerful molecular spectroscopic technique with the capability of ultradetection sensing is a reliable analytical tool that is expanding its realm of applications from diagnosis and biomedical applications to environmental monitoring with potential multiplexing and real time analysis. In serious medical issues the fast and accurate detection of the pathogen is literally a matter of life and death. SERS biosensors can be applied in the detection of biological samples and diseases, including various types of cancer,¹¹⁵ prionic diseases such as Alzheimer and Parkinson¹¹⁶ or infections.¹¹⁷ Therefore, there is a potential substitution of the time consuming and more costly traditional immunological detection assays which employ antibody methods as the enzyme-linked immunosorbent assay (ELISA) by SERS immunosensors with the ability to provide information in the complex biological environments with minimum sample preparation and high spatial resolution.

2.2.4. MICROORGANISMS

The etymology of the word microorganism is derived from the Greek word *μικρόβιος* [microbes], which is composed of *μικρός* [Micros] and *βίος* [bios]. That means a very small living being that can only be viewed with a microscope, also called micro-organism. The concept of microorganism does not imply a taxonomic or phylogenetic relationship, as it encompasses unicellular and multicellular organisms that have no evolutionary relationship to each other. The group includes both, prokaryotic microorganisms (bacteria, etc.) and eukaryotes (protozoa, etc.), also some algae and fungi, and even acellular biological entities with an ultramicroscopic size such as viruses or prions. The latter generally are not considered living beings and therefore are not strictly microorganisms; however, they are also included in the study field of microbiology.¹¹⁸

Because of evolution and natural selection, nowadays, there is vast microbial diversity which can be seen in many ways, for example, in variations in cell size, morphology, motility, metabolic strategies, etc.

All organisms contain ribosomes and thus ribosomal RNA, this molecule has been used to construct a phylogenetic tree of all life forms, prokaryotic and eukaryotic.¹¹⁹ From comparative ribosomal RNA sequences three phylogenetically distinct lineages of cells have been identified; two of these lineages contain only prokaryotes, while the third is composed of eukaryotes. The lineages, referred to as evolutionary domains, are called The Bacteria, The Archaea and The Eukaryota (Figure 2.19). These domains are thought to have diverged from a common ancestral organism called The LUCA.

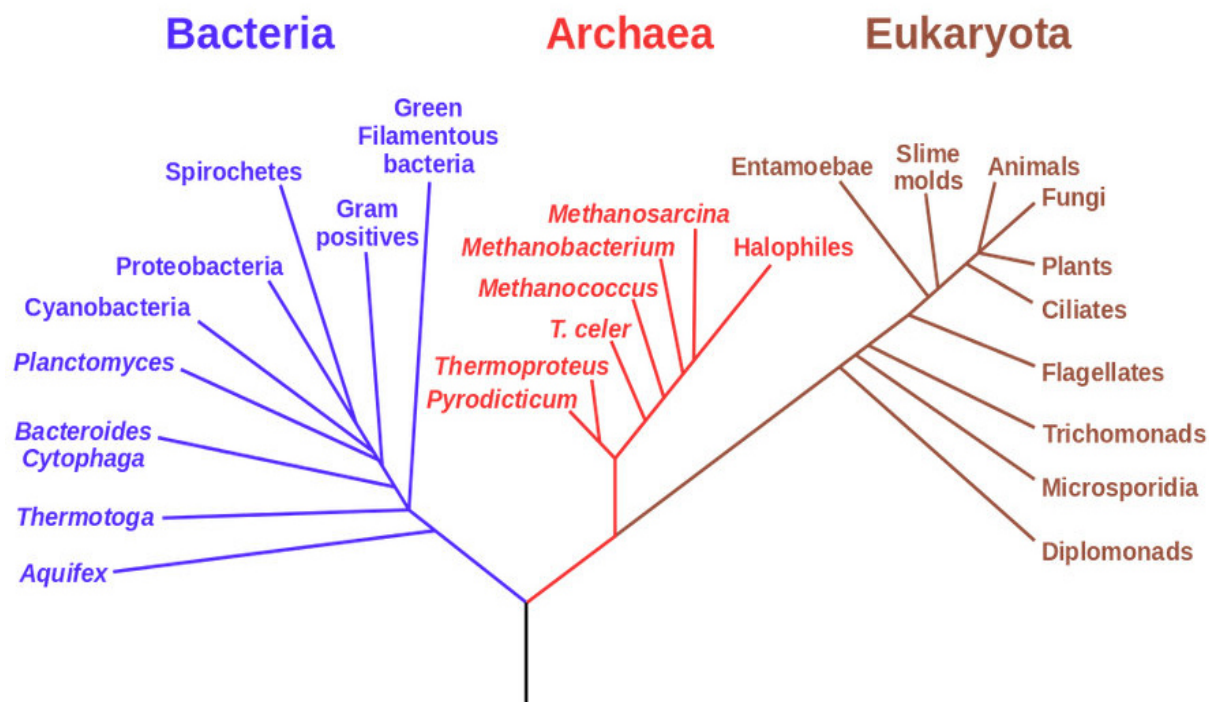


Figure 2.19 Universal phylogenetic tree. This tree is derived from comparative sequencing of ribosomal RNA (16S or 18S). Adapted from <https://commons.wikimedia.org/w/index.php?curid=26075698>

The term "bacteria" is still widely used in a general sense to mean "the prokaryotic organisms" and in this sense it includes all the prokaryotes. However, molecular studies have indicated that the prokaryotes can be divided into two fundamentally different groups (domains): the domain Bacteria and the domain Archaea.¹²⁰

Most Bacteria are free-living, they do not necessarily form specific associations with other organisms. Bacteria normally occur as members of mixed communities which include fungi, algae, protozoa and other organisms. Such communities can be found in a wide variety of natural habitats water, surfaces of plants, soil, within the bodies of mammals. Those microorganisms which are normally present in a particular habitat are referred as the microflora of that habitat.^{121,122}

Bacteria which colonize a given habitat may affect each other in various ways; for example, they may have to compete for primary requirements like as nutrients,

oxygen, space, light, etc. and those organisms which cannot compete effectively are likely to be eliminated from the habitat.¹²³

One important reason for study Bacteria because the cause some major diseases as well as a number of minor ones; the prevention and control of these diseases depend largely on the efforts of medical, veterinary and agricultural bacteriologists. Importantly, the pathogenic bacteria are only a small proportion of the bacteria as a whole meanwhile most bacteria are innocuous or even positive to humans.^{124,125}

2.2.4.1. Bacteria Pathogens

Some diseases are due to "errors" in the body's chemistry, but in many diseases symptoms result from the activities of certain microorganisms, on or within the body; any microorganisms which can cause diseases is called a pathogen. Sometimes a disease is due to an organism which does not usually behave as a pathogen and which may actually be a member of the body's own microflora, called opportunist pathogens. Disease does not necessarily follow exposure to a give "causal agent". In fact, the occurrence of a disease typically depends on various factors, including the degree or resistance of the host and the virulence of the pathogen.^{126,127}

Different pathogens act in different ways. Some produce toxins or other substances which disrupt specific physiological processes, while others invade particular cells or tissues and may also form toxins. Even when localized in the body, infections often have systemic effects.¹²⁸

Some pathogens are able to synthesize a biofilm; increasing therefore their virulence. Biofilms can be defined as an organized group of microorganisms living within a self-produced matrix of polymeric substances which gets attached to several surfaces.¹²⁹ These microbial collectives are found to be ubiquitous in almost

every environment.¹³⁰ Biofilms can be found in both biotic and abiotic surfaces.¹³¹ Biofilms have been seen to be present on liquid surfaces as a floating mat and in submerged state also.¹³²

2.2.4.2. Isolation of Pathogens from clinical specimens

A clinical examination of a patient, may suspect that an infectious disease is present. Samples of infected tissues or fluids are then collected for microbiological, immunological, and molecular biological analyses **Figure 2.20**. The swab is streaked over the surface (i.e. an agar plate) or placed directly in a liquid culture medium. In some cases, small pieces of living tissue may be also sampled for culture. **Figure 2.20** summarizes current recommendations for initial culture of organisms isolated from typical clinical specimens.

If clinically relevant organisms are to be isolated and identified, the specimen must be obtained properly. The clinician must ensure that the specimen is removed from the actual site of the infection. In addition, recovery of pathogens may not be possible if insufficient inoculum is taken.¹³³ The sample must also be taken under aseptic conditions so that further contaminations are avoided. Care must also be taken to ensure that metabolic requirements for certain organisms, such as anoxic conditions, are maintained. Once obtained, the sample must be analyzed as soon as possible.¹³⁴

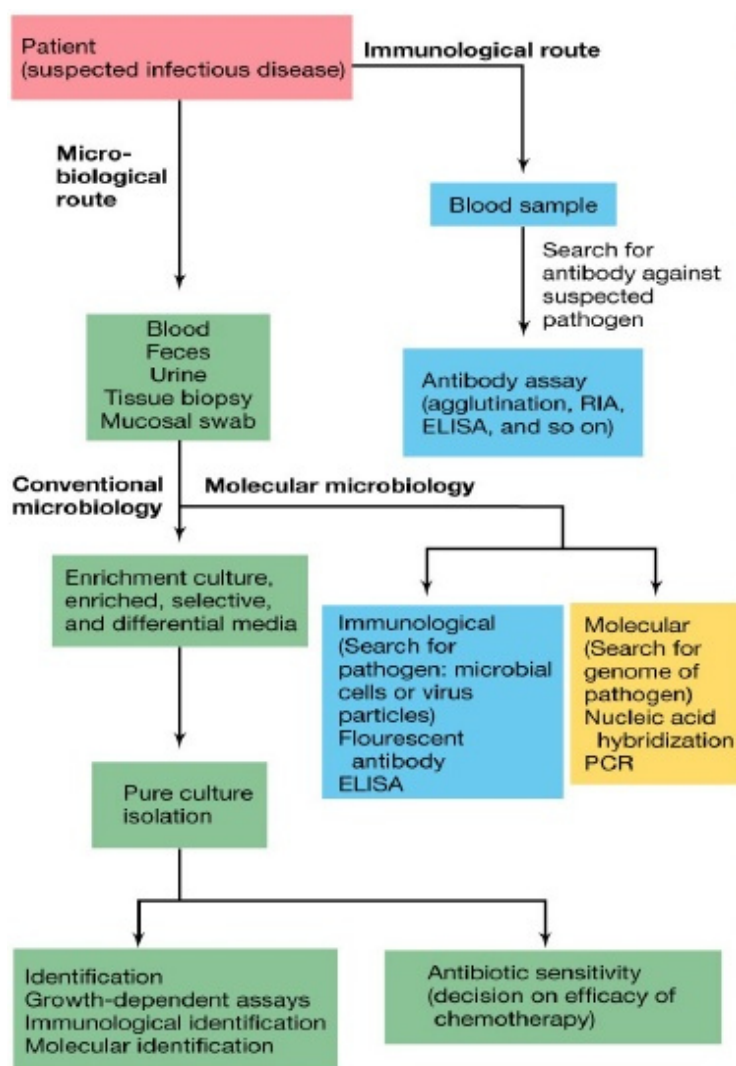


Figure 2.20. Clinical and diagnostic methods used for isolation and identification of infectious pathogens.¹³⁵

An aspect to bear in mind is the term "quorum sensing" was first introduced by Fuqua et al. (1994)¹³⁶, and later explained by Wuster and Babu (2007).¹³⁷ In some cases, cells in a high-density population exhibit characteristics which are absent in the same cells in low- density populations. The cells secrete signal molecules of a special kind, and if cell density reaches a certain minimum "quorum" these molecules accumulate to a level which activates certain genes within the cells. The low- molecular- weight signalling molecule is called an autoinducer, because the

cells themselves produce it. Different bacteria may produce different autoinducers which regulate different characteristics; in some cases different species produce the same autoinducer, but for regulating different genes. Some bacteria produce a range of autoinducers for controlling the expression of various properties.

2.2.4.3. Gram + / Gram -

Gram staining is a method used to differentiate bacterial species into two large groups called: gram-positive and gram-negative. The name comes from the Danish bacteriologist Hans Christian Gram, who published his method in 1884¹³⁸ Gram staining differentiates bacteria by the chemical and physical properties of their cell walls (see **Figure 2.21**) by detecting peptidoglycan, which is present in the cell wall of Gram-positive bacteria.¹³⁹ Gram-positive bacteria retain the crystal violet dye, and thus are stained violet, while the Gram-negative bacteria do not; after washing, a counterstain is added, commonly safranin or fuchsine that will stain the Gram-negative bacteria in pink meanwhile for the Gram-positive bacteria the counterstain is unseen because of the darker crystal violet stain.

The Gram stain is almost always the first step in the preliminary identification of a bacterial organism. However, while Gram staining is a valuable diagnostic tool, not all bacteria can be definitively classified by this technique. This gives rise to *gram-variable* and *gram-indeterminate* groups.¹³⁵

This differentiation enables it to prescribe adequate drugs. Generally, Gram-negative bacteria are more resistant to antibodies and antibiotics than Gram-positive, because they have a largely impermeable cell wall.¹⁴⁰

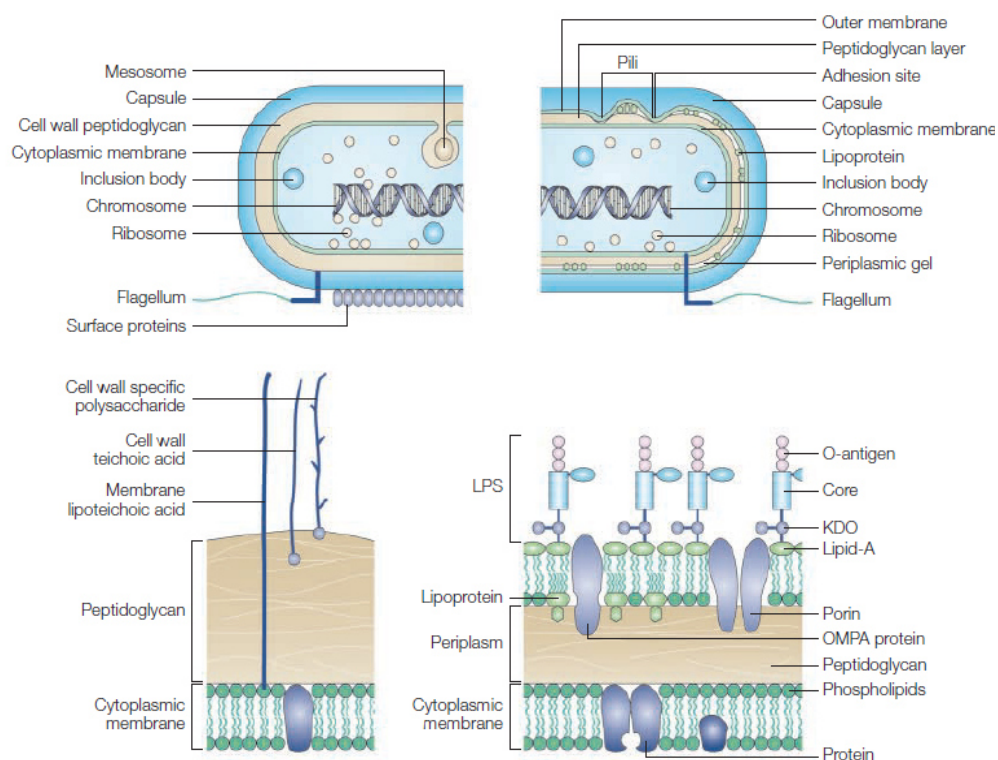


Figure 2.21. Structural features of the cell wall that distinguishes the Gram-positive from the Gram-negative bacteria, which are two principal classes of pathogenic bacteria.¹⁴⁰

2.2.5. ANTIBIOTICS

Usually, when we are suffering from a bacterial infection doctors' prescribe antibiotics. However, there is a wide range of antibiotics available, and vary both in its use and its mechanism of action. As previously described, bacteria can be divided into two major classes: Gram-positive and Gram-negative. Gram-negative bacteria are more resistant to antibodies and antibiotics than Gram-positive bacteria, because they have a largely impermeable cell wall.^{140,141} **Figure 2.22** summarizes the main classes of antibiotics giving also a brief overview of their effectiveness for different bacterial infections.

DIFFERENT CLASSES OF ANTIBIOTICS - AN OVERVIEW

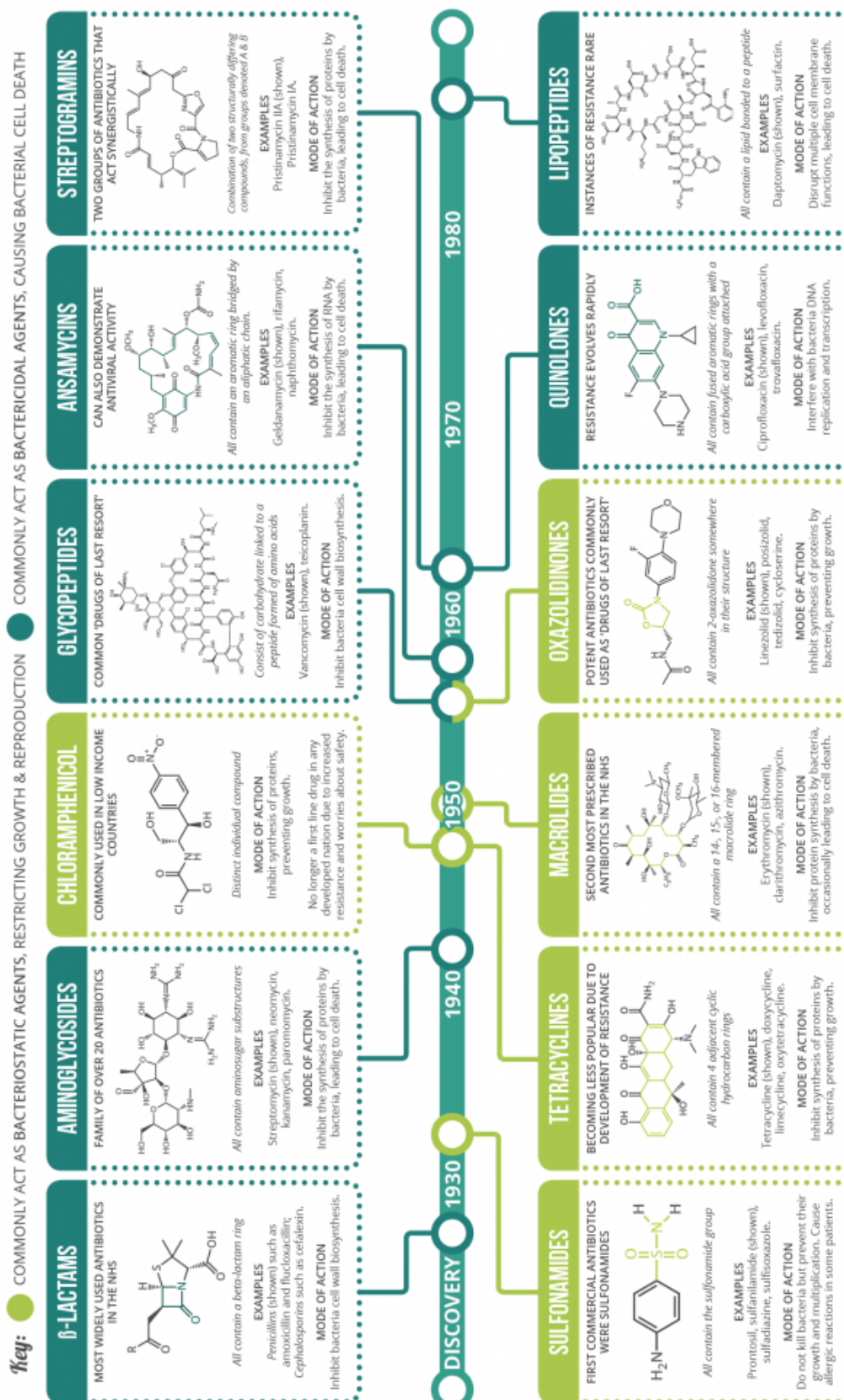


Figure 2.22. Adapted from <http://www.compoundchem.com/wp-content/uploads/2014/09/Major-Classes-of-Antibiotics-Summary-v2.png>

2.2.5.1. AntiMicrobial Resistance (AMR)

Resistance to antimicrobials (AMR) is a natural process that has been observed since the first antibiotics were discovered and, indeed, the genes that confer drug resistance upon some strains of bacteria predate antibiotics by millions of years.¹⁴²

AMR arises when the micro-organisms which cause infection survive exposure to a medicine that would normally kill them or stop their growth. This allows those strains that are capable of surviving exposure to a particular drug to grow and spread, due to a lack of competition from other strains.¹⁴³ This has led to the emergence of 'superbugs' such as Methicillin-resistant *Staphylococcus aureus* (MRSA) and extremely drug-resistant tuberculosis, bacteria which are difficult or impossible to treat with existing medicines.¹⁴⁴

AMR has increasingly become a problem in recent times because overuse of antimicrobials has increased the rate at which resistance is developing and spreading. In the past, resistant infections were associated predominantly with hospitals and care settings, but over the last decade resistant infections have been seen in the wider community too.^{67-144a}

2.2.6. SEPSIS

Sepsis is a syndrome which results from the body's response to an infecting microorganism. Upon activation, the immune competent cells, cause the release of cytokines and activation of different cascade systems that ultimately, affect the endothelium. This course of events results in what is known as inflammation. In sepsis, the inflammatory process is systemic; it affects every organ system in the body, even remote from the original infection site. If unrecognized and left untreated, there is a considerable risk of progression to the most severe form, septic shock. Despite enormous advances in understanding the disease processes

and technical progress sepsis is still increasing.¹⁴⁵⁻¹⁴⁹ In Table are summarized the most frequently microorganisms causing sepsis.

Microorganisms of Special Relevance				
Bacteria	Aerobes	Gram positive	<i>Streptococcus pneumoniae</i>	
			<i>Streptococcus pyogenes</i> (Grupo A)	
			<i>Streptococcus agalactiae</i> (Grupo B)	
			<i>Staphylococcus aureus</i>	
		Gram negative	<i>Neisseria meningitidis</i>	
			"Enterics"	<i>Escherichia coli</i>
				<i>Klebsiella</i>
				<i>Enterobacter Serratia</i>
				<i>Citobacter Salmonella</i>
			"Non-enterics"	<i>Pseudomona aeruginosa</i>
<i>Acinetobacter</i>				
Anaerobes	<i>Bacteroides fragilis</i>			
Viruses	<i>Flavivirus</i>			
	<i>Coronaviridae</i>			
Fungi	<i>Candida</i>			
	<i>Histoplasma</i>			
	<i>Aspergillus</i>			

Table 1. Sump up of microorganisms that acquired a special relevance or high incidence rates in hospitals. The division is shown separated by domain and some characteristics of microorganisms such as oxygen tolerance, staining of grams and subdivision between enteric and non-enteric. Highlighted in bold the selected microorganisms.¹⁵⁰

2.2.7. Characteristics of the bacteria used in this thesis

To develop the microbiology part of this thesis, we selected four bacterial strains with high incidence rates in hospitals. Specifically, two gram + strains that are *Streptococcus agalactiae* (Table 2) and *Staphylococcus aureus* (Table 3) and other two gram- strains, *Escherichia coli* (Table 4) and *Pseudomonas aureginosa* (Table 5).

2.2.7.1. *Streptococcus agalactiae*


<i>Streptococcus agalactiae</i>		<u>Lehmann and Neuman 1896</u>
Scientific classification	<p>Domain Bacteria</p> <p>Kingdom Eubacteria</p> <p>Phylum Firmicutes</p> <p>Class Bacilli</p> <p>Order Lactobacilles</p> <p>Family Streptococcaeae</p> <p>Genus <i>Streptococcus</i></p> <p>Specie <i>agalactiae</i></p>	
Characteristics	<p>Morphology</p> <p>Appearance single, in pairs, or chains</p> <p>Size 0.5- 2.0 µm in diameter</p> <p>Colour creamy / tan</p> <p>Texture dry</p> <p>Optical Quality opaque</p> <p>Hemolysis Beta</p> <p>Gram positive</p> <p>Movility Non motile</p> <p>Spore Non spore-forming</p> <p>metabolism facultative anaerobes</p> <p>Capsule variable, virulents strains encapsulated.</p> <p>Salt tolerance variable</p> <p>Chemo-organotrophic fermentative metabolism producing mainly lactose, no gas</p> <p>Catalse negative</p> <p>Oxidase negative</p> <p>Hipurate positive</p> <p>Bile esculin negative</p>	
Human	It can be commonly found in normal flora to the mouth, nouse and throat.	
Most common diseases	The most commonly associated it is with neonatal infections such as sepsis, pneumonia and meningitis . ¹⁵¹ It is only fatal in adults in the immunocompromised or elderly (mortality rate of 15% in patients aged 65 or older). ^{151,152}	
Biofilm	Biofilm production has been suggested to be important for Group B <i>Streptococcus</i> pathogenesis along side many other elements, including phylogenetic lineage and virulence factors, such as pili and capsule type. ¹⁵³	
Clinically significance	It is a commensal bacterium colonizing the intestinal tract of a significant proportion of the human population. However, it is also a pathogen which is the leading cause of invasive infections in neonates and causes septicaemia, meningitis and pneumonia. ¹⁵⁴	
Host defenses	Phagocytosis is the major mechanism for combatting streptococcal infection. D-alanylation of lipoteichoic acid (LTA) contributes to the virulence of <i>S. agalactiae</i> . This allows Gram-positive bacteria to modulate their surface charge, regulate ligand binding and control the electromechanical properties of the cell wall. ¹⁵⁵	

Table 2. Short characterization and description of *Streptococcus agalactiae*. Image and text adapted from references ¹⁵¹⁻¹⁵⁵ and <https://www.yooniqimages.com/kr/images/detail/105652534/Editorial/streptococcus-agalactiae-bacteria-sem>.

2.2.7.2. *Staphylococcus aureus*

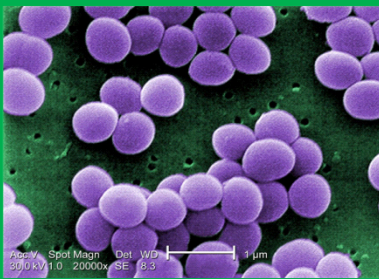
<i>Staphylococcus aureus</i>		<u>Rosenbach 1884</u>
Scientific classification	<p>Domain Bacteria</p> <p>Kingdom Eubacteria</p> <p>Phylum Firmicutes</p> <p>Class Bacilli</p> <p>Order Bacillales</p> <p>Family Staphylococcaceae</p> <p>Genus <i>Staphylococcus</i></p> <p>Specie <i>aureus</i></p>	
Characteristics	<p>Morphology</p> <p>Appearance single, in pairs, or irregular grape-like clusters</p> <p>Size 0.5-1.5 µm in diameter</p> <p>Colour Creamy / tan</p> <p>Texture dry</p> <p>Optical Quality opaque</p> <p>Hemolysis Alpha Prime or Beta</p> <p>Gram positive</p> <p>Movility Non motile</p> <p>Spore Non spore-forming</p> <p>metabolism Facultatives anaerobes</p> <p>Capsule variable, virulents strains ecapsulated.</p> <p>Salt tolerance High salt tolerance (up to 10% NaCl)</p> <p>Catalase positive</p> <p>Oxidase negative</p> <p>TGA test black colonies</p> <p>Coagulase positive</p> <p>MSA test Colorless; colonies Yellow; Medium</p>	
Human microbiom	The genus <i>Staphylococcus</i> is part of normal flora widespread over the body surface.	
Most common diseases	It is common for this bacteria to cause impetigo, toxic shock, syndrome, bacteremia, endocarditis, folliculitis furncle and osteomelity. ¹⁵⁶	
Biofilm	Many strains have the ability to form biofilms wich can then colonize structures such as medical catheters, stents, heart valves, prostheses, shunts and valves. ¹⁵⁷	
Clinically significance	Generally it is possible separated the <i>Staphylococcus</i> species into coagulase-negative, like as <i>S. epidermidis</i> or coagulase-positive wich includes <i>S. aureus</i> ,this especie are a major cause of morbidity and mortality in nosocomial infections. ¹⁵⁸	
Host defenses	Phagocytosis is the major mechanism for combatting staphylococcal infection. Antibodies are produced which neutralize toxins and promote opsonization. The capsule and protein A may interfere with phagocytosis. Biofilm growth on implants is impervious to phagocytosis. ¹⁵⁹	

Table 3. Short characterization and description of *Staphylococcus aureus*. Image and text adapted from references¹⁵⁶⁻¹⁵⁹ and https://es.wikipedia.org/wiki/Staphylococcus_aureus#/media/File:Staphylococcus_aureus_VISA_2.jpg

2.2.7.3. *Escherichia coli*

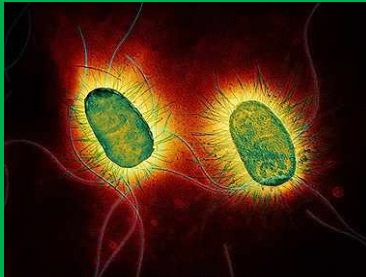
<i>Escherichia coli</i>		<u>Mingula 1895</u>
Scientific classification	<p>Domain Bacteria</p> <p>Kingdom Eubacteria</p> <p>Phylum Proteobacteria</p> <p>Class Gammaproteobactea</p> <p>Order Enterobacteriales</p> <p>Family Enterobacteriaceae</p> <p>Genus <i>Escherichia</i></p> <p>Specie <i>coli</i></p>	
Characteristics	<p>Morphology</p> <p>Appearance single</p> <p>Size 0,5 µm in diameter and 1.0-3.0 µm in length.</p> <p>Colour Creamy / tan</p> <p>Texture dry</p> <p>Optical Quality opaque</p> <p>Hemolysis Occasionally, Beta.</p> <p>Gram negative</p> <p>Movility motile, peritrichous.</p> <p>Spore Non spore-forming</p> <p>metabolism Facultatives anaerobes</p> <p>Oxidasa negative</p> <p>Catalasa positive</p> <p>Methyl red tests positive</p> <p>Indole positive</p> <p>manitol positive</p> <p>lactose positive</p> <p>Voges-Proskauer negative</p>	
Human microbiome	It can be commonly found in lower intestines of human and mammals. When <i>E.coli</i> locates in human large intestines, it can help digestion processes, food breakdown and absorpction, and vitamin K production. ¹⁶⁰	
Most common diseases	Extraintestinal <i>E. coli</i> infections, such as urinary tract infections and neonatal sepsis, represent a huge public health problem. ¹⁶¹	
Biofilm	The formation of biofilm is very frequent, but also variable. Despite the various studies on the factors and genes that regulate this process; results are not conclusive. ¹⁶²	
Clinically significance	They are caused mainly by specialized extraintestinal pathogenic <i>E. coli</i> strains that can innocuously colonize human hosts but can also cause disease upon entering a normally sterile body site. ¹⁶³	
Host defenses	<i>E. coli</i> strains are confronted with a formidable array of host defenses, including urine flow and a panoply of antimicrobial factors. To counteract, usually <i>E. coli</i> strains encode surface filamentous adhesive organelles called pili type 1 that can mediate bacterial binding and invasion. ¹⁶⁴	

Table 4. Short characterization and description of *Escherichia coli*. Image and text adapted from references¹⁶⁰⁻¹⁶³ and <http://es.globedia.com/mutacion-bacteria-coli-transgenicos>.

2.2.7.4. *Pseudomona aeruginosa*

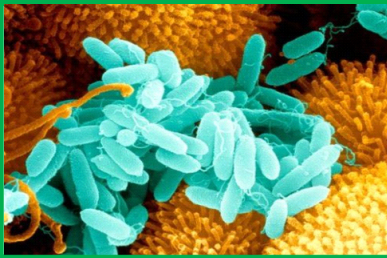
<i>Pseudomona aeruginosa</i>		<u>Schröter 1872</u>
Scientific classification	<p>Domain Bacteria</p> <p>Kingdom Eubacteria</p> <p>Phylum Proteobacteria</p> <p>Class Grammaproteobacteria</p> <p>Order Pseudomonadales</p> <p>Family Pseudomonadaceae</p> <p>Genus <i>Pseudomona</i></p> <p>Specie <i>aeruginosa</i></p>	
Characteristics	<p style="text-align: center;">Morphology</p> <p style="text-align: center;">Appearance rod</p> <p style="text-align: center;">Size 1-5 µm long and 0.5-1.0 µm wide</p> <p style="text-align: center;">Colour Creamy / tan</p> <p style="text-align: center;">Texture mucous / dry</p> <p style="text-align: center;">Optical Quality opaque</p> <p style="text-align: center;">Hemolysis Ocasionaly, Beta.</p> <p style="text-align: center;">Gram negative</p> <p style="text-align: center;">Movility Motile, unipolar</p> <p style="text-align: center;">metabolism aerobic</p> <p style="text-align: center;">Odor in vitro likes a grapes, caramel or strawberry.</p> <p style="text-align: center;">gas No</p> <p style="text-align: center;">Catalse positive</p> <p style="text-align: center;">Oxidase positive</p> <p style="text-align: center;">Lactose negative</p> <p style="text-align: center;">Citrate test positve</p> <p style="text-align: center;">Pigments Produce water-soluble pigments which diffuse through the medium: pyocyanin (blue-green), pyoverdine (yellow-green, fluorescent), and pyorubin (red-brown, produced by a small proportion of strains).</p>	
Human microbiome	<p>The genus <i>Pseudomonas</i> is distributed practically everywhere, for example in water, soil, vegetation, gasoline, inanimate objects, in humans, animals, etc. The vectors of transmission are: By air, contaminated water is a good source and it is possible to transmit the bacteria through the medium of saliva droplets.¹⁶⁵</p>	
Most common diseases	<p>It is common for this bacteria to cause nosocomial infections like pneumonia, meningitis, endocarditis or bacteremia.¹⁶⁴</p>	
Biofilm	<p>It produce robust biofilms. <i>P. aeruginosa</i> biofilms cause severe problems in immunocompromised patients including those with cystic fibrosis or wound infection.¹⁶⁶</p>	
Clinically significance	<p>The Immunocompromised individual is possible that will be infected by <i>P. aeruginosa</i>. It is one of the main leading causes (18%–20%) of nosocomial lung infections. Chronic obstructive pulmonary disease patients are also frequently colonized in their lungs with <i>P. aeruginosa</i> and present diverse symptoms ranging from mild bronchitis to pneumonia with sepsis.¹⁶⁷</p>	
Host defenses	<p>Despite innate and adaptive immune responses upon infection, <i>P. aeruginosa</i> is capable of efficiently escaping host defenses, but the underlying immune mechanisms remain poorly understood.¹⁶⁸</p>	

Table 5. Short characterization and description of *Pseudomona aeruginosa*. Image and text adapted from reference ¹⁶⁴⁻¹⁶⁸ and <http://beforeitsnews.com/health/2012/08/is-this-the-cause-of-all-inflammation-allergies-and-respiratory-infections-2445282.html>.

2.2.8. BIOLOGICAL TARGETS

Biological targets or recognition elements are molecules that have the ability of binding highly specific to concrete targets through molecular recognition. Nature offers a large variety of organic molecules of different composition, size and complexity that serve to provide structure and function to biological process and organisms.¹⁶⁹ Conjugation of inorganic nanoparticles to biomolecules generates hybrid materials that can be used to let the nanoparticles interact specifically with biological targets (see **Figure 2.23**)¹⁷⁰. Nanoparticle-biomolecule conjugates bring together the unique properties and the ability of biomolecules for highly specific binding by molecular recognition. The biological targets used in this thesis are further discussed.¹⁷¹

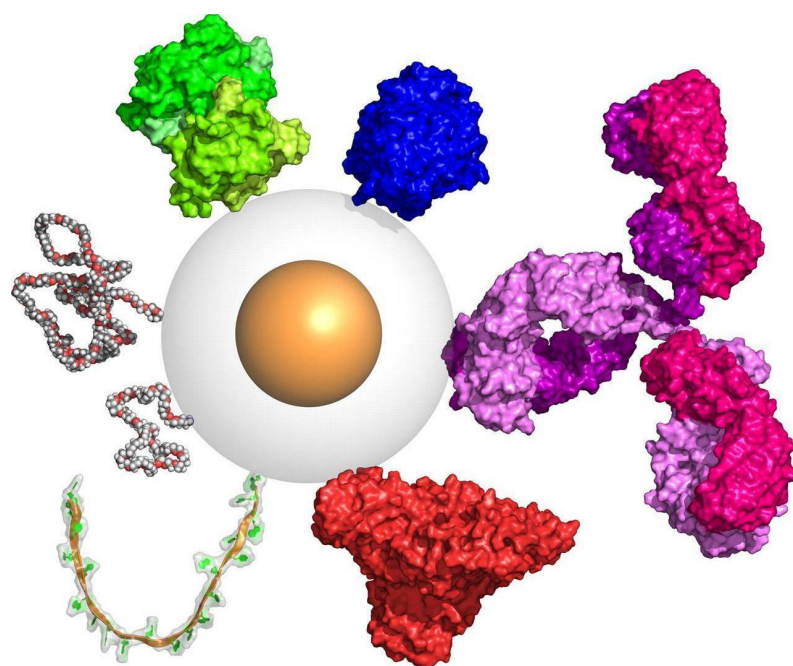


Figure 2.23. Relative size of nanoparticles and biomolecules, drawn to scale. Schematic representation of a nanoparticle with 5nm core diameter, 10nm shell diameter, with PEG molecules of 2000 and 5000g mol^{-1} (on the left, light grey), streptavidin (green), transferrin (blue), antibody (IgG, purple), albumin (red), single-stranded DNA (20mer, cartoon and space filling). Proteins are crystal structures taken from the Protein Data Bank (<http://www.rcsb.org>) and displayed as surfaces; PEG and DNA have been modelled from their chemical structure and space filling.¹⁷⁰

2.2.8.1. Antibody

Antibodies or immunoglobulins (Ig), are proteins that interact specifically with antigenic determinants (epitopes). They are found in serum and other body fluids. Serum containing antigen-specific antibodies is called antiserum. Ig can be separated into five major classes on the basis of their physical, chemical, and immunological properties: IgG, IgA, IgM, IgD and IgE, see **Figure 2.24.**¹⁷²

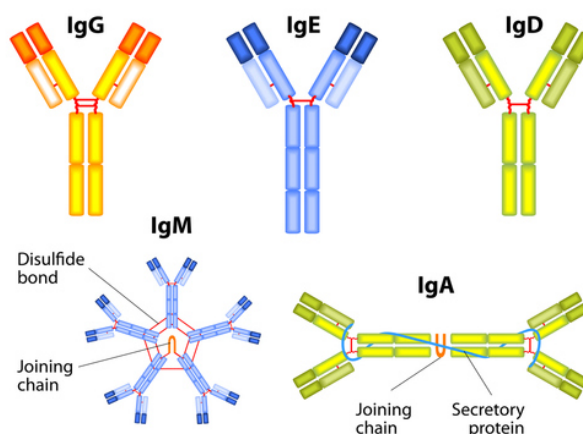


Figure 2.24. Schematic representation of an antibody molecule and its fragments. For detailed description, see text. Adapted from <https://www.labome.com/method/Mouse-Antibody.html>

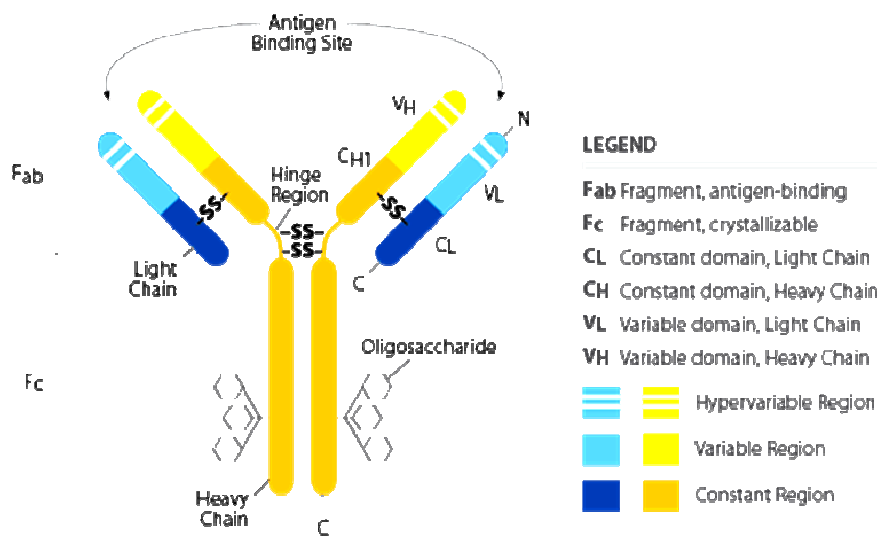


Figure 2.25. Schematic of a typical IgG. Adapted from <http://www.ebioscience.com/knowledge-center/antigen/immunoglobulin/structure.htm>

An antibody has a molecular weight of about 150 kDa, it contains two couples of polypeptide chains in a Y-shaped structure.¹⁷³ From top to bottom, the molecule measures about 10 nm¹⁷⁴ and the two arms are about 15 nm apart.¹⁷⁵ As is shown in **Figure 2.25**, each couple contains a heavy and light chain. The two heavy chains (blue) are linked by disulfide bonds and have a molecular weight of 50 kDa, the light chains (orange) of 25 kDa.¹⁷⁶ The structure of IgG molecule comprises two types of fragments, Fab and Fc. The Fab (fragment antigen binding) is used for binding specific antigens and contains two identical Fab fragments, which are held together by disulfide linkages in the hinge (H) region. A Fab fragment consists of the heavy (H) and light (L) variable (V) chains (VH and VL) and the constant (CH 1 and CL) chains. Other segments are the Fv (variable fragment) consisting of the VH and VL chains. The Fc (fragment, crystallizable) contains antibody-effector functions.¹⁷⁷⁻¹⁷⁹ These are, for instance, complement activation, cell membrane receptor interaction and transplacental transfer.¹⁸⁰

2.2.8.2. Antibody-Antigen-Interaction

In immunology an antigen is defined as a substance to which a specific antibody binds with a dedicated affinity. Antigens are in the majority of cases proteins or polysaccharides.¹⁸¹ The antigen-binding sites of all antibodies are formed by cooperative interaction between the variable domains of both, heavy and light chains.¹⁷⁷ The variable regions of the V subunits (VL and VH) form connecting segments, which occur in spatial proximity in the three dimensional structure. The specificity and affinity of antigen-binding-sites are determined by the sequence of these variable regions.¹⁷⁶

The interacting variable domains form a receptor that binds the antigen strongly but non-covalently. An antibody reacts only with subdomains of this antigen – the epitopes. Natural occurring antigens are mostly multivalent, i.e. they have multiple epitopes. An antigen-antibody reaction is similar to a ligand-receptor- or enzyme-

substrate-bond. The effective forces are steric complementarity, hydrogen bonds, van der Waals forces and hydrophobic interactions. The measurable strength of antibody-antigen-bindings is called binding affinity. A high-affinity antibody binds tightly to its antigen. The production of antibodies by organism is a complex process and the main function of the humoral immune system.

2.2.8.3. Aptamer

During the 1980's, studies into the replication of HIV-1 and adenoviruses revealed short regulatory RNA sequences that interacted with specific proteins. These studies revealed that short sequences of nucleic acids could interact with and affect the function of proteins. In 1990, the first organic aptamers were independently produced by two different groups,¹⁸² and Turk and Gold.¹⁸³ Ellington and Szostak coined and defined the term aptamer, a short sequence of RNA or single-stranded DNA (ssDNA) selective to a target molecule. They selected RNA aptamers from a pool of 1013 unique sequences towards two chemically similar dyes. Although the dyes were similar in structure, they found that the sequences were specific towards the dye they selected and did not cross react. It was therefore demonstrated that aptamers were able to differentiate between similar targets.¹⁸² During Tuerk and Gold's study, RNA aptamers were selected from a pool of 65,000 unique sequences derived from a wild-type sequence already known to interact with the target. It was noted that selected sequences were structurally similar to the wild-type and the synthetic aptamers disassociation constant (Kd) was similar to the wild-type. As well as showing aptamers selected synthetically were just as good as those selected by nature, Tuerk and Gold pioneered the simple methodology which can be applied to select specific aptamers to a target. They coined this process Systematic Evolution of Ligands by Exponential Enrichment (SELEX).¹⁸³ It is important to say that aptamers have the ability to distinguish between proteins that are 96% similar and this allows for

aptamers to be selected towards analogous proteins with high selectivity and affinity.

2.2.8.4. Identification of aptamers by SELEX

SELEX is the basic process used to identify functional aptamers to an employed target.¹⁸³ During SELEX, a starting pool of 10¹⁵ unique oligonucleotides is amplified and incubated with a counter selection, which is analogous to the target. Unbound sequences are then exposed to the target of choice.¹⁸⁴ Aptamers bound to the target are eluted and amplified via polymerase chain reaction (PCR), utilising constant regions flanking either side of the randomised sequence. The amplified aptamers are then purified and concentrated in-order to control the reaction volume for the following round of selection. A summary of SELEX can be seen in **Figure 2.26**.

SELEX is produced in iterative cycles to evolve the starting naive library in to a pool of aptamers selective for the desired target. As rounds are produced, the competition for the epitope increases, however conditions can be made more stringent which impacts the aptamer affinity and K_d for the target. Over the last 20 years, the original SELEX process has been modified and updated to produce more than 25 different variations of the method.¹⁸⁵ Whilst the basic foundations of selection, elution, amplification and purification have stayed consistent, updated and less laborious technologies have been introduced producing aptamers of higher quality with better functionality.

2.2.8.5. Aptamers vs antibodies

In comparison to antibodies, aptamers are relatively small and are able to penetrate the cell once bound to the target present on the cell surface, which would improve delivery of chemotherapeutic payloads. Whilst antibodies are the

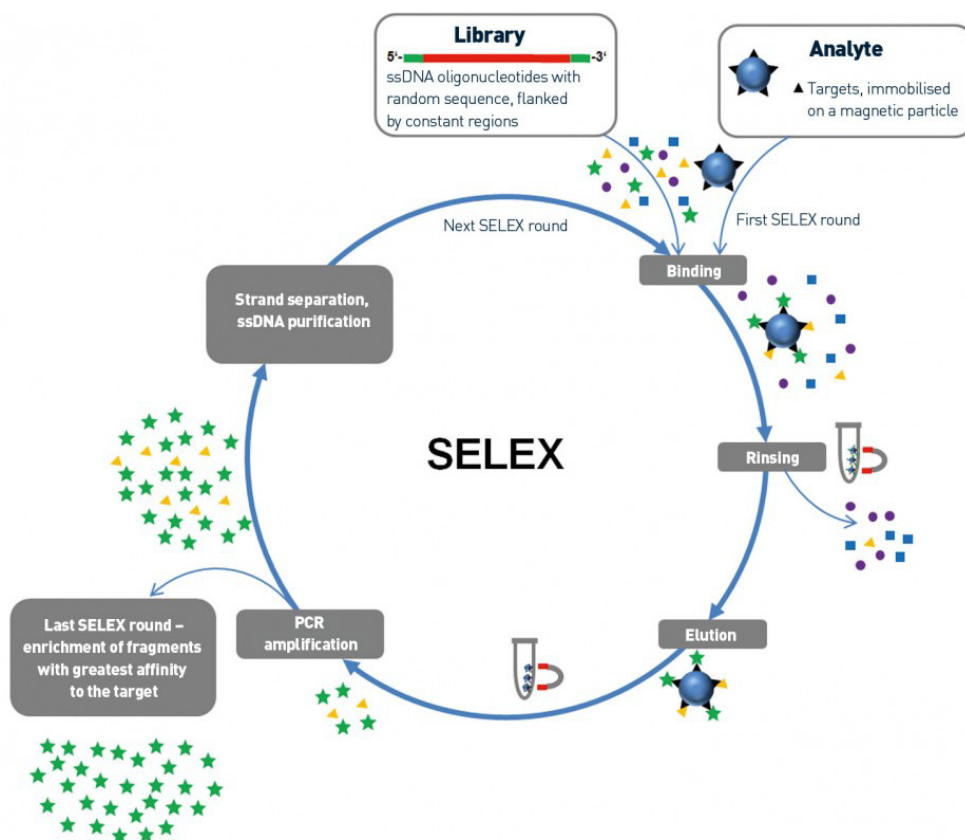


Figure 2.26. Selex method. Systematic Evolution of Ligands by Exponential Enrichment (SELEX). A nucleic library is incubated and filtered using a negative control and a positive selection. The aptamers eluted from the positive selection are amplified, concentrated and are used for further rounds of SELEX selection until a minority emerge. Figure adapted from Sefah et al.¹⁸⁶

commercially established targeting ligand, aptamers are identified through the *in vitro* process of SELEX and do not need the use of animals. As specific aptamers are isolated *in vitro*, the process can be controlled and changed to suit the application for which it is meant for. Aptamers, unlike antibodies, are able to be counter selected against a compound that is analogous to the target.¹⁸⁶ This reduces the chances of the aptamer cross reacting and increases specificity to the target of choice.

Aptamers are the rivals of Antibodies as they are stable, easy to develop and functionalized. More detail about aptamer advantages over antibody is given in **Table 6**.

	Aptamers	Antibodies
1	Binding affinity (KD) usually ranges from nanomolar to picomolar	Binding affinity (kD) in low nanomolar to picomolar range
2	Aptamer selection is a chemical process carried out in vitro and can therefore target any protein	Antibody generation requires a biological system, therefore difficult to raise antibodies to toxins (not tolerated by animal) or non-immunogenic targets
3	Can select for ligands under a variety of conditions for in vitro diagnostic	Limited to physiologic conditions for optimizing antibodies for diagnostics
4	Aptamer selection is an iterative process and usually requires 5-10 rounds and even more in some cases (varied from target to target)	Screening of monoclonal antibodies is a time-consuming and expensive
5	Uniform activity regardless of batch synthesis	Activity of antibodies varies from batch to batch
6	Pharmacokinetic parameters can be changed on demand	Difficult to modify pharmacokinetic parameters
7	Investigator determines target site of protein	Immune system determines target site of protein
8	Wide variety of chemical modifications to molecule for diverse functions (Fluor and biotin labeling etc.)	Limited modifications of molecule
9	Return to original conformation after temperature insult	Temperature sensitive and undergo irreversible denaturation
10	Unlimited shelf-life	Limited shelf-life
11	No evidence of immunogenicity	Significant immunogenicity
12	Cross-reactive compounds can be isolated through SELEX strategy	No method for isolating cross-reactive compound
13	Aptamer-specific anti-toxic can be developed to reverse the inhibitory activity of the drug	No rational method to reverse molecules

Table 6. Aptamer advantages vs antibodies.¹⁸⁷

3

Multiplex bacteria quantification in blood samples

Multiplex bacteria quantification in blood samples

3.1. INTRODUCTION

Septicemia affects nearly 20 million people per year with a mortality rate of 30–40%.^{188,189} These patients require intensive care with associated high costs, which impose significant health-care, economic, and social burdens. In particular, each septic patient in the United States incurs costs of approximately \$25,000 during hospitalization, totalling a nationwide annual bill in excess of \$17bn.¹⁸⁹ The time to initiation of effective antimicrobial therapy is known to be the single strongest predictor of outcome, as every hour delay in its administration increases by 8% the risk of death.^{4,5} Besides the obvious economic benefits, the development of fast, accurate, and inexpensive diagnostic methods thus appears as a major goal for alleviating human pain. Microbial culture remains the most widespread technique for identifying the infectious agent, but unfortunately it requires 24-72 hours to provide a conclusive diagnosis for common infections.¹⁹⁰ Understandably, a large deal of work has been devoted over the last three decades to developing alternative methods for fast identification of bacteria in suspected patients.¹⁹¹ These methods include immunology-based approaches (e.g., enzyme-linked immunosorbent assay (ELISA), as well as fluorescence and radio immunoassays),¹⁹² nucleic acid identification (e.g., polymerase chain reaction, PCR),¹⁹³ and, lately, spectrometry-based procedures (e.g., matrix-assisted laser desorption/ionization-time-of-flight, MALDI-TOF, mass spectrometry).¹⁹⁴ Although generally faster than just sequential microbial culture, these techniques still require hours to days, depending on the pathogen. Additionally, immunological and nucleic-acid tests are expensive (around \$200 each) and monoplex (one test per target microorganism), while MALDI-TOF still relies on microbial culture to isolate pure colonies. As a

consequence, a cocktail of broad-spectrum antibiotics is generally recommended to cover all potential pathogens until obtaining a conclusive identification. Apart from its inherent cost and adverse health effects, this indiscriminate use of antibiotics induces bacterial resistance,¹⁹⁵ a growing problem of modern pharmacopeia.¹⁹⁶ Despite recent advances in fast recognition of bacterial resistance, society urges for the development of new diagnostic systems capable of providing fast, accurate, inexpensive, and if possible multiplexed identification of infectious agents in body fluids that will yield a rapid and guided treatment that avoids the use of spurious drugs.^{197,198} Recent advances in nanoscience, spectroscopy, magnetism, plasmonics, and microfluidics^{193,199-203} have generated great expectations for the development of new approaches to bacteria characterization²⁰⁴ and detection.^{71,205-209} Unfortunately, the methods so far proposed are generally time consuming, capable of only exploring small sample volumes (~microliters) not relevant for clinical diagnosis of septicemia,^{200,210} working exclusively for one *a priori* selected pathogen,^{71,205-211} not truly multiplex,²⁰⁵ requiring from multiple external labels,²⁰⁹ or relying on additional steps to record a suitable signal for identification.^{71,200} Here, we report a microorganism optical detection system (MODS) and demonstrate exhaustive pathogen identification through fast screening of large body-fluid volumes (milliliters of blood) for bacterial content, down to the single colony forming unit detection, as required by standard medical practice for the analysis of biological samples.¹⁹⁰ Specifically, we achieve detection and quantification of bacteria in real time and in a multiplexed manner.

4.2. EXPERIMENTAL SECTION

3.2.1. MATERIALS

Silver nitrate (99.99%, AgNO₃), trisodium citrate dihydrate (≥99.5%), L-ascorbic acid (≥99.0%), magnesium sulfate (≥99.0%, MgSO₄), ethanol (99.5%, EtOH), 11-mercaptoundecanoic acid (95%, MUA), 4-mercaptobenzoic acid (99%, 4MBA) 2-mercaptobenzoic acid (97%, 2MBA), 3,4-difluorobenzenethiol (96%, DFBT), 2-(trifluoromethyl)benzenethiol (96%, TFMBT), 1-(4-hydroxyphenyl)-1H-tetrazole-5-thiol (97%, HPTZT), bovine serum albumin (≥98.0% , BSA), *N*-(3-dimethylaminopropyl)-*N'*-ethylcarbodiimide hydrochloride (BioXtra, EDC), sodium chloride (BioXtra, ≥99.5%, NaCl), Dulbecco's phosphate buffered saline (D8537, DPBS), and human blood (BCR634 FLUKA) were purchased from Sigma-Aldrich. All reactants were used without further purification. MilliQ water (18 MΩ cm⁻¹) was used in all aqueous solutions. All the glassware and magnetic stirrers were cleaned with aqua regia and with potassium hydroxide solution in isopropanol/water before all the experiments.

3.2.2. ANTIBODIES AND BACTERIA

Antibodies selected for this study are the same that those used in the clinical practice for the immunological methods. *Escherichia coli* (ab30522, *E. coli*) and *Streptococcus agalactiae* (ab41203, *S. agalactiae*) antibodies (Ab) were purchased from Abcam. *Pseudomonas aeruginosa* (MA1-83430, *P. aeruginosa*) and *Staphylococcus aureus* (MA1-83467, *S. aureus*) antibodies were purchased from Life Technologies. Enriched thioglycollate medium (221742, BBL) was purchased from BD (Becton, Dickinson and Company) and Columbia agar + 5% sheep blood plates (43 041) were purchased from bioMérieux. Bacterial samples were obtained from the Department of Clinical Microbiology, Hospital Clinic i Provincial, School of Medicine, University of Barcelona, Barcelona, Spain.

3.2.3. SYNTHESIS OF CITRATE-STABILIZED SPHERICAL SILVER NANOPARTICLES

Spherical silver nanoparticles (Ag NPs) of approximately 62 nm in diameter were produced by a combination of previously reported approaches.^{55,212-214} Briefly, 250 mL of MilliQ water were heated under vigorous stirring. A condenser was used to prevent solvent evaporation. Next, aqueous solutions of trisodium citrate (3.41 mL, 0.1 M) and ascorbic acid (0.25 mL, 0.1 M) were consecutively added into the boiling water. After 1 min, a premixed aqueous solution containing AgNO₃ (0.744 mL, 0.1 M) and MgSO₄ (0.56 mL 0.1 M), which was previously incubated at room temperature for 5 min, was rapidly injected into the reaction vessel under vigorous stirring. The color of the solution quickly changed from colorless to yellow and then gradually into dark orange. Boiling was continued for 1 h under stirring to ensure the completeness of the reaction. The silver concentration of the synthesized particles was 2×10^{-4} M (i.e., $\sim 10^{10}$ NPs per mL).

3.2.4. MUA FUNCTIONALIZATION AND CODIFICATION OF Ag NPs

After NP synthesis, MUA was used in order both to provide colloidal stability to the Ag NPs during the encoding process and later on to use the carboxylic functionality for the coupling of the antibodies. Specifically, five aliquots (25 mL each) of the synthesized Ag NPs were cleaned by centrifugation (5400 rpm, 30 min) and redispersed via sonication (during 5 min) in a solution containing MilliQ water (3.27 mL) and EtOH (21.67 mL). Subsequently, the Ag NPs were functionalized with a small amount of MUA ($2.4 \text{ molecules nm}^{-2}$) by rapidly adding a solution containing MUA (24.76 μL , 1.0×10^{-3} M in EtOH) and NH₄OH (30 μL , 29% aqueous solution) to each aliquot under vigorous stirring. Agitation was continued for 28 h to assure the complete MUA functionalization on the silver surface. Finally, the MUA functionalized Ag NPs aliquots were encoded with five different Raman labels (1.6 molecules per nm² of 4MBA, 2MBA, DFBT, TFMBT, and HPTZT, respectively). To this

end, 16.51 μL of a 10^{-3} M stock solution of the five different SERS codes were added to the aliquots under strong magnetic stirring. Once again, stirring was continued for another 28 h. The encoded Ag NPs solutions were then centrifuged and redispersed twice in MilliQ water to remove the excess of NH_4OH , EtOH, and any unreacted Raman label prior to antibody coupling. The concentration of NPs was calculated for each aliquot using the Lambert-Beer law and an extinction coefficient of $7.79 \times 10^{10} \text{ M}^{-1} \text{ cm}^{-1}$, derived from literature²¹⁵ and adjusted to 0.14 nM for all of them.

Additionally, another aliquot (25 mL) of the synthesized Ag NPs was cleaned by centrifugation (5400 rpm, 30 min) and redispersed in MilliQ water (25 mL). The Ag NPs were then functionalized with MUA by adding, under vigorous stirring, 24.76 μL (1.0×10^{-3} M in EtOH). Agitation was continued for 28 h to ensure the complete MUA functionalization on the silver surface. Finally, Ag NPs were further modified with BSA (41.26 μL , 1.0×10^{-3} M in MilliQ water) under magnetic stirring for 24 h, followed by one cleaning step centrifugation to remove excess of BSA and any unreacted MUA molecules (5400 rpm, 30 min, redispersed in MilliQ water). The concentration of these NPs was calculated and adjusted to 0.034 nM.

3.2.5. ANTIBODY CONJUGATION TO Ag NPs

200 μL of DPBS and EDC (39.2 μL , 250 nM in DPBS) were added over each codified Ag NPs solution (1 mL, 0.14 nM, Raman labels: 4MBA, 2MBA, DFBT, TFMBT, and HPTZT), the mixtures were shaken for 5 min at room temperature, and then the antibodies solutions were added (1.46 μL , ~ 6.67 μM , *E. coli*, BSA, *P. aeruginosa*, *S. agalactiae*, and *S. aureus*, respectively). The resulting mixtures were first shaken for 2 h at room temperature, then cleaned twice by centrifugation to remove the excess of unreacted EDC and antibodies (3000 rpm, 10 min), and redispersed in DPBS/MilliQ water (1:3). The concentration of each Ab-modified Ag NPs solution

was measured and adjusted to 0.14 nM. The resulting NP solutions were stored at 4 °C.

3.2.6. CHARACTERIZATION OF THE NANOPARTICLES

UV-Vis spectroscopy (Lambda 19, PerkinElmer) and transmission electron microscopy (TEM, JEOL JEM-1011 operating at 100 kV) were used to characterize the optical response, structure, and size of the nanoparticles during the functionalization process. To characterize the codification process, SERS spectra were collected in backscattering geometry with a Renishaw Invia Reflex system equipped with a 2D-CCD detector. The spectrograph used a high resolution grating (1200 g cm^{-1}) with additional band-pass filter optics. A 785 nm diode laser was focused onto the colloidal solution ($[\text{Ag}^0] = 0.1 \text{ mM}$) by a long-working distance objective (0.17 NA, working distance 30 mm). The spectra were acquired with an exposure time of 1 s (depending on Raman intensity saturation) and a laser power at the sample of ca. 300 mW.

3.2.7. MICROFLUIDIC DEVICE MANUFACTURING

The microfluidic device was fabricated with polydimethylsiloxane (PDMS) by replica molding using an aluminum master mold. PDMS (Sylgard 184, Dow Corning) was prepared by mixing pre-polymer and curing agent at a standard 10:1 ratio. The mixture was poured onto the mold, degassed in vacuum, and cured at 80 °C. After one hour, PDMS was peeled off the mold and the fluidic access holes (inlet and outlet) were punched. The final device was obtained by bonding the PDMS layer to a slide cover (130-170 μm -thick) after oxygen plasma treatment (100 W, 3% O_2 , 0.2 4MBAr, 40 s) (Plasma Flecto 10, Plasma technology GmbH). The microfluidic device consisted of a single channel with variable dimensions. The inlet channel had a width of 200 μm and a depth of 100 μm , which was enlarged to 400 μm -width and 2 mm-depth in the outlet channel (i.e., the optical detection section). A detailed

schema showing the dimension of the detection region in the chipset can be seen in Figure 3.1.

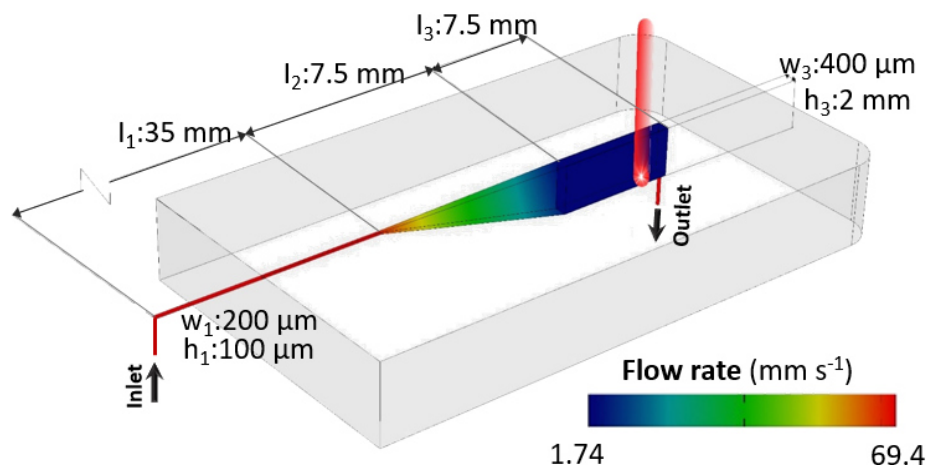


Figure 3.1. Detailed schematics of the detection region in the millifluidic chipset that is shown in Figure 3.8. The channel is divided in three sections: an initial narrow section used to increase pressure and reduce the flow to finely control the fluid discharge with the micropump; a second segment of increasing larger section; and, a third wide segment (0.4 mm width, 2 mm depth), with suitable dimensions to continuously screen the sample at flow rates of 1.74 mm s^{-1} , at a spectral capture rate of 1.83 mm s^{-1} .

3.2.8. BACTERIAL SAMPLES

Bacteria were inoculated in enriched thioglycollate medium (BBL), incubated at 37 °C for 18 h and then diluted with saline solution (NaCl 0.9%). Next, the required amount of bacterial solution, to reach the desired final concentration, was added into the corresponding fluid, that is, saline solution or human blood containing Ab-modified Ag NPs (1 μL of each encoded particle per mL of sample) and twice as many serum-albumin protected unlabeled AgNPs as the total amount of codified AgNPs. Bacterial culture is the gold standard for bacterial quantification in environmental and clinical microbiology. Essentially, it is based in the spread of a known volume of the target liquid onto a blood agar plate. After some time (24-

48h for most bacteria) the single colony forming units (CFUs), dispersed in the liquid, multiply in the blood agar plate to form colonies that can be counted visually. Each colony is equivalent to a single CFU in the initial bacterial solution.^{216,217} Thus, to verify the final bacterial concentration per sample, several aliquots of each solution were spread in agar-blood plates and incubated for 24-48 h at 37 °C. After this time, the number of colonies in each plate was counted in order to calculate their concentration of CFU per mL. To further corroborate the interaction between the Ab-modified Ag NPs with the corresponding bacteria, equal volumes of Ag NPs (0.14 nM) and bacterial solution ($\sim 10^6$ CFU mL⁻¹) were mixed, and incubated for 15 min at 37 °C. Small fractions (10 μ L) of these mixtures were deposited on carbon coated copper grids and the samples were allowed to dry before performing TEM analysis.

3.2.9. MEASUREMENT SYSTEM SETUP

The PDMS microfluidic device was integrated in a stage comprising an inlet vessel with the precharged NPs where the sample is placed, a micropump (mp6, Bartels) and an outlet vessel. All these elements were connected with polytetrafluoroethylene (PTFE) 0.8 mm wide tubes. The flow rate was controlled with a Bartels extend Micropump Controller and set to 1.74 mm s⁻¹. SERS measurements were collected with a Renishaw Invia Reflex. The laser (785 nm, 300 mW) was focused with a macro-objective (6 mm aperture and -18 mm focal distance), providing an efficient spot of 0.5 mm. The scan collection time was set to 270 ms per spectrum, providing an acquisition speed of 1.85 mm s⁻¹, which results in an evaluation speed of 13.3 min per mL of sample, during which 3000 scans are obtained. Data deconvolution was carried out by principal component analysis and classical least squares using the Wire 4.1 software from Renishaw.

3.2.10. ELECTROMAGNETIC SIMULATIONS

The simulation of the electric near-field and SERS enhancements were carried out with a fully converged multiple elastic scattering of multipolar expansions (MESME) method²¹⁸ or using the boundary-element method (BEM)²¹⁹ for bacteria covered with NPs.

3.3. RESULTS AND DISCUSSION

3.3.1. DIMERS ELECTROMAGNETIC SIMULATIONS

The simulations shown in **Figure 3.2 – 3.4** were carried out with a fully converged multiple elastic scattering of multipolar expansions (MESME) method.²¹⁸ In particular, the SERS enhancement at a given position was approximated as the product of the field enhancements calculated at that position for wavelengths corresponding to the incident and emitted light. Each of these field enhancements was averaged over incidence light directions and polarizations before multiplying them to yield the SERS enhancement.

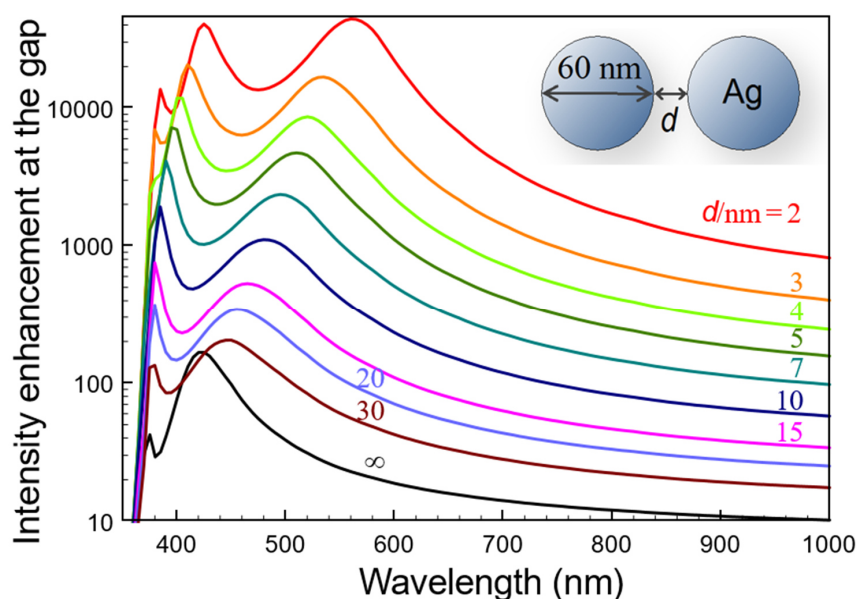


Figure 3.2. Electric field intensity enhancement $|E/E_{ext}|^2$ generated by a dimer of silver nanoparticles (60 nm diameter) embedded in water ($\epsilon = 1.77$). The intensity is calculated at a

distance of 1 nm from the surface of one of the particles in the gap region. Different surface-to-surface separations d are considered (see labels). A significant intensity enhancement of several orders of magnitude is still observable at the off-resonance light wavelength of 785 nm used throughout this work.

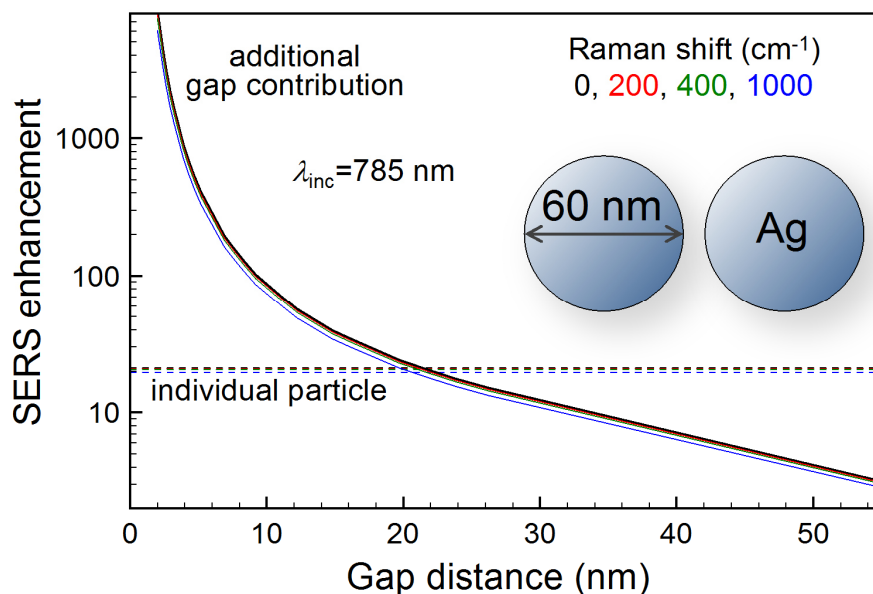


Figure 3.3. SERS enhancement produced by Ag NP dimers in aqueous solution. We show the increase in SERS enhancement factor due to inter-particle interaction (solid curves) compared with the values for individual particles (dashed lines) as a function of gap distance. This quantity is averaged over randomly distributed sampling molecules placed 1 nm outside the metal surface. An average over light polarizations and incidence directions is also carried out. The different Raman shifts under consideration (see labels) produce similar results because the incident light wavelength (785 nm) is not resonant with the particle plasmons (see **Figure 3.2**).

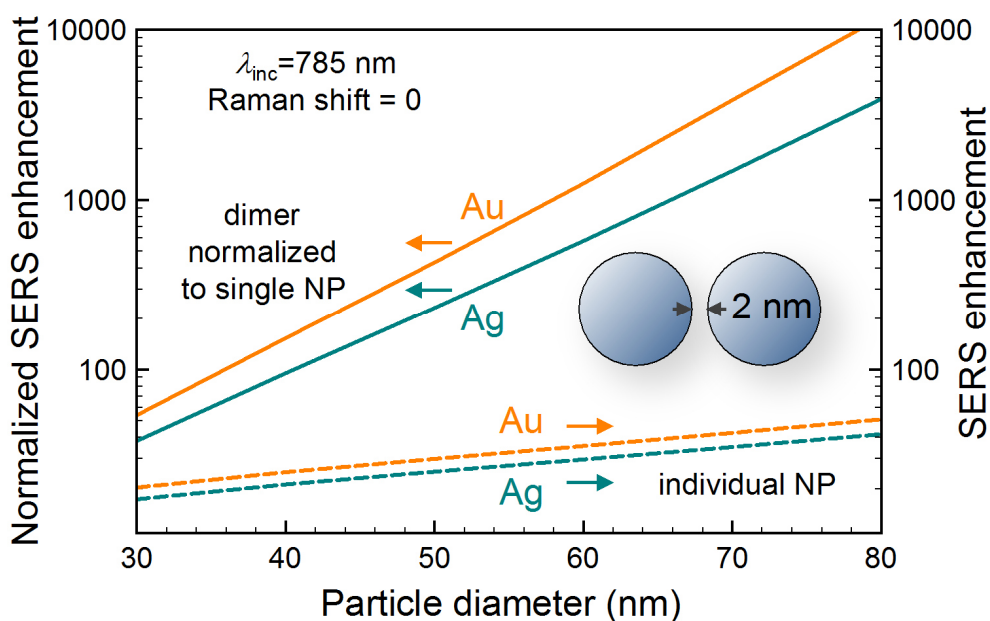


Figure 3.4. SERS enhancement for Au and Ag dimers of different size. We show the SERS enhancement averaged over molecule positions (1 nm outside the metal), light polarizations, and directions of incidence for gold and silver dimers as a function of particle size. The gap distance and the light wavelength are both fixed to 2 nm and 785 nm, respectively. The solid curves are the results for dimers normalized to the average over individual NPs (left vertical axis). The dashed curves show the absolute averaged enhancement for individual NPs (right vertical axis).

3.3.2. SIMULATION OF PARTICLE ATTACHMENT

We simulated the process of NP attachment on the membrane of the targeted bacteria by implementing a Monte Carlo method in which particles landed on the microbe surface at random spots, following either randomly oriented trajectories (Figure 3.19 B, and solid curves in Figure 3.5 left and Figure 3.16) or approaching it along the surface normal (dashed curves in Figure 3.5 left and Figure 3.16). Particles colliding with any previously stuck particle were disregarded. The probability distribution of random-incidence orientations was taken to be proportional to $\sin\theta\cos\theta$ as a function of incidence angle θ relative to the surface normal, where the \cos function reflects the average particle flux for a surface tilted by that angle, whereas the \sin function comes from the Jacobian of spherical coordinates. Statistical analysis of the particle positions produced by these

simulations allowed us to obtain the time-dependent particle density (**Figure 3.19 B**) and the distribution of inter-particle gap distances (**Figure 3.6**). Each of the results here presented was averaged over 10^5 simulation runs for a square membrane of large side compared with the particle diameter. Opposite sides of the square were identified (toroidal topology) to minimize edge effects. Convergence was achieved for a side length ~ 20 particle diameters.

In the resulting **Figure 3.5 left** and **Figure 3.6**, the time axis is expressed in units of the average interval between collisions over an area equal to the unit cell of a closed-packed arrangement of the NPs (i.e., a time unit is defined as the average time needed to have one particle colliding for each element of area equal to $3^{1/2}D^2/2$, where $D=60$ nm is the particle diameter). For the sake of readability, the time in **Figure 3.9 B** is instead normalized to the average interval separating consecutive particle collisions on an area of $1 \mu\text{m}^2$. Finally, for the comparison with experiment in **Figure 3.9 A**, the theory curve is scaled to have 17.3 collisions per second per μm^2 , as predicted by the impingement rate equation.²²⁰

$$n \sqrt{\frac{k_B T}{2\pi M}}$$

Where $n=10^9$ NP/mL is the particle density (notice that the NP dispersion used to study the kinetics in **Figure 3.19 A** was diluted with respect to the cocktail used for MODS analyses), $T=300$ K is the temperature, and $M=2.2 \times 10^{-18}$ kg is the NP mass corresponding to 60 nm silver spheres. Although this equation is a result of frictionless kinetic theory, we apply it here assuming that the collision rate is dictated by microscopic random displacements aimed by Brownian motion.

The field enhancement of **Figure 3.5** was obtained using the boundary-element method (BEM).²¹⁹ The dielectric functions of gold and silver used in these

simulations were taken from tabulated measurements.²²¹ The media inside and outside the bacteria were both assumed to have the permittivity of water ($\epsilon = 1.77$).

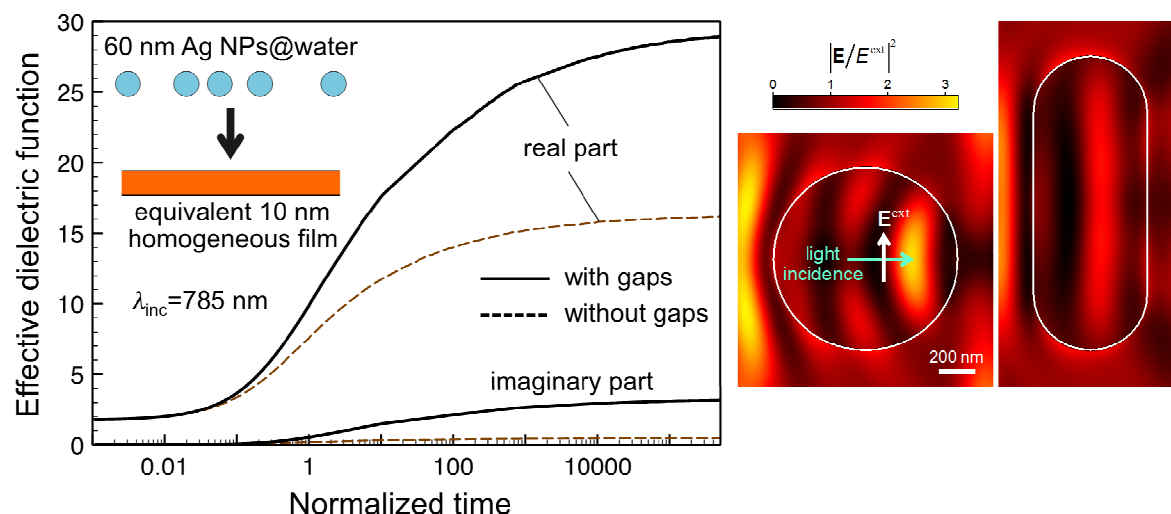


Figure 3.5. Near-field intensity in bacteria covered with nanoparticles. We assimilate the NP coating to a thin film with an effective dielectric function that is represented in the left plot. This dielectric function depends on the assumed film thickness (10 nm), but the calculated near field (right plot) is only mildly dependent on this parameter. The left plot shows that the dielectric function increases with the normalized time (see **Figure 3.6** for time normalization), as a result of the increase in particle density. Similar to the SERS enhancement (see **Figure 3.19 B** of the main paper), the gaps produce a large effect, creating additional polarization that further increases the dielectric function. The near-field intensity shown on the right density plots is calculated by replacing the NPs by an equivalent homogeneous film that is conformally covering sphere-like and rod-like microbes, respectively, with the media inside and outside the film both described as water ($\epsilon=1.77$). The light wavelength is 785 nm. Based on the results of the left plot, we model the coating as a 10 nm thick layer with permittivity equal to $28 + 3i$. The intensity is observed to undergo relatively weak variations due to the coating, and therefore, the bulk of the SERS enhancement is produced by hotspots, as shown in **Figure 3.19 C**.

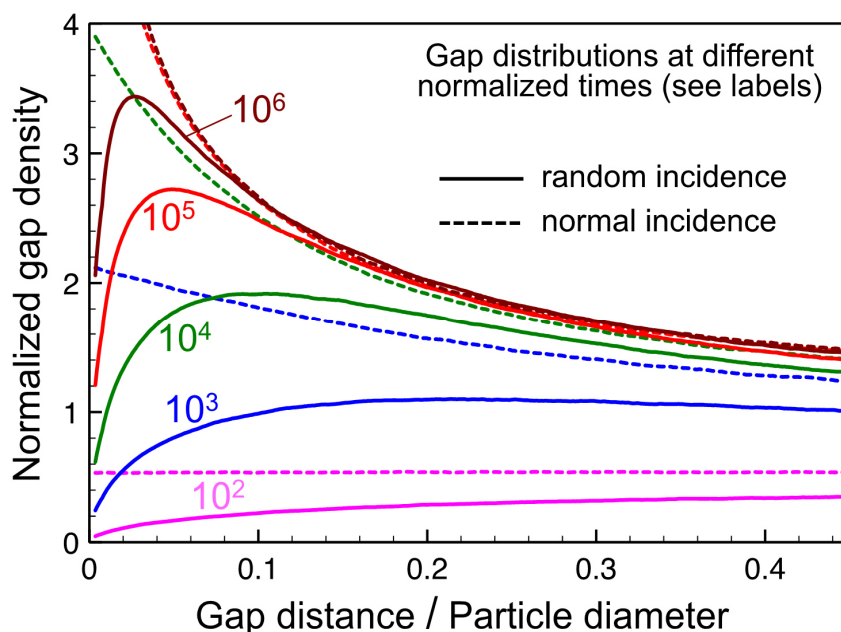


Figure 3.6. Simulated distribution of gap distances between NPs attached on the pathogen membrane at different normalized times (see labels), both under random (solid curves) or normal (dashed curves) incidence directions relative to the membrane surface. The gap density distribution is normalized to the maximum NP density at regular close-packed coverage and it is given per unit of gap-to-diameter ratio. A time unit is defined here as the interval over which the number of particles colliding with the surface is equal to the number of attached particles under close-packed coverage.

3.3.3. SIMULATION OF SERS ENHANCEMENT PRODUCED BY PARTICLE ATTACHMENT

We obtained the temporal evolution of the SERS signal (**Figure 3.19 B**) by combining the gap-mediated SERS enhancement (**Figure 3.3**) and the time-dependent particle (**Figure 3.19 B**) and gap (**Figure 3.6**) densities. The SERS enhancement was calculated from the weighted contributions of both the individual NPs (**Figure 3.3**, dashed lines) and the gaps formed between them (**Figure 3.3**, solid curves). Incidentally, multiple inter-particle interactions beyond dimers formed by nearest neighbors have a relatively weak effect (**Figure 3.19 C** and **Figure 3.5**), which should be further reduced when averaging over random NP

arrangements and light incidence directions and polarizations. Consequently, we approximated the SERS enhancement at the gaps by simulating isolated dimers (**Figure 3.3**). For simplicity, we considered a zero Raman shift in our simulations (i.e., we used the black solid curve of **Figure 3.3**). We found the effect of finite Raman shift to be marginal, as the particles were operating at an off-resonance wavelength ≥ 785 nm (see **Figure 3.2**). Incidentally, the SERS enhancement of **Figure 3.19 B** is normalized to the emission from an individual NP.

3.3.4. SIMULATION OF THE EFFECTIVE PERMITTIVITY OF THE NP COATING DESCRIBED AS A METAMATERIAL

In order to quickly assess the effect of the NP coating on the near-field at the large scale commensurate with the microbe, we assimilated the NPs to an equivalent homogeneous thin film with an effective dielectric function calculated in such a way that the film had the same normal-incidence reflection coefficient as a layer of randomly distributed particles (i.e., the layer was treated as a metamaterial). We estimated the effective dielectric function from the dipoles induced per gap and per particle, as obtained from electromagnetic simulations of the gap-size-dependent polarizability of NP dimers using MESME. The effective dielectric function was then expressed as $\epsilon + (4\pi / t) \beta$, where β is the sum of NP and gap polarizabilities normalized per film-surface area, t is the equivalent film thickness, and $\epsilon = 1.77$ is the permittivity of the surrounding medium (water). The dependence on the choice of t was found to be very mild, and actually, the results obtained for the near-field distribution calculated with $t=10$ nm and $t=20$ nm were nearly indistinguishable on the scale of **Figure 3.5 right**.

3.3.5. MICROORGANISM OPTICAL DETECTION SYSTEM (MODS)

Motivated by the need for an accessible, highly sensitive, and selective platform for the screening of pathogens in large samples of biological fluids (i.e., serum or blood), we have engineered a device as described in **Figure 3.7**. Our MODS device relies on the use of plasmonic nanoparticles (NPs) tagged with Raman-active molecules and functionalized with selective antibodies. In contrast to previous demonstrations of *in vivo* imaging using silica or polymer protected nanoparticles,²²² our plasmonic colloids are unprotected in order to facilitate their plasmonic interaction. For each targeted pathogen receptor, we prepare NPs (silver spheres, ~60 nm diameter) with a unique combination of Raman label and selective antibody. The NPs produce a relatively weak Raman signal when they are dispersed in a fluid. In contrast, the presence of one of the targeted pathogens triggers the accumulation of its partner NPs on the antigen-carrying membrane of the microorganism, rapidly reaching full random coverage.²²³ Multiple gaps between NPs are then formed, which act as optical hotspots in which Raman scattering is enhanced by several orders of magnitude relative to the same number of non-interacting NPs.^{56,224-226}

The resulting surface-enhanced Raman scattering (SERS)²²⁷ signal is sufficiently intense as to allow us to record pathogen-specific inelastic light spectra (**Figure 3.8 A**) from the NP-covered bacteria (**Figure 3.8 B**). By driving the sample through a millifluidic channel (0.4 mm x 2 mm section, aimed by a micropump, see **Figure 3.1** and **Figure 3.7**), where a backscattered detecting laser (785 nm) continuously monitors the liquid stream (one spectrum every 270 ms over an illuminated volume of ~0.32 μL), we successfully and simultaneously quantify multiple different types of bacteria at a pace of 13 minutes per mL of blood or serum. Importantly, this method can be readily scaled to cope with many more pathogens including viruses or eukaryotic

cells such as fungi or protozoa, in a single pass without increasing the sampling time, simply by preparing NPs functionalized with more combinations of Raman labels and selective antibodies or aptamers.

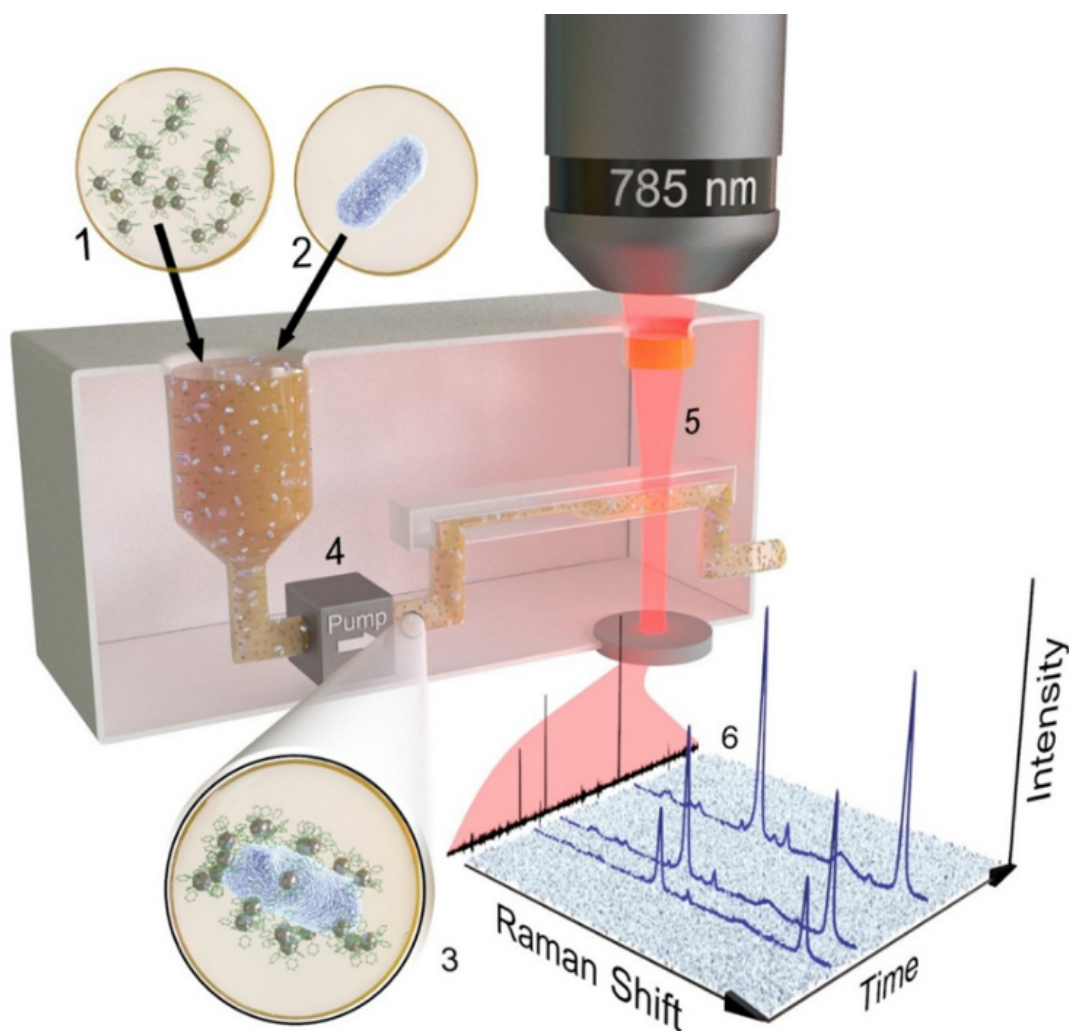


Figure 3.7. Conceptual view of the Microorganism optical detection system (MODS) and its relevant components. Silver nanoparticles (NPs) are separately labelled with different Raman-active molecules and functionalized with bacteria-selective antibodies (1). A nanoparticle dispersion is mixed in a vessel (3 mL) with the sample fluid, possibly infected (2). Several types of bacteria are targeted using NPs prepared with different specific combinations of Raman molecules and antibodies. The presence of one of these microorganisms induces aggregation of antibody-matching NPs on its membrane, rapidly evolving towards full random coverage (3). The mixture is

circulated through a millifluidic channel with a micropump (4) and passing through the focus of a 785 nm laser (5), which is in turn spectrally analysed to record the SERS signal generated by the Raman-active molecules (6). Targeted bacteria produce a large increase in SERS signal, whose spectral fingerprints allow us to identify the type of pathogen.

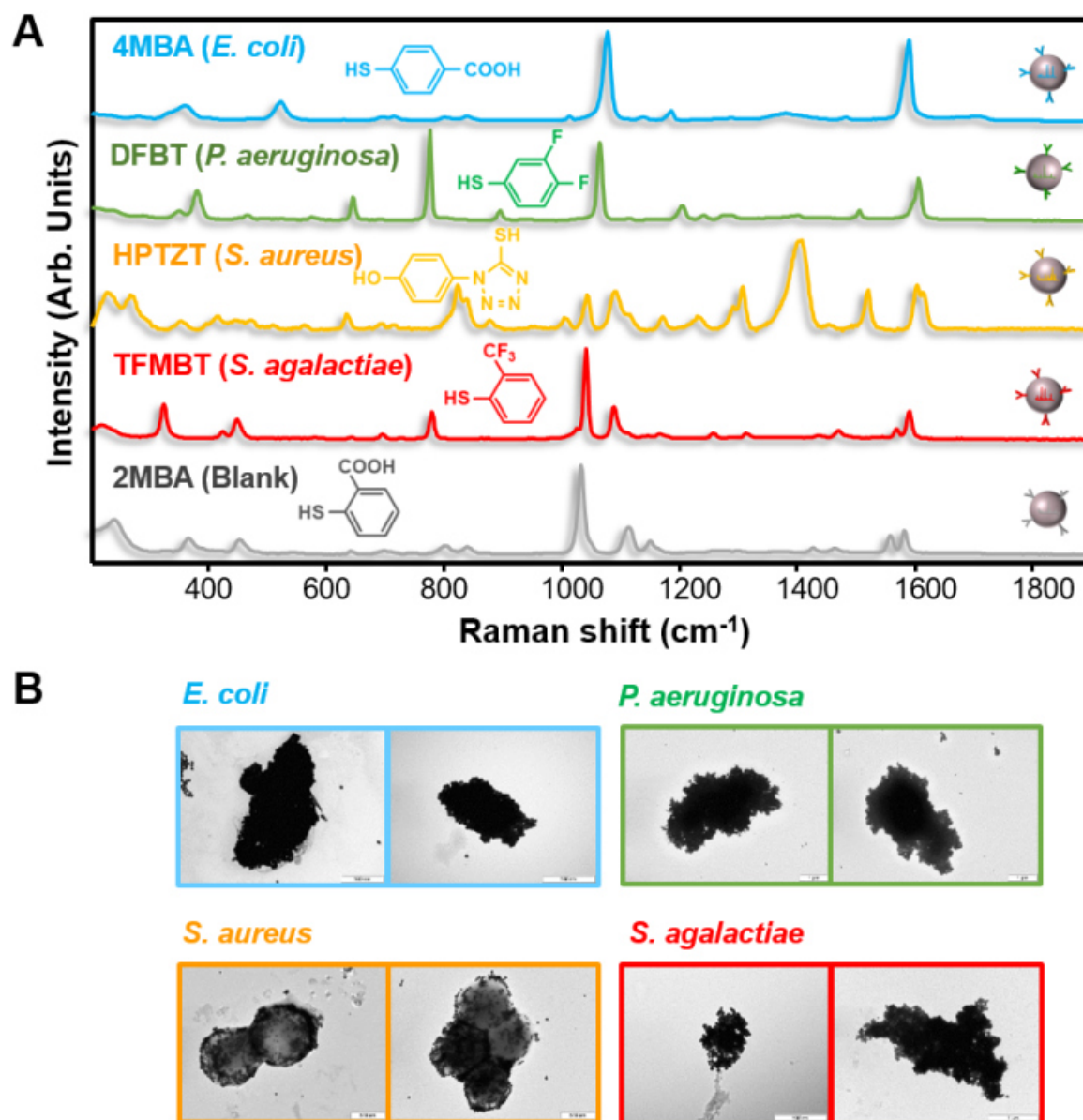


Figure 3.8. Encoded nanoparticles and their interaction with bacteria. (A) SERS spectra of the different coded particles here used for each targeted pathogen, along with their corresponding labelling molecules. (B) Transmission electron microscope images of the targeted bacteria (*E. coli*, *P. aeruginosa*, *S. aureus*, and *S. agalactiae*) coated with their respective matching NPs.

MODS DEMONSTRATION IN SERUM.

For demonstration of bacteria detection, we prepared five dispersions of coded NPs, each of them functionalized with a different aromatic thiol that yields a unique Raman spectrum (Figure 3.8 and Figure 3.9). The coded NPs were subsequently and separately functionalized with the corresponding membrane-selective antibody, at low concentration, for recognition of *E. coli* and *P. aeruginosa* (gram negative rod-like bacteria), as well as *S. aureus* and *S. agalactiae* (gram positive spheroidal coccus). The fifth NP dispersion was functionalized with serum albumin and used as a blank. All five NP dispersions were then mixed in the MODS vessel (Figure 3.7) at a concentration of $\sim 10^7$ NPs per mL per Raman code, which was found to be optimum for yielding fast NP-pathogen attachment with a minimum background SERS signal of unattached NPs (see Figure 3.10).

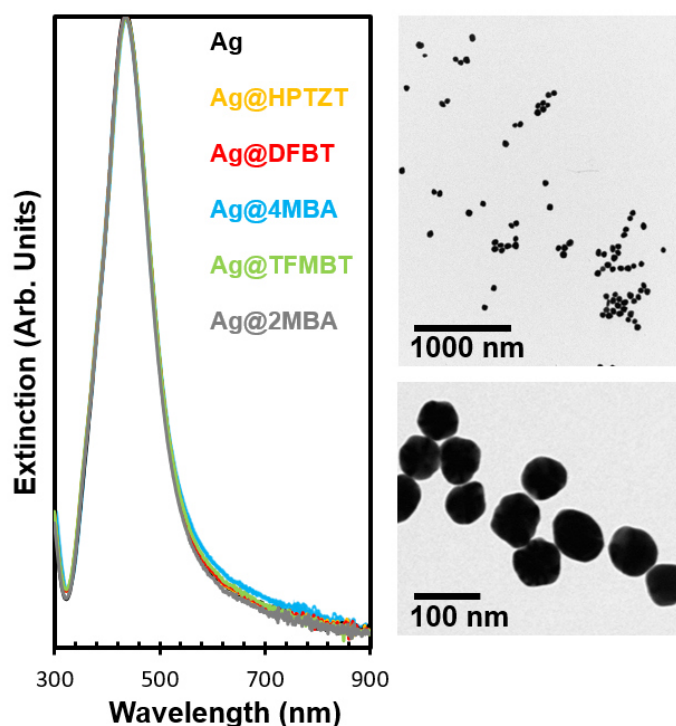


Figure 3.9. Left: Optical extinction of functionalized Ag NPs in aqueous solution, showing a prominent plasmon consistent with the nominal diameter of 62 nm, and indicating that the coating molecules have a minor effect on the optical response. Right: Representative TEM images of as prepared encoded nanoparticles.

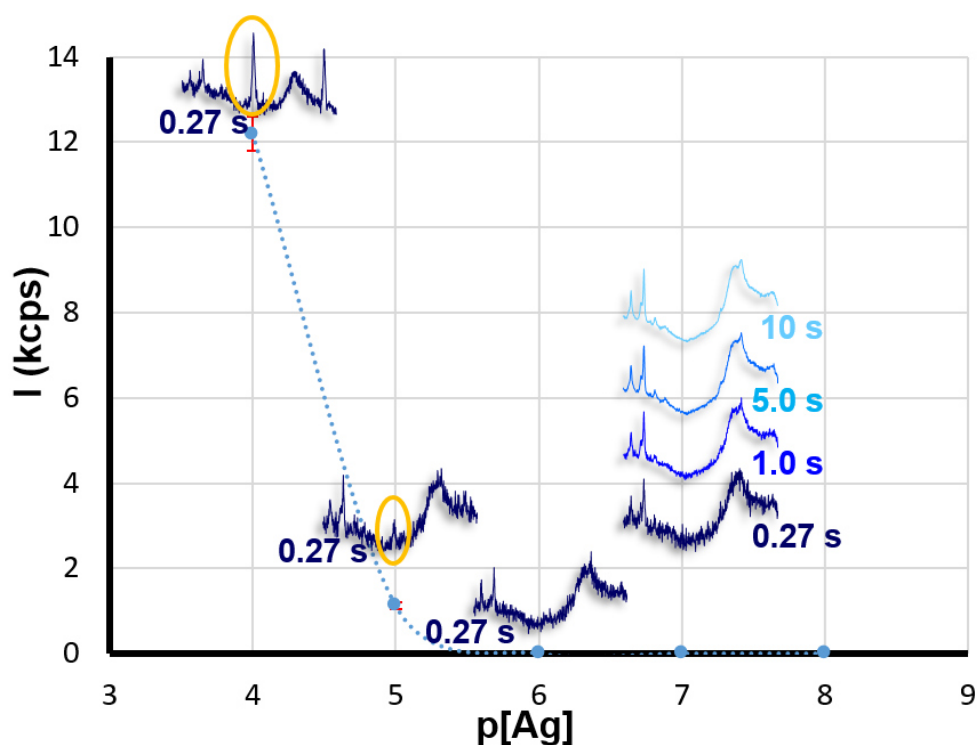


Figure 3.10. Optimization of the concentration of encoded NPs for reduction of background noise from the codes of dispersed NPs against the signal of decorated pathogens in the measurement area of the millifluidic chipset. We show SERS spectra of different dispersions of NPs arranged as a function of NP density (p is $-\log_{10}$ of the Ag molar concentration). A harmless, smooth, nearly constant background is produced by the chipset material. A SERS signal from the codes (circled features) can be clearly identified above 10^{-5} M in silver, but the spectrum disappears at 10^{-6} M. We operate at a silver concentration of 10^{-7} M ($\sim 10^7$ NPs per mL), for which no signal is achieved even after long acquisition times.

Further, to limit the formation of spurious aggregates in the colloidal solution, which may lead to false positives, we added to the mixture twice as many non-coded BSA-protected NPs to the mixture. As a first demonstration, serum contaminated with only one of the four mentioned bacteria was then added to the MODS mixing vessel, and a time series of SERS spectra were collected as the mixture was circulated through the laser focus (**Figure 3.11 A** and **Figure 3.12 – 3.15**). The majority of the time steps only sampled dispersed NPs, which produced a weak or none SERS signal. Occasionally, a targeted colony forming unit (CFU)

traversed the laser focus, giving rise to $\sim 10^3$ higher SERS signal due to the concentration of particles on the bacterial surface and the subsequent formation of NP gaps, as discussed above. We then calculated the correlation of the recorded spectra with the reference ones for each of the Raman codes (**Figure 3.8 A**), and obtained clear identification of the added pathogen. The experiment was successfully repeated for samples containing mixtures of two bacteria (**Figure 3.16**). Importantly, we note that no false identifications were observed in any of the analyses (i.e., no signatures from the bacteria types that were absent from the serum), and no positives were recorded from blank samples (**Figure 3.11 A** and **Figure 3.12– 3.17**). Incidentally, a significant dispersion in correlation was observed (i.e., absolute SERS intensity per recognition event), which we attribute to the size of the detected CFUs, ranging from single cells to larger colonies (**Figure 3.18**). Remarkably, all of the obtained concentrations were consistent with those found using conventional cell culture, but with a considerably lower standard deviation (**Figure 3.12 – 3.17**).

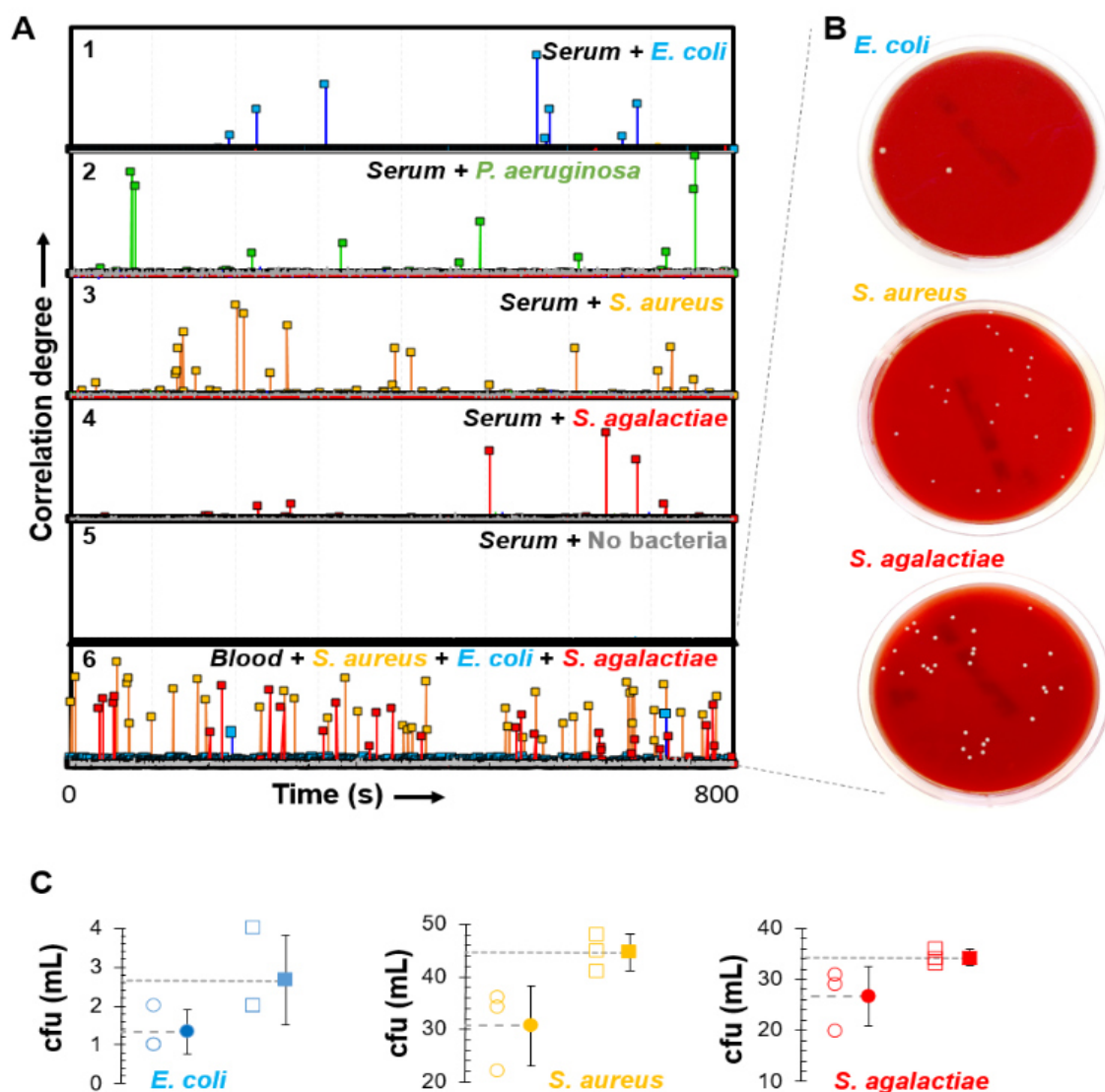


Figure 3.11. MODS performance for contaminated samples. **(A)** Correlation between a temporal series of spectra collected over 270 ms intervals and the SERS reference of the labelled NPs. The analysed serum samples contain either one pathogen (1-4, see labels) or no pathogen (5, blank). Series 6 shows the result for a blood sample spiked with a combination of three different bacteria and concentrations (*S. aureus*, *E. coli*, and *S. agalactiae*). Large correlation values reveal the passage of an individual bacteria or CFU. **(B)** Cellular cultures (24-48 hours) for the microorganism inoculated in the blood samples (series 6). White spots correspond to CFUs. **(C)** Comparison of the bacteria concentrations (CFUs per mL) as determined by MODS (open squares) for the sample contaminated with three pathogens (series 6) versus traditional cultures (open circles). Averages over three runs of both MODS and culture experiments are shown by the corresponding solid symbols.

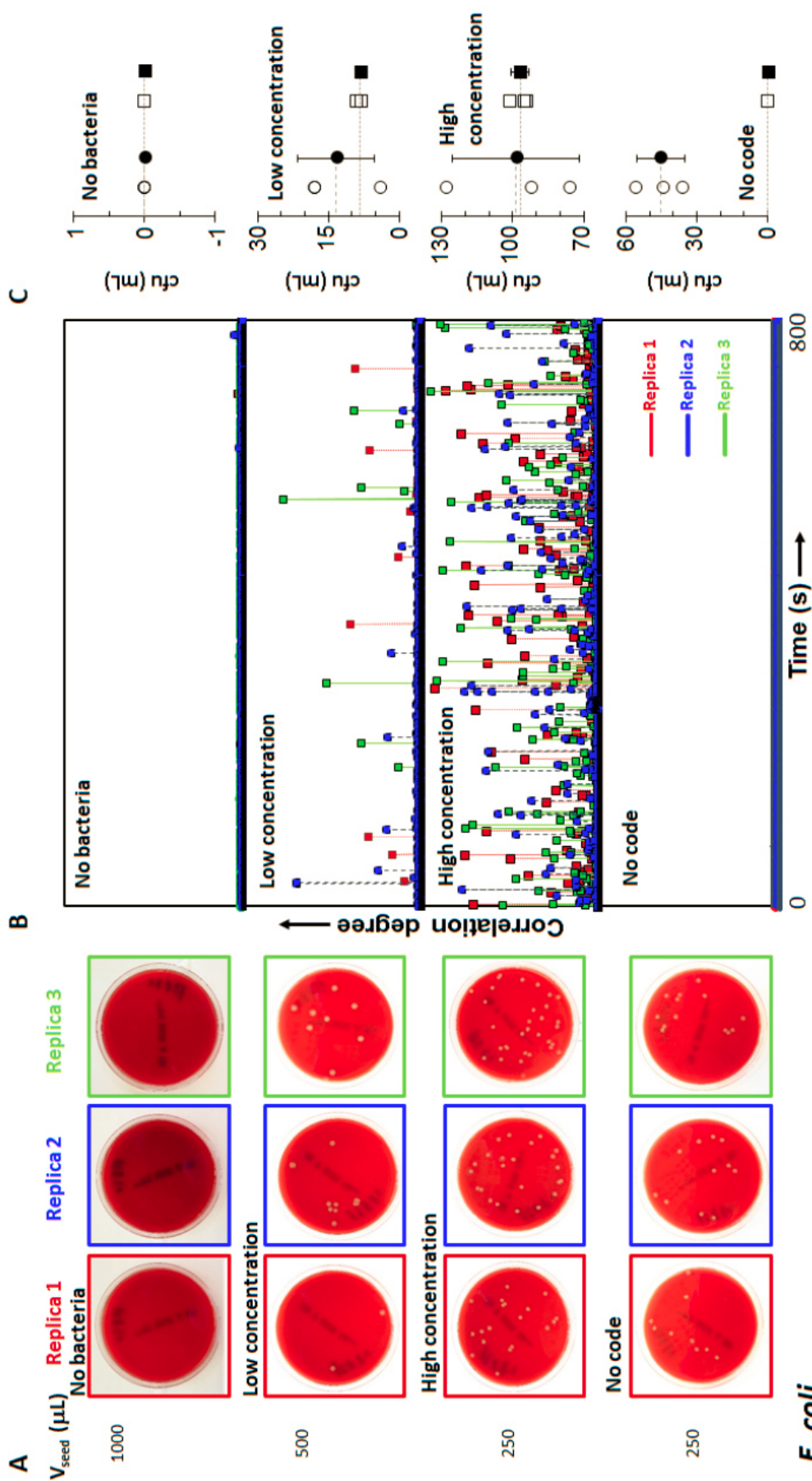


Figure 3.12 Results for serum sample spiked with *E. coli* at different concentrations. **(A)** Cellular cultures. **(B)** Detection and quantification results obtained in our MODS device, from top to bottom: With no bacteria present, at low pathogen concentration, high concentration, and high concentration but without the encoded nanoparticle that identifies this bacteria. **(C)** Statistical comparison of bacteria concentrations (CFUs per mL) as determined by MODS (open squares) versus traditional cultures (open circles). Averages over three runs of both MODS and culture experiments are shown by the corresponding solid symbols.

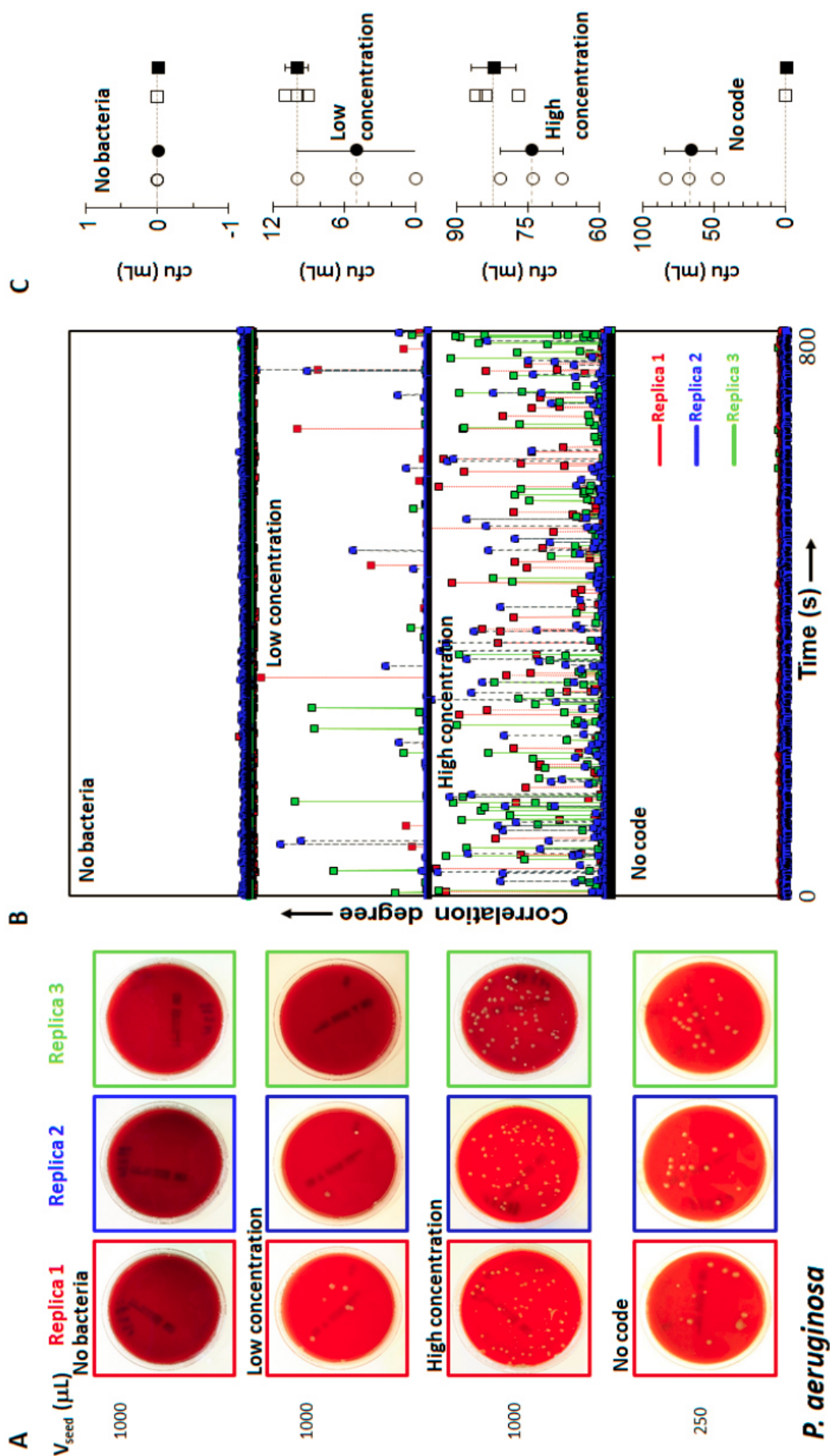


Figure 3.13. Same as Figure 3.12 for *P. aeruginosa* instead of *E. coli*.

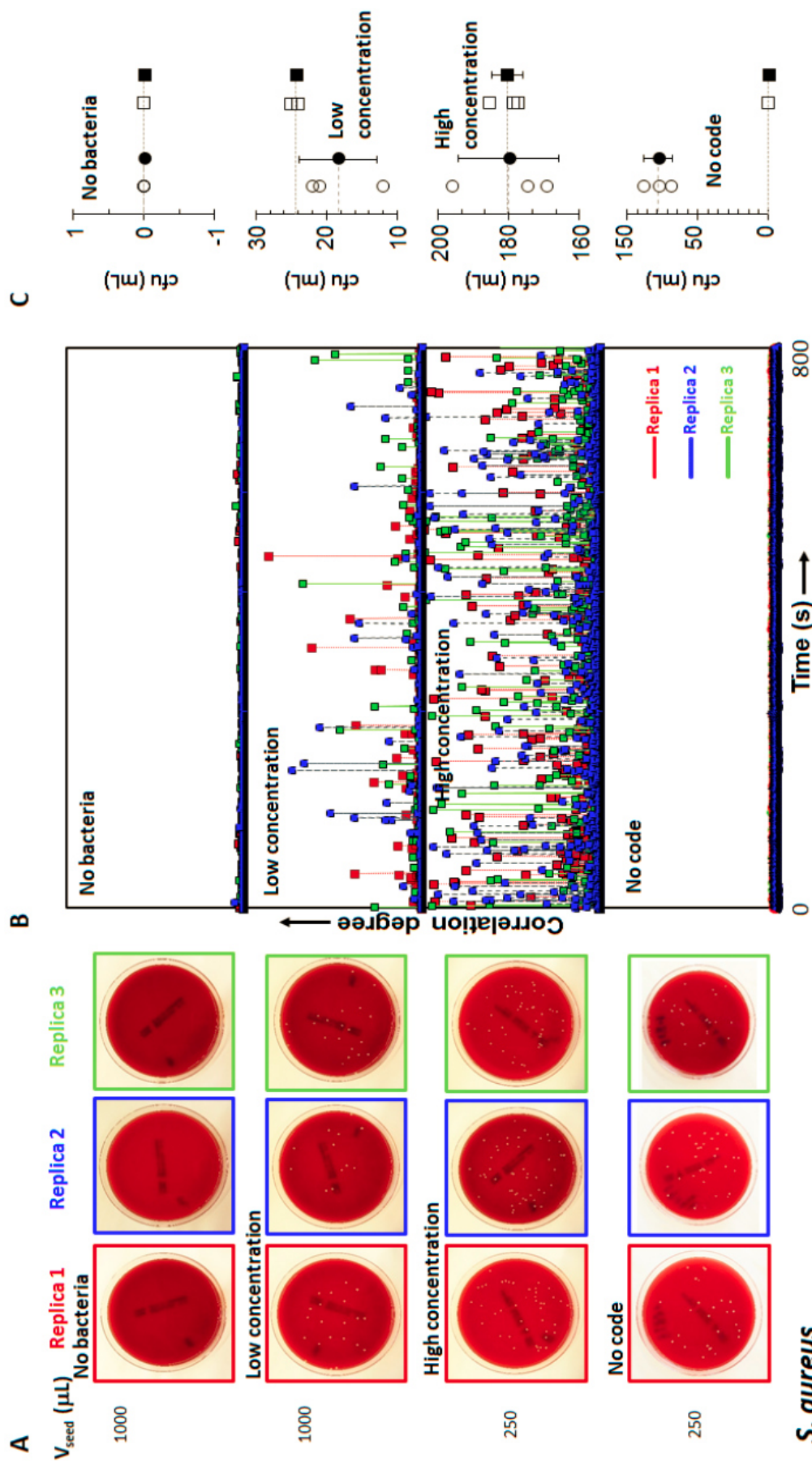


Figure 3.14. Same as Figure 3.12 for *S. aureus* instead of *E. coli*.

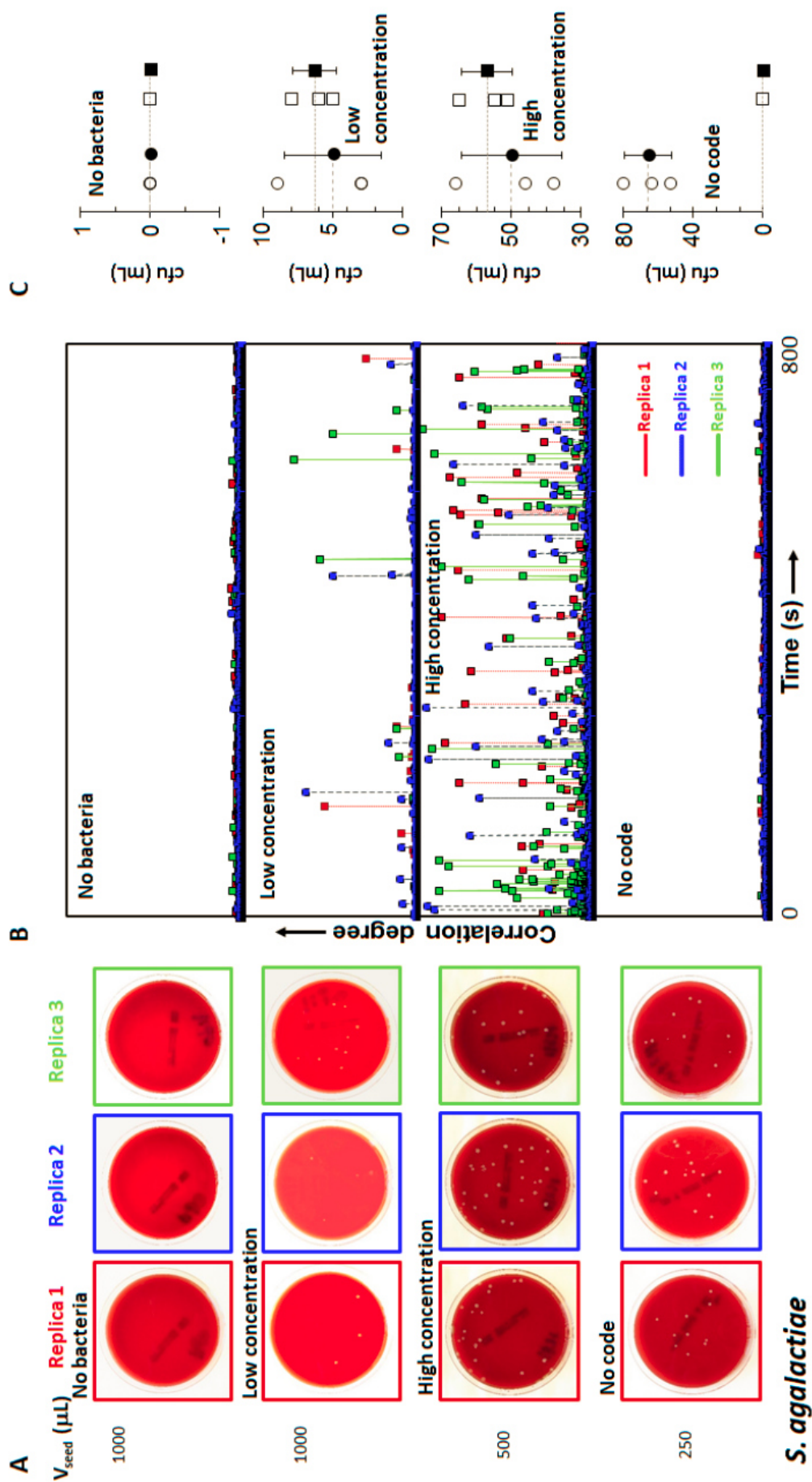


Figure 3.15. Same as Figure 3.12 for *S. agalactiae* instead of *E. coli*.

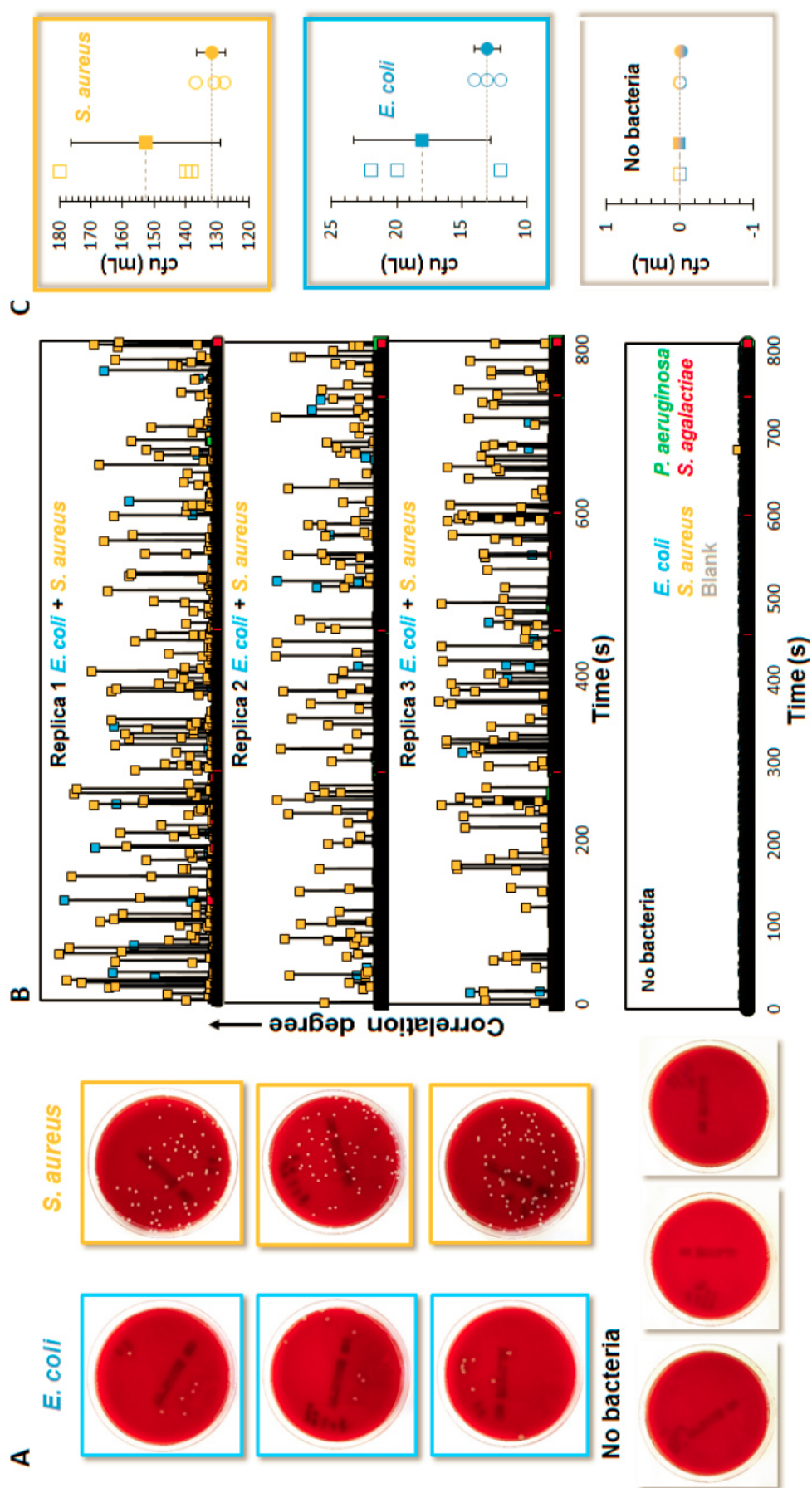


Figure 3.16. Results for serum sample spiked with both *E. coli* and *S. aureus*. **(A)** Cellular cultures for each bacteria (the volume seeded is 1 mL for *E. coli* and 0.5 mL for *S. aureus*). **(B)** Detection and quantification results obtained with MODS. **(C)** Statistical comparison of bacteria concentrations (CFUs per mL) as determined by MODS (open squares) versus traditional cultures (open circles). Averages over three runs of both MODS and culture experiments are shown by the corresponding solid symbol

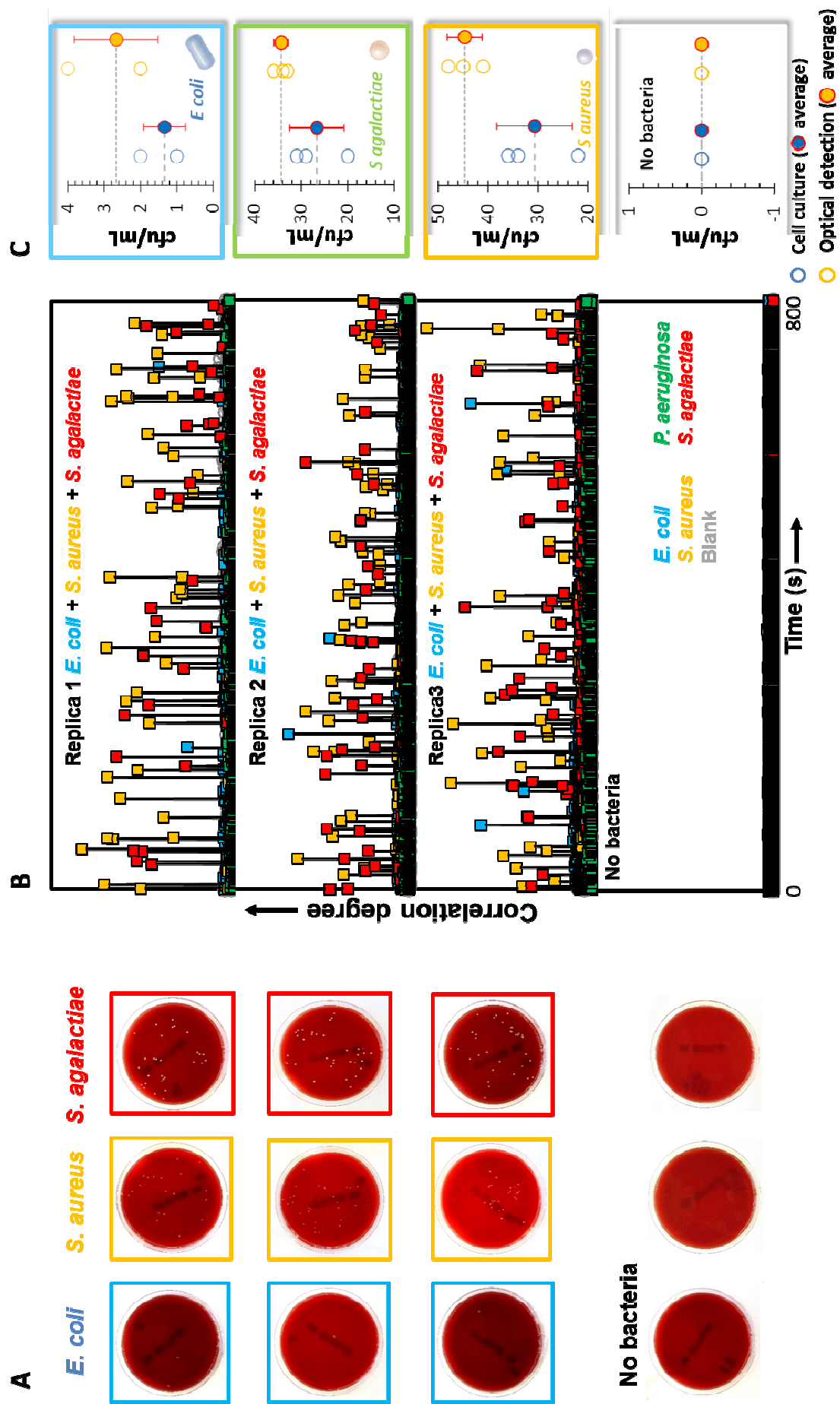


Figure 3.17. Blood sample spiked with *E. coli*, *S. agalactiae*, and *S. aureus*. (A) Cellular cultures for each bacteria (a volume 0.5 mL for each). (B) Detection and quantification results obtained in MODS. A statistical comparison of these results is presented in (C).

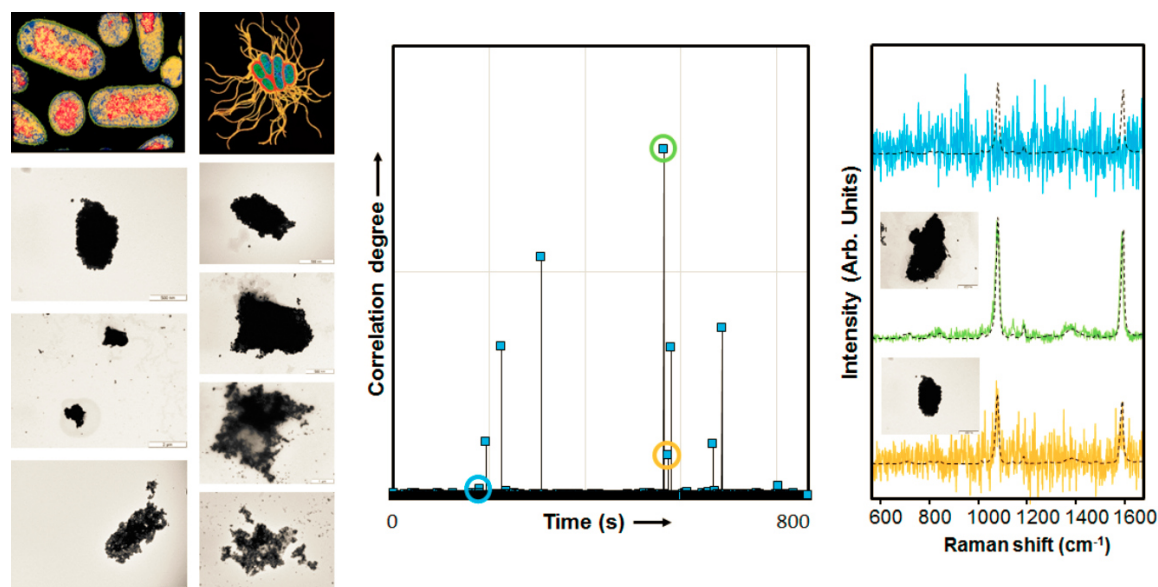


Figure 3.18. Biodiversity of *E. coli*. Left: TEM images of several single or clustered *E. coli* CFU's coated with nanoparticles. Center: SERS detection results on the millifluidic MODS device for one of the samples of **Figure 3.14** at low bacterial concentration. Right: Spectra corresponding to the events highlighted by circles in the previous plot, showing that the degree of correlation of the SERS spectra of the encoded particles strongly depends on the signal-to-noise ratio. Consequently, bigger clusters of bacteria give rise to larger signal and higher correlation.

3.3.6. MODS DEMONSTRATION IN BLOOD.

We demonstrated selectivity and multiplexing of MODS in whole blood samples by contaminating blood simultaneously with *S. aureus*, *E. coli*, and *S. agalactiae* in different concentrations ranging from units to tens of CFUs per mL. It is important to note that blood samples spiked with microorganisms constitute a good model to emulate bacterial infection in actual patients, as an infection in the latter originates in spiking of biological fluids from an external source. MODS analysis of this sample revealed all three pathogens (**Figure 3.11 A** and **Figure 3.17**), while a statistical analysis of the results based on three runs of the experiment **Figure 3.11 C**)

determined their respective concentrations in excellent agreement with cellular cultures (**Figure 3.11 B** and **Figure 3.17**). Incidentally, positive events varied in the degree of correlation, as expected from the bacterial diversity (**Figure 3.18**). We stress that each MODS analysis took 13 min, which is a substantial reduction in time compared with cellular cultures (24-72 hours). These results further demonstrate the ability of MODS to accurately resolve pathogen concentrations in complex samples infected simultaneously with different pathogens at very different concentrations in a single pass, as illustrated in **Figure 3.11** and **Figure 3.17**, where *E. coli* is present in a much lower density than *S. aureus* and *S. agalactiae*.

3.3.7. NANOPARTICLE AGGREGATION ON BACTERIA.

The kinetics of functionalized NP aggregation on the pathogen membrane is a key factor of MODS. As a representative example, after adding a large concentration of *E. coli* to the pool of five coded NPs (time 0), we found three distinct stages in the temporal evolution of the resulting SERS signal (**Figure 3.19 A**): NP aggregation is initially very slow due to the relatively infrequent NP-bacteria encounters before sample and NPs fluids are fully intermixed, yielding just a slow increase in Raman signal; diffusion eventually brings the NPs closer to the bacteria after ca. 300 s, resulting in more frequent encounters and a faster linear increase in SERS intensity; the signal eventually reaches a plateau after ca. 700 s, consistent with previous literature,²²⁸ indicating saturated coverage of the membrane. The latter stage is also affected by signal depletion produced by flocculation, as the increased weight of NP-covered CFUs pulls them away from the laser focus. Insight into these experimental results is provided by a Monte Carlo simulation of particle sticking (**Figure 3.19 B**, right scale), which reveals a characteristic saturation at a NP random coverage ~60% of the maximum close-packed density.²²³ A large occurrence of NP

gaps takes place at high NP coverage (Figure 3.6). Although the laser wavelength is far from the NP plasmons (Figure 3.2 and Figure 3.9), these gaps produce a dramatic enhancement in the Raman signal (Figure 3.3). Averaging over the gap distribution (Figure 3.5), we find an increase in SERS intensity by 3 orders of magnitude compared with non-interacting NPs (cf. solid and broken red curves in Figure 3.19 B, left scale). The signal resulting from positive CFU encounters is further amplified by the effect of attached NP accumulation. We note that the modelled temporal evolution of the SERS signal agrees rather well with the measured kinetics (Figure 3.19 A), without adjustable parameters other than the time after which sample and NPs fluids are considered to be fully intermixed (~500 s).

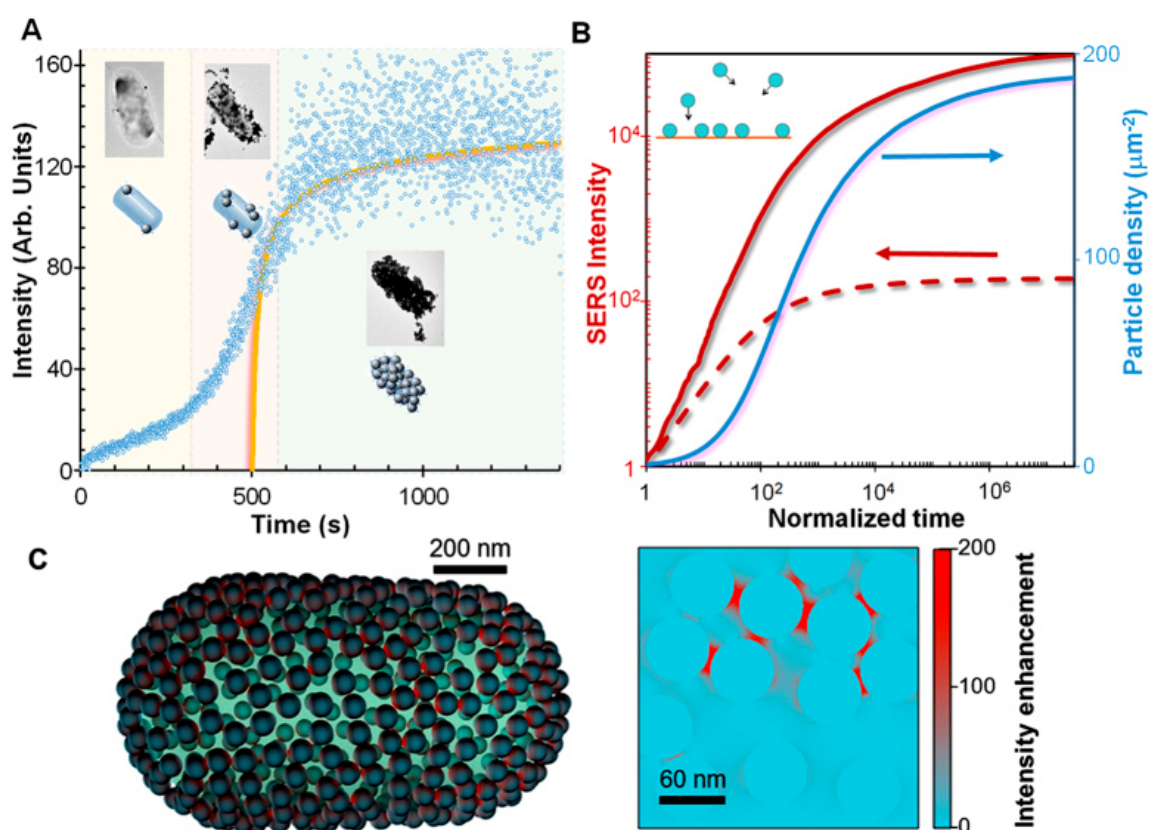


Figure 3.19. (A) Kinetics of NP aggregation as measured through the time-dependent SERS signal (symbols) after adding *E. coli* to the mixture of coded NPs. Solid curve: theory from (B). (B) Simulation of the temporal evolution of 60nm Ag NP aggregation on the bacteria membrane produced by random NP-membrane encounters, resulting in a rapidly growing NP density (right

scale) and SERS intensity (left scale, calculated per μm^2 of membrane area and normalized to the signal from an individual NP). The latter is given with (solid curve) and without (broken curve) inclusion of the effect of NP gap hotspots. The time is normalized to the average delay interval between consecutive NP arrivals. The theory curve in A is scaled to 17.3 arrivals per second, as estimated from kinetic theory. (C) Near-electric-field intensity in a rod-like individual *E. coli* covered with Ag NPs (top, intensity plotted on the NP surfaces) and detail of the array (bottom, intensity on a surface passing by the NP centers), revealing the formation of optical hotspots. The intensity is averaged over light incidence directions and polarizations, the light wavelength is 785 nm, and the color scale is saturated to improve visibility.

3.3.8. OPTICAL EFFECTS OF THE NANOPARTICLE AGGREGATION ON BACTERIA.

Particle accumulation, gap formation, and the resulting SERS enhancement are thus pivotal elements that allow us to obtain intense signals from bacteria content well above the background of dispersed NPs. In support of this conclusion, we further simulate the near-electric-field light intensity at 785 nm wavelength for a rod-like structure mimicking an *E. coli* specimen (**Figure 3.19 C**), which reveals large enhancements at the gaps between neighbouring NPs, accompanied by relatively weak modulations away from the gaps (see also **Figure 3.5**). Additional simulations of SERS enhancement for different particle compositions and sizes (**Figure 3.4**) suggest that an improvement in sensitivity can be gained by optimizing these parameters. In particular, the optimum particle size may depend on the dimensions and morphology of the pathogen and its affinity for the NP ligand biomolecules, as the figure of merit for MODS is the ratio of the SERS signal coming from the microorganisms to that originating in the dispersed NPs.

4 Antibody vs Aptamer for SERS detection in human fluids: The case of *Staphylococcus aureus*

Antibody vs Aptamer for SERS detection in human fluids: The case of *Staphylococcus aureus*

4.1. INTRODUCTION

Staphylococcus aureus (*S.aureus*), Gram-positive cocci, are a common cause of community-acquired skin and soft tissue infections, septic arthritis, osteomyelitis, endocarditis, pneumonia or bacteremia.²²⁹ Also, *S. aureus* is one of the five most common causes of hospital-acquired infections and is often the cause of many postsurgical wound infections. Each year, around 500,000 patients in hospitals of the United States contract a staphylococcal infection mainly by *S. aureus*.²³⁰ Mortality rates for *S.aureus* can be set at 25 to 60% for infective endocarditis, 39 to 67% for pulmonary infections, 22 to 48% for bacteremia without a focus, and 7 to 21%, 15 to 17%, and 10% for catheter, skin and soft tissue, and urinary tract infections related bacteremias, respectively.^{230,231} Mortality can be largely reduced by early administration of active antibiotic treatment.²³⁰ Unfortunately, the time needed for obtaining a definitive bacterial identification using conventional blood cultures,¹⁹⁰ including matrix-assisted laser desorption/ionization-time-of-flight (MALDI-TOF) mass spectrometry,¹⁹⁴ is around 12-24 hours. Thus, during the last decades an enormous work has been devoted to develop alternative methods for faster identification of infection.¹⁹¹ Between these alternatives, the most popular are those based on immunology approaches (e.g., enzyme-linked immunosorbent assay (ELISA) as well as fluorescence and radio immunoassays¹⁹²) and the identification of nucleic acids (i.e., polymerase chain reaction, PCR¹⁹³). However, these techniques are expensive, time costly, and/or exhibit low sensibility.

Thus, in order to detect rapidly and sensitively bacteria and, therefore, avoiding the use of spurious drugs^{197,198} and decreasing the mortality of patients, several

detection alternatives^{71,204-210} have been proposed based on concepts such as nanoscience, spectroscopy, magnetism, plasmonics, and microfluidics.^{193,199-203} However, most of these methods are time consuming, capable of exploring only small sample volumes (~microliters) which, especially in cases of bacteremia, are not relevant for clinical diagnosis,^{4,200} or rely on additional steps, such as bacterial culture, to acquire target concentration high enough to record a suitable signal for identification.^{71,200,232} In recent years, surface-enhanced Raman scattering (SERS) encoded particles have been extensively employed, mostly in proof-of-concepts studies, as efficient optical tools for biomedical detection and diagnosis,^{92,233,234} including in combination with other methods such as microfluidics.²³⁵⁻²³⁷ The next breakthrough is possibly the integration of such SERS platforms into spectroscopic devices for clinical human applications.²³³ In this regard, our groups have recently proposed a translational alternative based on the use of SERS encoded plasmonic particles and microfluidics.²³⁸ In this approach, the particles form a dense collection of electromagnetic hot spots on the surface of the target bacteria allowing for an exponential increase of the SERS intensity as compared to the signal of free particles in solution. Quantification is achieved by passing the sample through a microfluidic device with a collection window where a laser interrogates and classifies each of the induced bacteria-nanoparticle aggregates in real time. This approach was demonstrated using SERS encoded nanoparticles functionalized with antibodies as chemoselective receptors to recognize bacteria in saline solutions. Although antibodies are an excellent option for the accurate recognition of specific targets, they are expensive to produce, delicate to handle, and rather large in size (a factor that limits the formation of active hot-spots). During the last years, a new family of biomolecules (aptamers) has been developed as an efficient alternative to antibodies. Aptamers display similar or even larger target specificity^{239,240} while providing key advantages in terms of stability, immunogenicity, facility of production, functionalization and reduced size. Further, although saline solutions are a good starting point for conceptual demonstrations,

they cannot be assimilated to real, complex human fluids as changes in medium composition can severely affect the physicochemical properties of the nanoparticles, perturbing their colloidal stability,²⁴¹ as well as suppressing the function of the surface biorecognition elements.²⁴²

Herein, we produce SERS encoded nanoparticles capable of remaining colloidally stable in real human samples, test the efficiency of these nanoparticles upon functionalization with either antibodies or aptamers against *S. aureus*, and demonstrate its rapid identification/quantification (1 mL/10 min), down to the single CFU, through a microfluidic device in large samples of real human fluids (i.e., urine, blood, and pleural and ascites fluids) where the early detection of these bacteria may impact the final outcome of the patient.

4.2. EXPERIMENTAL SECTION

4.2.1. MATERIALS

Dihydrated trisodium citrate ($\geq 99.5\%$, $C_6H_5Na_3O_7 \cdot 2H_2O$), ethanol absolute ($\geq 99.9\%$, EtOH), L-ascorbic acid ($\geq 99.0\%$), 4-mercaptobenzoic acid ($\geq 99\%$, MBA), silver nitrate ($\geq 99.9999\%$, $AgNO_3$), sodium hydroxide ($\geq 98\%$, NaOH), *O*-(2-Mercaptoethyl)-*O'*-(2-carboxyethyl) heptaethylene glycol ($\geq 95.0\%$, HS-PEG-CO₂H), magnesium sulfate ($\geq 98\%$, $MgSO_4$), *N*-(3-dimethylaminopropyl)-*N'*-ethylcarbodiimide hydrochloride (BioXtra, EDC), sodium chloride (BioXtra, $\geq 99.5\%$, NaCl), sodium docecyl sulfate (BioReagent, SDS), and Dulbecco's phosphate buffered saline (D8537, DPBS) were purchased from Sigma-Aldrich (Munich, Germany); 10X TBE buffer was acquired from Fisher Scientific; and *Staphylococcus aureus* antibody (MA1-10708, *S. aureus*), and thiol-modified *Staphylococcus aureus* aptamer²⁴³ were purchased from Life Technologies. All reactants were used without further purification. Milli-Q water ($18\text{ M}\Omega\text{ cm}^{-1}$) was used in all aqueous solutions, and all glassware was cleaned with aqua regia before the experiments. *Staphylococcus aureus* was supplied by the Hospital Clínic y Provincial de Barcelona; the aseptic biological fluids (urine, blood, and pleural and ascites fluids) were supplied by the Hospital Universitario Hm Madrid-Torrelodones. Personal and clinical data were recorded according to standard clinical procedures. All specimens were obtained with informed consent. The study was approved by the local Ethics and Clinical Research Committee.

4.2.2. SYNTHESIS OF CITRATE-STABILIZED SPHERICAL Ag NPs.

Spherical silver nanoparticles (AgNPs) of approximately 56 nm in diameter were produced by a modification of the previously reported protocol.²⁴⁴ Briefly, 250 mL of Milli-Q water were heated to reflux under strong magnetic stirring. Once it boils energetically, a mixture containing ascorbic acid (250 μ L, 0.1 M) and trisodium citrate (1.7 mL, 0.1 M) was added. After 1 minute, a solution containing $AgNO_3$

(496 μL , 0.1 M) and MgSO_4 (392 μL , 0.1 M), previously incubated for 5 min at room temperature, was injected into the reaction vessel under vigorous stirring. Boiling and stirring were continued during 1 h to ensure the precursors reduction. During this time, the color of the solution quickly changed from colorless to yellow, and gradually into dark orange. Finally, NPs were cleaned by centrifugation (5400 r.p.m., 20 min) and redispersed in Milli-Q water, to a final $[\text{Ag}^0] = 5 \times 10^{-4}$ M.

4.2.3. Ag NPs CODIFICATION AND ANTIBODY CONJUGATION.

In order to provide colloidal stability to AgNPs during the encoding process and antibody conjugation, 15 mL of the as produced spherical silver nanoparticles were functionalized with a small amount of HS-PEG- CO_2H . To this end, a solution containing HS-PEG- CO_2H (7.5 mL, 1.83 μM in EtOH) and MBA (7.5 mL, 5.48 μM in EtOH) was prepared. This solution was then rapidly added to silver colloids ($[\text{Ag}^0] = 5 \times 10^{-4}$ M) and sonicated during 30 s (the number of molecules/ nm^2 was 1 for HS-PEG- CO_2H and 3 for MBA). Subsequently, NaOH (150 μL , 0.23 M) was added to the mixture under vigorous stirring and sonicated again for 30 s. 1 h later, AgNPs were cleaned twice by centrifugation (4.200 r.p.m, 12 min) and redispersed in Milli-Q water to achieve a final $[\text{Ag}^0] = 5 \times 10^{-4}$ M. Afterwards, in order to conjugate the antibody to the nanoparticles, DPBS (200 μL) and EDC (20.3 μL , 250 nM in DPBS) were added to the colloidal dispersion (1 mL, $[\text{NPs}] = 92.8$ pM), the mixture was shaken for 5 min at room temperature, and then the antibody solution was added (0.7 μL , ~ 7.3 μM). The resulting mixture was shaken for 2 h at room temperature, then cleaned twice by centrifugation to remove the excess of unreacted EDC and antibody (3000 rpm, 10 min), and redispersed in DPBS/Milli-Q water (1:3). The concentration of the Ab-modified AgNPs solution was measured, adjusted to 18.6 pM ($[\text{Ag}^0] = 1 \times 10^{-4}$ M), and the solution was stored at 4 °C.

4.2.4. Ag NPs CODIFICATION AND APTAMER CONJUGATION.

5'-alkyl-thiol-modified *S.aureus* aptamer (1.5 mL, 3.1 nM) was added to a 92.8 pM AgNPs solution (0.5 mL, $[Ag^0] = 5 \times 10^{-4}$ M), and the mixture was shaken overnight at room temperature. Then, 20 μ L of 1% SDS and 50 μ L of 10X TBE were added, and the resulting solution was shaken overnight at room temperature. The following morning, sodium chloride was added 5 times at 1 h intervals to a final concentration of 20, 40, 60, 80, and 100 mM. One hour after the last addition, 2.2 μ L of a 100 μ M MBA solution (0.4 molecules/nm²) were added, and the mixture was shaken overnight at room temperature. Finally, the NPs were cleaned by centrifugation (3000 r.p.m., 10 min) and redispersed in Milli-Q water. The concentration of the aptamer-modified AgNPs solution was measured, adjusted to 18.6 pM ($[Ag^0] = 1 \times 10^{-4}$ M), and the solution was stored at 4 °C.

4.2.5. NANOPARTICLE CHARACTERIZATION.

UV-vis spectra were recorded using a Thermo Scientific Evolution 201 UV-vis spectrophotometer. Silver concentration for AgNPs colloids was calculated by the Lambert-Beer law using an extinction coefficient of $6.61 \times 10^{10} \text{ M}^{-1} \text{ cm}^{-1}$.^{55,215} Electron micrographs were recorded with a transmission electron microscopy (JEOL JEM-1011 operating at 80 kV) and an environmental scanning electron microscopy (JEOL 6400) for the structural characterization of the samples. SERS spectra were collected in backscattering geometry with an in-house Raman system (Technospex, Singapur) equipped with a CCD detector and a macrolense. The spectrograph used a high resolution grating (1200 g cm⁻¹) with additional band pass filter optics. Excitation of the sample was carried out with a 785 nm diode laser line, with acquisition times of 0.4 s and power at the sample of 500 mW.

4.2.6. MICROFLUIDIC DEVICE MANUFACTURING.

The microfluidic device was fabricated with polydimethylsiloxane (PDMS) by replica molding. The device consisted of a single microchannel of 600 μm -width, 2 mm-depth, and 50 mm-length. Briefly, PDMS was mixed with curing agent (10:1) (Sylgard 184, Dow Corning) and poured onto a poly(methyl methacrylate) (PMMA) mold. Once degassed in vacuum, the mixture was cured at 80 $^{\circ}\text{C}$ for 1 h. Then, the PDMS layer was peeled off from the master, and inlet/outlet holes were punched with a biopsy punch. The final device was obtained by bonding the PDMS layer to a slide cover (130-170 μm -thick) after oxygen plasma treatment (100 W, 3% O_2 , 0.2 mbar, 40 s) (Plasma Flecto 10, Plasma technology GmbH).

4.2.7. BACTERIAL SAMPLES

Bacteria were inoculated in enriched thioglycollate medium (BBL), incubated at 37 $^{\circ}\text{C}$ for 18 h, and then diluted with saline solution (0.9% NaCl). Next, the required volume of bacterial solution was diluted into serum or biological fluids in order to reach the desired final concentration. Then, the modified AgNPs, with antibody or aptamer of *Staphylococcus aureus*, were added to the bacterial solutions at a concentration of 10 μL (10^{-4} M of Ag^0)/mL of sample, in the case serum and 1 mL (2×10^{-6} M of Ag^0)/mL of sample for the biological fluids. To verify the final bacterial concentration per sample, three replicates of each solution were spread in agar-blood plates and incubated for 24-48 h at 37 $^{\circ}\text{C}$. After this time, the number of colonies in each plate was counted in order to calculate their concentration of CFUs per mL.

4.2.8. MEASUREMENT SYSTEM SETUP

The microfluidic device was placed onto the stage of the system and appropriately aligned. Inlet and outlet were connected to a syringe and a waste container,

respectively, via 0.8 mm-diameter polytetrafluoroethylene (PTFE) and 1.1 mm-diameter tygon tubes. The syringe was pre-charged with the sample and nanoparticles. A standard syringe pump (NE-1000, New Era Pump Systems, Inc.) was used to push the sample at a flow rate of 6 mL/h. The laser (785 nm, 500 mW) was focused with a macrolense providing an efficient spot of 0.6 mm. The scan collection time was set to 400 ms per spectrum, providing an acquisition speed of 1.5 mm/s (for a flow speed of 1.48 mm/s), which results in an evaluation speed of 10 min per mL of sample, during which 1500 scans are obtained. Data deconvolution was carried out by principal component analysis and classical least squares using the Wire 4.1 software.

4.3. RESULTS AND DISCUSSION

4.3.1. DESIGN AND PREPARATION OF AB /Apt FUNCTIONALIZED Ag NPs

SERS encoded particles usually consist of a plasmonic core tagged with an organic molecule with a large SERS cross-section, and a thick coating of inorganic oxides or polymers. The external shell aims at protecting the SERS code, stabilizing the particle in the medium, and providing an easy (bio) functionalizable surface.^{55,245,246}

In our case, however, due to the requirements of the detection scheme and the chemical conditions of the analytical matrix, SERS encoded nanoparticles had to be design to sustain high colloidal stability in biological media (usually characterized by their high ionic strengths) while minimizing the thickness of the external coating layer (a key condition to maximize the efficient plasmonic coupling of the nanoparticles retained on the bacterial membrane²⁴⁷).

Notably, although antibodies and aptamers fulfill the same bio-recognition function, their chemical nature is significantly different. Thus, for preparing our encoded nanoparticles, two different protocols were developed that can be observed schematically in **Figure 4.1**.

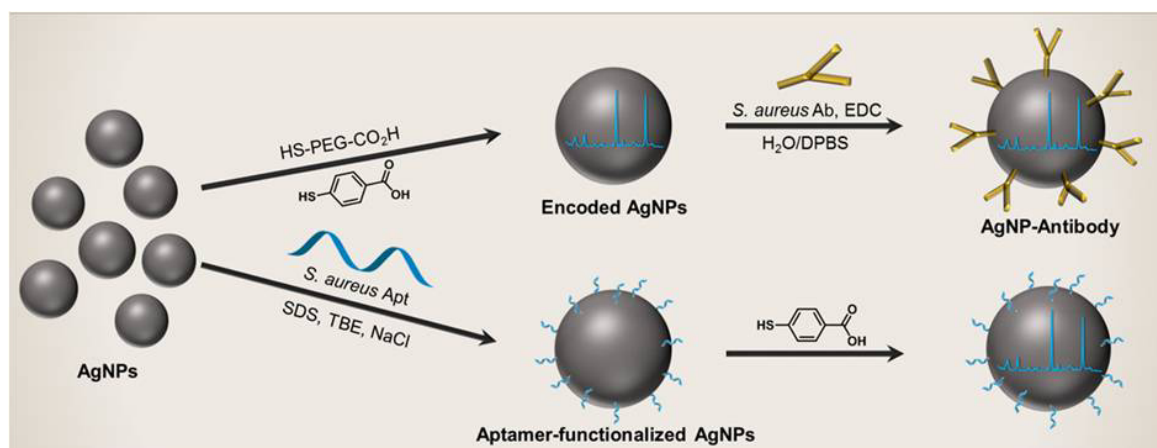


Figure 4.1. Schematic representation of the nanoparticle SERS encoding and functionalization with antibodies and aptamers.

First, silver nanoparticles of ≈ 56 nm diameter were prepared using ascorbic and sodium citrate as reducing agents by modifying a previously reported protocol.²⁴⁴ The encoded nanoparticles conjugated with antibodies were functionalized with a small amount of *O*-(2-Mercaptoethyl)-*O'*-(2-carboxyethyl)heptaethylene glycol (HS-PEG-CO₂H) in order to improve their colloidal stability, and outfit the surface with a suitable group for the antibody coupling. Then, the molecular code (4-mercaptobenzoic acid, MBA) was added. In order to maximize the SERS signal while preventing loss of stability, the molecular ratio between HS-PEG-CO₂H to MBA was optimized to 1:3. The antibody coupling to the nanoparticles was achieved using EDC as activating agent, forming a peptide bond in between the carboxylic group of the HS-PEG-CO₂H and an amine group of the antibody.

In the case of the aptamer functionalized nanoparticles, a 5'-alkyl-thiol-modified *S.aureus* aptamer was first self-assembled onto the silver surfaces followed by the subsequent encoding with MBA. Concentration of MBA was set to be similar to that of the particles functionalized with antibodies. In this case, no extra stabilizing agents were necessary as the aptamer surface modification maintains the colloidal integrity of the particles.

Figure 4.2 shows the localized surface plasmon resonance (LSPR); **Figure 4.3** shows SERS response of the particles encoded with MBA and functionalized with either antibodies or aptamers and finally **Figure 4.4** shows transmission electron microscopy (TEM) images. Notably, both optical and physical characteristics of all the materials remain similar, without appreciable changes in between samples (**Figure 4.2 A**, **Figure 4.3** and **Figure 4.4**) and over time (**Figure 4.2 B** and **Figure 4.2 C**).

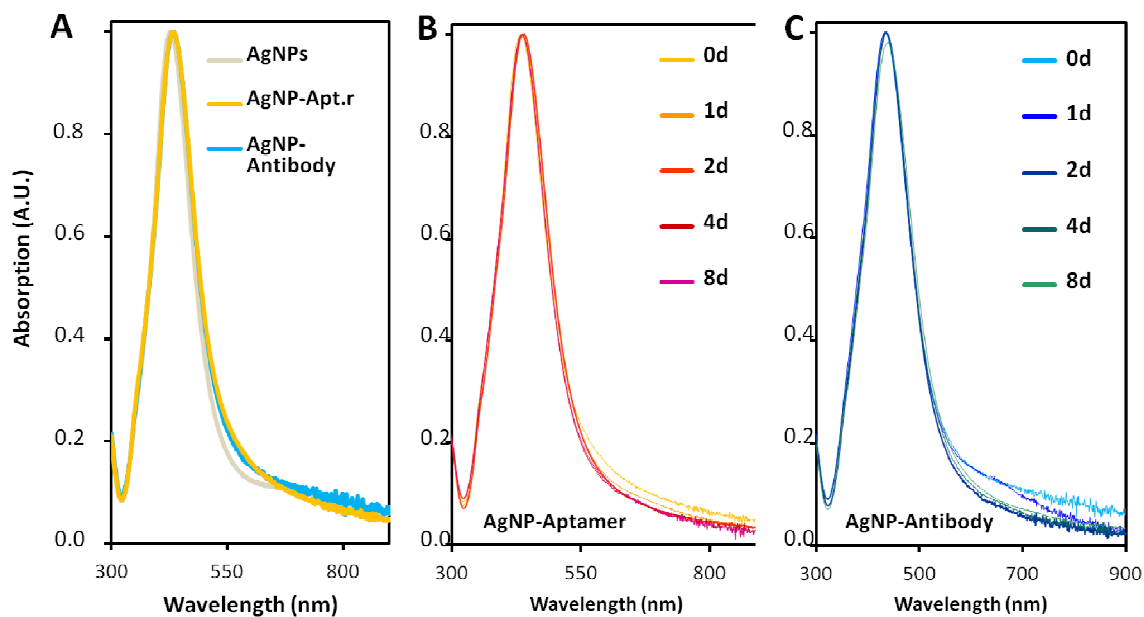


Figure 4.2. (A) Localized surface plasmon resonances of MBA-encoded silver nanoparticle before and after bioconjugation with aptamers or antibodies (B, C). Time-monitoring of the optical properties for SERS encoded nanoparticles, conjugated either with aptamers (B) or antibodies (C) in PBS (d = days).

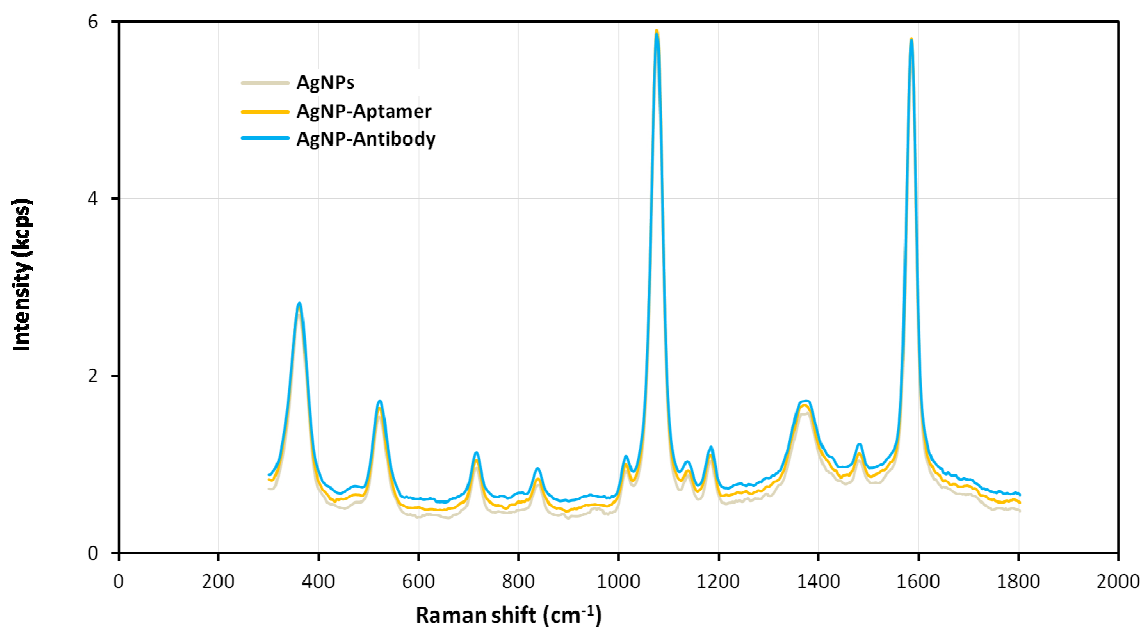


Figure 4.3. SERS response in suspension of MBA-encoded silver nanoparticles before (grey) and after bioconjugation with aptamers (yellow) or antibodies (blue).

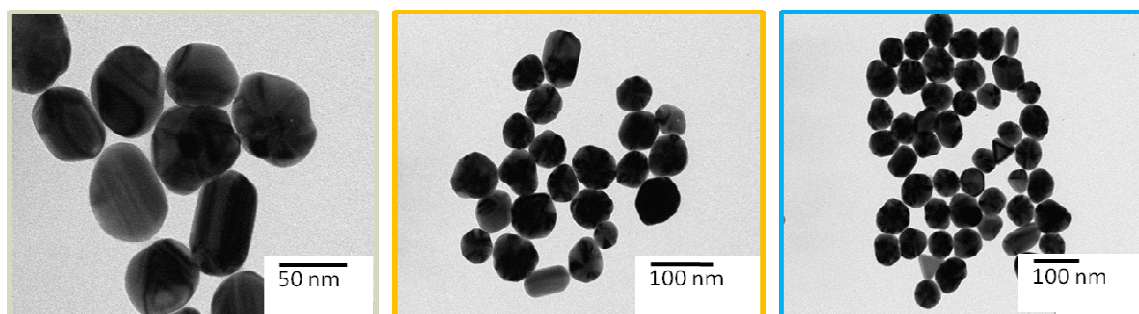


Figure 4.4. Representative TEM images of MBA-encoded silver nanoparticles before (grey frame) and after bioconjugation with aptamers (yellow frame) or antibodies (blue frame).

4.3.2. AgNPs-Apt vs AgNPs-AB FOR *S. aureus* QUANTIFICATION

To test the efficiency of antibodies vs aptamers functionalization, we designed an experiment comprising a serum solution spiked with around 7×10^3 CFUs/mL of *S. aureus*. **Figure 4.5**.

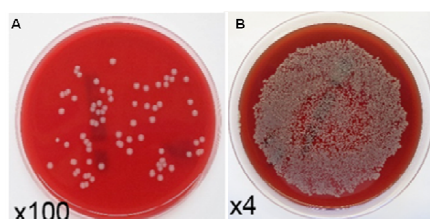


Figure 4.5. Bacterial culture of the *S. aureus* solution in image A 10 μ L and image B, 250 μ L.

It is worth noting that, as solitary cells are the exception in nature, the colony-forming unit (CFU) is the unit used in microbiology to estimate the number of viable bacteria in a sample. The *S. aureus*-spiked solution was mixed with the same volume (10 mL, 10^{-6} M of Ag^0) of SERS encoded nanoparticles, either uncoated or functionalized with antibodies or aptamers. The resultant solutions were passed through a microfluidic device comprising a syringe with the sample and nanoparticles, a pump, and a laser that interrogates the flow in real time. (**Figure 4.6**).

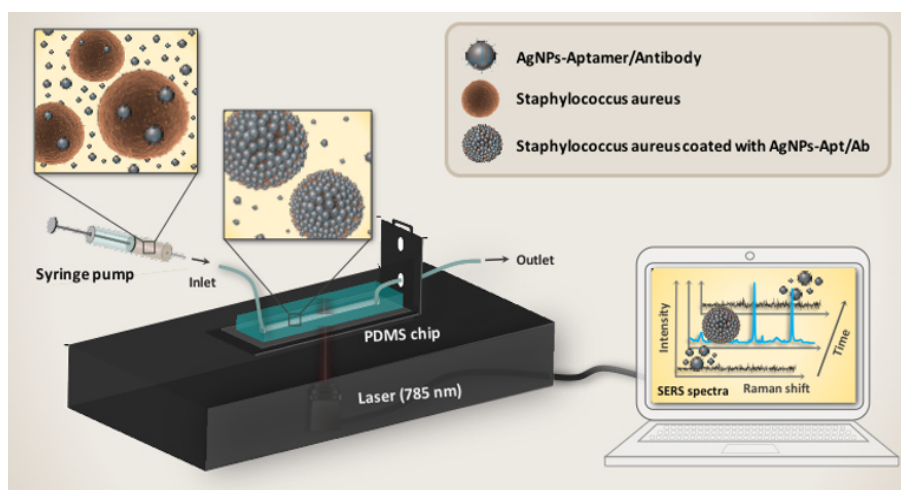


Figure 4.6. Conceptual view of microfluidics-optical device for bacterial quantification and its relevant components. SERS encoded silver nanoparticles functionalized with *S.aureus* selective antibodies or aptamers are mixed with the infected fluids. The presence of microorganism induces aggregation of the nanoparticles on its membrane, rapidly evolving toward full random coverage. The mixture is circulated through a microfluidic channel with a pump and passing through the focus of a 785 nm laser, which interrogates the sample in real time. Targeted bacteria produce a large increase in SERS signal, whose spectral fingerprints allow us to identify and quantify the type of pathogen.

In **Figure 4.7** shows the results for the three materials. The MBA ring breathing feature at 1078 cm^{-1} was selected as a spectral marker to monitor the SERS intensity.

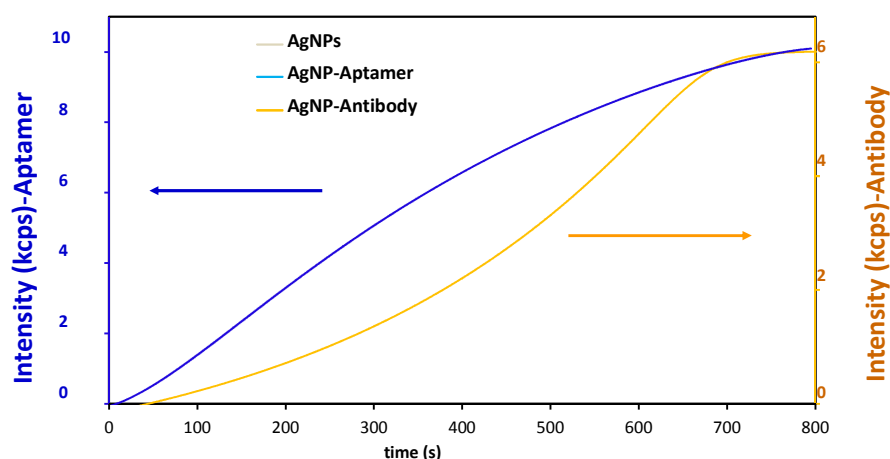


Figure 4.7. Comparison of the SERS intensity of the band at 1078 cm^{-1} (ring breathing of MBA).

First the SERS encoded AgNPs lacking of surface biorecognition elements do not show any detectable SERS signal. Conversely, both antibody- and aptamer-functionalized particles yield intense SERS signals that increase with time up to ≈ 800 s, when a plateau is reached. The comparison of aptamers with antibodies displays, however, notable differences.

First, aptamers exhibit much larger affinity for bacteria than antibodies. Second the final SERS intensity registered for aptamers (at $t = 800$ s) is around 40% larger than that for antibodies. To understand this behaviour, samples of bacteria with nanoparticles were studied at different incubation times with electronic microscopy (**Figure 4.8**). At $t = 0$ s, both samples show low interaction with nanoparticles. At $t = 400$ s, the amount of nanoparticles retained on the bacteria increases, but to a much larger extent in the case of aptamers, thus resulting in stronger SERS signals. Such discrepancy can be attributed to a larger affinity constant of the overall ensemble of aptamer molecules bound to the metallic surface as compared with the antibody.

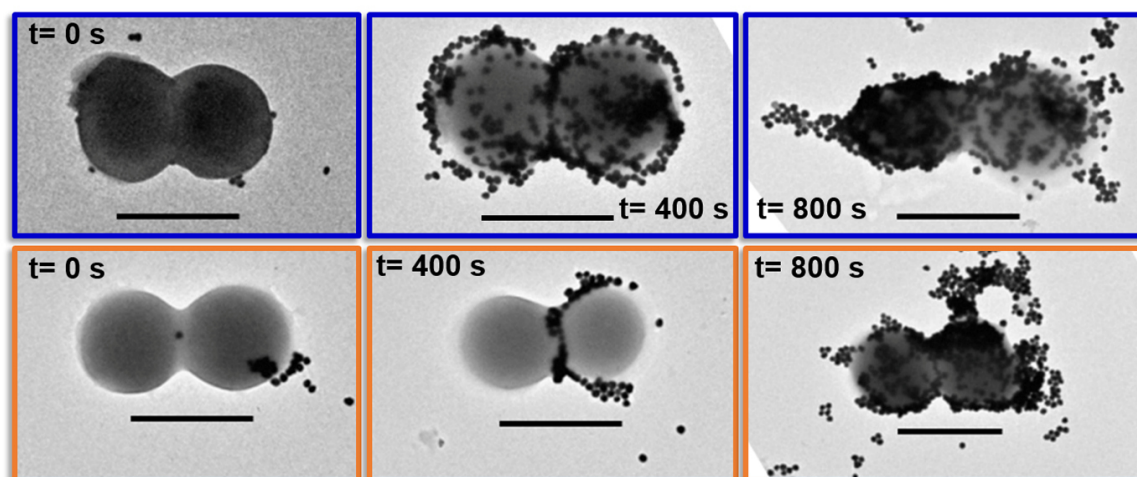


Figure 4.8. TEM images of *S.aureus* as a function of the incubation time with the SERS encoded silver particles functionalized with either aptamers (blue) or antibodies (orange). Scale bar: $1\mu\text{m}$.

Notwithstanding, aptamers can be easily functionalized/modified without any loss of their activity and, then, their conjugation on the nanoparticle surface can be directed to yield a conformation suitable for their efficient interaction with the target entity. In contrast, the functionalization of antibodies may affect their biological response and, further and more importantly, the coupling protocol always leads to a random orientation of the protein on the nanoparticle surface. As a result, a portion of the antibody molecules can be coupled through sensitive amino groups inactivating their binding site (i.e., paratope).²⁴⁸ Finally, at $t = 800$ s, the TEM images show a similar coating of particles for both aptamers and antibodies, while aptamer-modified SERS encoded nanoparticles still yield a remarkable larger SERS intensity. This may be ascribed to the smaller aptamer size,^{249,250} which allows the formation of smaller interparticle gaps at the bacterial surface, leading to an overall increase of the electromagnetic energy generated at the hot spot.

Figure 4.9 shows the results obtained for serum samples infected with *S.aureus* at different concentrations, either measured with regular bacterial culture (48 h of incubation, **Figure 4.9 A**) or via our optical system (**Figure 4.9 B**).

As in the previous case, we added $10\ \mu\text{L}$ (10^{-4} M of Ag^0) of nanoparticles per mL of sample. After incubating the samples for 15 min, several millilitres of each solution were passed through our microfluidic optical device at a flow rate of 6 mL/h. Positive events are associated with the detection of targeted CFUs. Both, antibody and aptamer functionalized nanoparticles offer similar results (**Figure 4.9 C**).

When no bacteria are present in the sample, no detectable signal is, which is consistent with the outcome of the bacterial culture analysis. However, at low or moderate concentrations of bacteria, both give rise to slightly larger quantification than the CFU count in bacterial cultures.

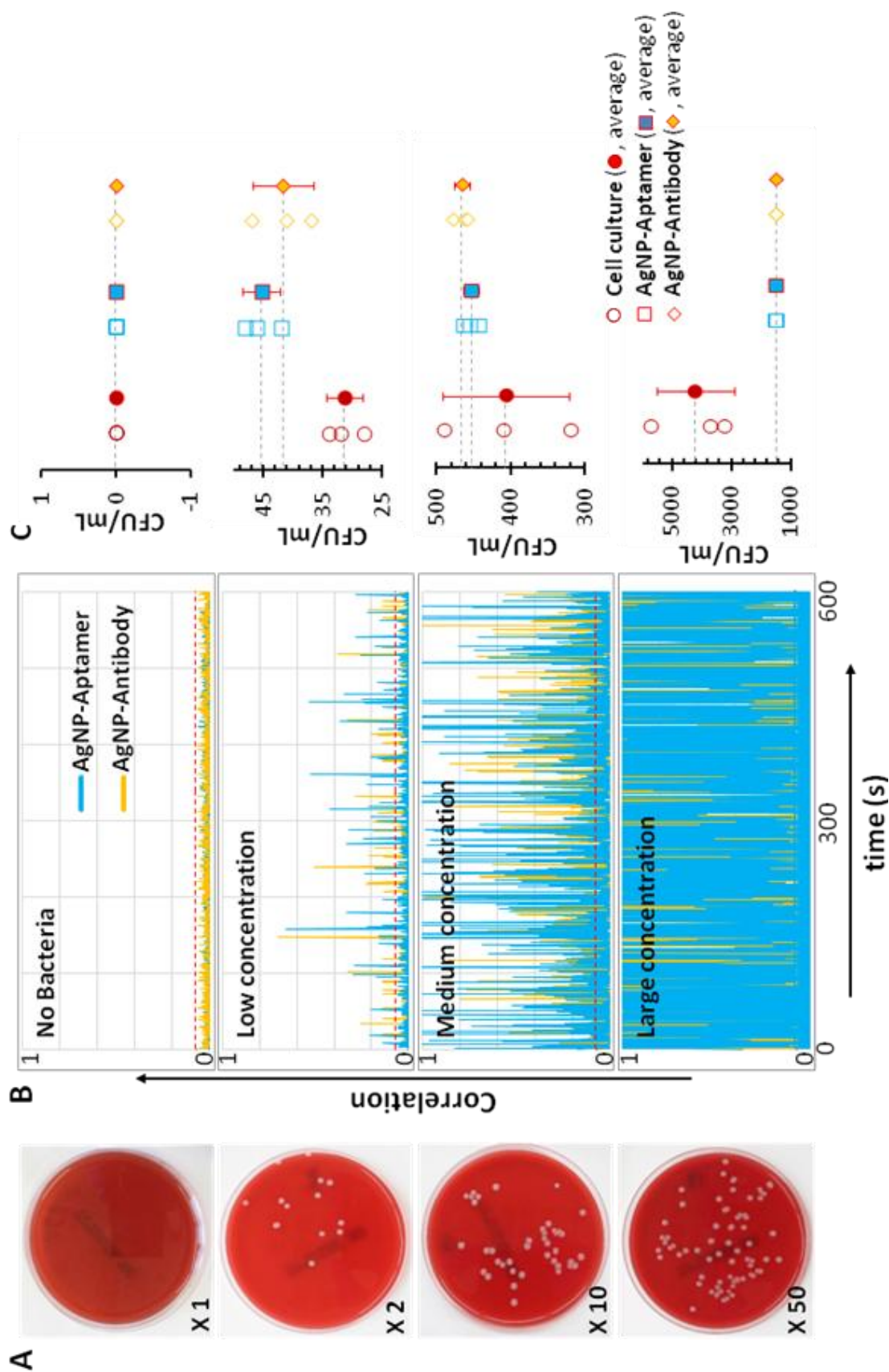


Figure 4.9. Quantification of *S. aureus* in different bacteria concentration through (A) bacterial culture and (B) our microfluidic optical system. The number in the bacterial culture images indicates the volume of initial solution spread in the blood agar plates (x4, 250 μ L). Conditions for the microfluidic optical device were: flow speed 6 mL/h with acquisition times of 0.4 s. Y axis represents the similarity of the obtained SERS spectrum of the sample at a given time with the reference SERS spectrum of MBA obtained from a concentrated solution (10^{-3} M of Ag⁰) of MBA encoded nanoparticles. (C) Comparison of the bacteria concentrations (CFU/mL) as determined by traditional cultures (open circles) and aptamers (open squares). Averages over three cultures or runs are shown by the corresponding solid symbols.

This difference is not significant for the clinical diagnosis, as these values are in the same order of magnitude.²⁵¹ In this regard, it is worth stressing that bacteria concentrations which are considered significant in clinical practices are always low. For instance, sepsis is diagnosed when the detected bacteria concentration is as low as one single CFU per mL of blood.²⁵¹ Conversely, for high bacteria concentrations, bacterial culture yields considerable larger results than our optical-based device. Notably, for bio-functionalized SERS encoded nanoparticles, the graph plotting correlation vs time shows a continuous positive. This is consistent with the acquisition times and flow speeds set for the optical measurement. In fact, for a flow rate of 6 mL/h and SERS acquisition time of 0.4s; The volume investigated per each measurement corresponds to $\sim 0.67 \mu\text{L}$ with an overall acquisition of 1500 scans per mL of sample. Consistently, a continuous positive signal is observed for such high concentrations under the actual experimental conditions (**Figure 4.9 B**). Finally, for low bacteria concentrations ($<100 \text{ CFU/mL}$), only one CFU is statistically present in the single scanned volume, while for very large quantities, such as those above 1500 CFU/mL, more CFUs are likely to occur simultaneously. A possible solution for the issues associated with high bacteria contents is the dilution of the sample to concentrations below the temporal resolution.

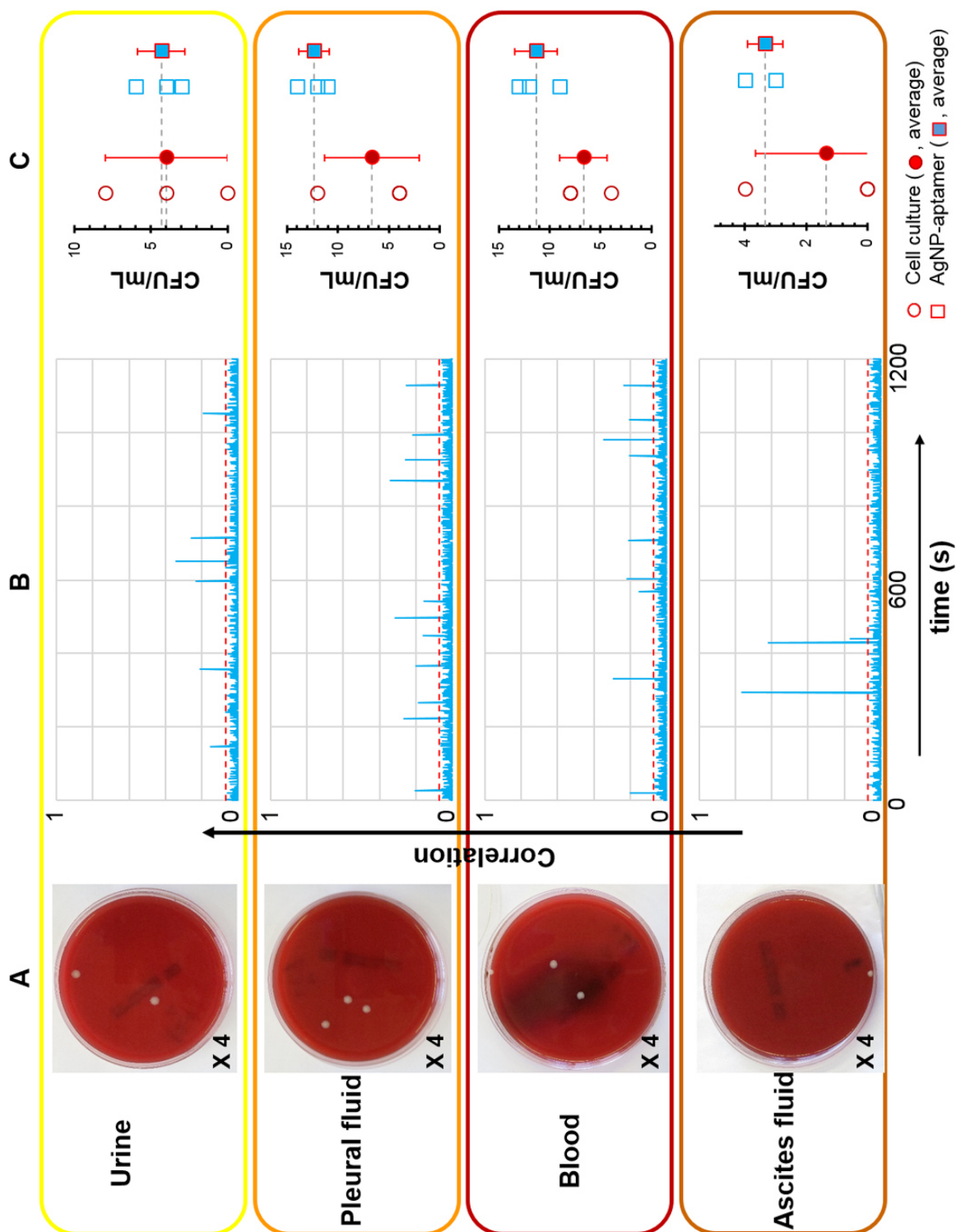


Figure 4.10. Quantification of *S. aureus* in different biofluids through (A) bacterial culture and (B) our microfluidic optical system. (C) Comparison of the bacteria concentrations (CFU/mL) as determined by traditional cultures (open circles) and nanoparticles with aptamers (open squares). Averages over three cultures or runs are shown by the corresponding solid symbols.

4.3.3. *Staphylococcus aureus* quantification in human fluids

Taking into account the results described in section 2.3, we selected SERS encoded nanoparticles conjugated with aptamers as optimal substrates for detecting *S.aureus* in several relevant human fluids. These fluids are aseptic in healthy conditions, and infection for most of them (i.e., blood, and pleural and ascites fluids) is defined by the presence of just one CFU per mL. Thus, we spiked the biological samples with a very low concentration of bacteria. Due to the lower laser penetration within blood, the experimental conditions were reset to 1 mL of diluted nanoparticles (2×10^{-6} M of Ag^0) per mL of sample. In order to compare the response for different biofluids, these new conditions were used for all the experiments. **Figure 4.10** shows the results obtained after infecting different human fluids with *S. aureus*. As in the case of serum, both bacterial culture and our optical system offered similar quantification results but with a dramatic difference in detection time: 48 h for the bacterial culture vs 20 min for the microfluidic SERS-based device.

5

Conclusions

Conclusions

Early diagnostic of sepsis in blood is a pressing clinical need. Consequently, in this doctoral thesis a microorganisms detection system (MODS) has been developed. This technique offers an accurate diagnostic for bacterial infections in very short times as compared with all other currently available methods. More concretely, we can state that, during this doctoral thesis, the following points have been achieved:

- A new method for the diagnosis of infections has been developed together with the detection device (MODS). This system can safely identify and quantify the presence of bacterial pathogens in biological fluids, with sensitivity down to the single CFU.
- The proposed method is able to recognize and quantify microorganisms within minutes, screening milliliters of liquid at a rate close to 10 min/mL; while traditional methods for bacterial culture such as microorganisms spreads on plaques, takes about 24-72 h.
- Comparing MODS results with those obtained from traditional methods such bacterial culture shows that the number of CFUs is usually slightly larger for MODS, while its standard deviation is consistently smaller. However, all the results, for both techniques, show the same order of magnitude of bacteria, which is the relevant parameter in clinical diagnosis.
- MODS mechanism is based in SERS encoded particles functionalized with a bio-recognition element, and therefore the particles selectively accumulate at the bacteria surface, forming a dense collection of electromagnetic hot spots. Consequently, an exponential increase of the SERS signal is detected and quantified by passing the sample through a microfluidic device with a collection

window where a laser interrogates and classifies each of the induced bacteria-nanoparticle aggregates in real time.

- The proof of concept here was just demonstrated with four bacterial agents at the same time. However, the detection method can be expanded to simultaneously identify many more of them by using the large number of available spectral codes and selective bio-recognition elements (antibodies and aptamers).
- Meanwhile the detection of those four bacterial agents was just carried out in serum and blood, the optical detection of *S aureus* was also demonstrated in more extended real human fluids such as urine, blood or pleural and ascites fluids achieving as before, also very short acquisition times (10 min/mL) for samples infected with low concentration of bacteria (such as <15 CFUs/mL).
- An extensive and detailed characterization comparing the efficiency of different bio-recognition elements (such antibodies and aptamers) to functionalize SERS encoded particles and its applicability in MODS, evidence that aptamers exhibit much larger affinity for bacteria than antibodies.
- Additionally, the final SERS intensity registered for aptamers is around 40% larger than that for antibodies.
- In addition, aptamers can be easily manipulated without affecting their biological response meanwhile antibodies are more delicate.
- For those reasons, this thesis also highlights the advantages of using aptamers over antibodies as bio-recognition elements.

Further, MODS cannot only guide in the choice of an accurate treatment for a given patient, but it can also monitor the effect of that treatment on the time evolution of the infection. Additionally, even though MODS is not yet capable of discerning in between resistant and non-resistant microorganisms directly, this method can be used to test the efficiency of antibiotics by just adding different

drugs to different aliquots of the patient sample with the subsequent determination of the bacterial population in the samples with MODS. Remarkably, the potential of MODS could be also expanded to analyse other microorganisms such as viruses, protozoa, fungus, and neoplastic cells in body fluids within minutes.

Recapitulating, this approach permits the monitoring of large volumes of sample within minutes and offers an interesting alternative to the common diagnosis of infections. Further, similar approach can be applied for the determination of other microorganisms and can be probably extended to the diagnosis of other relevant diseases. All these characteristics render our technology a great interest for both, the accurate diagnostic of patients and the screening of large populations, especially in suspected pandemics.

References

References

- 1 *Prevention of hospital-acquired infections [Internet]. 2012. Available from: <http://apps.who.int/medicinedocs/index/assoc/s16355e/s16355e.pdf>.*
- 2 Organization, W. H. Report on the burden of endemic health care-associated infection worldwide. (2011).
- 3 Brockmann, D. 1-24 (Wiley-VCH Verlag GmbH & Co. KGaA, 2010).
- 4 Dellinger, R. P. *et al.* Surviving sepsis campaign: international guidelines for management of severe sepsis and septic shock: 2012. *Crit Care Med* **41**, 580-637, doi:10.1097/CCM.0b013e31827e83af (2013).
- 5 Kumar, A. *et al.* Duration of hypotension before initiation of effective antimicrobial therapy is the critical determinant of survival in human septic shock. *Crit Care Med* **34**, 1589-1596, doi:10.1097/01.ccm.0000217961.75225.e9 (2006).
- 6 Efrima, S. & Zeiri, L. Understanding SERS of bacteria. *Journal of Raman Spectroscopy* **40**, 277-288, doi:10.1002/jrs.2121 (2009).
- 7 Long, D. A. & Long, D. *Raman spectroscopy*. (McGraw-Hill New York, 1977).
- 8 Comin, A. & Manna, L. New materials for tunable plasmonic colloidal nanocrystals. *Chem Soc Rev* **43**, 3957-3975, doi:10.1039/c3cs60265f (2014).
- 9 Murray, W. A. & Barnes, W. L. Plasmonic Materials. *Advanced Materials* **19**, 3771-3782, doi:10.1002/adma.200700678 (2007).
- 10 West, P. R. *et al.* Searching for better plasmonic materials. *Laser & Photonics Reviews* **4**, 795-808, doi:10.1002/lpor.200900055 (2010).
- 11 Wang, A. X. & Kong, X. Review of Recent Progress of Plasmonic Materials and Nano-Structures for Surface-Enhanced Raman Scattering. *Materials (Basel)* **8**, 3024-3052, doi:10.3390/ma8063024 (2015).
- 12 Abalde-Cela, S. *et al.* Surface-enhanced Raman scattering biomedical applications of plasmonic colloidal particles. *J R Soc Interface* **7**, S435-450 (2010).
- 13 Naik, G. V., Shalae, V. M. & Boltasseva, A. Alternative plasmonic materials: beyond gold and silver. *Adv Mater* **25**, 3264-3294, doi:10.1002/adma.201205076 (2013).
- 14 Zeng, S., Baillargeat, D., Ho, H. P. & Yong, K. T. Nanomaterials enhanced surface plasmon resonance for biological and chemical sensing applications. *Chem Soc Rev* **43**, 3426-3452, doi:10.1039/c3cs60479a (2014).
- 15 Zheng, Y. B., Kiraly, B., Weiss, P. S. & Huang, T. J. Molecular plasmonics for biology and nanomedicine. *Nanomedicine (Lond)* **7**, 751-770, doi:10.2217/nnm.12.30 (2012).
- 16 Pelaz, B. *et al.* Diverse Applications of Nanomedicine. *Acs Nano*, doi:10.1021/acsnano.6b06040 (2017).
- 17 Rycenga, M. *et al.* Controlling the synthesis and assembly of silver nanostructures for plasmonic applications. *Chem Rev* **111**, 3669-3712, doi:10.1021/cr100275d (2011).
- 18 Iravani, S., Korbekandi, H., Mirmohammadi, S. V. & Zolfaghari, B. Synthesis of silver nanoparticles: chemical, physical and biological methods. *Res Pharm Sci* **9**, 385-406 (2014).
- 19 Mittal, A. K., Chisti, Y. & Banerjee, U. C. Synthesis of metallic nanoparticles using plant extracts. *Biotechnol Adv* **31**, 346-356, doi:10.1016/j.biotechadv.2013.01.003 (2013).
- 20 P. Zhao, N. L., D. Astruc. State of the art in gold nanoparticle synthesis. *Coordination Chemistry Reviews* **257**, 638-665 (2013).
- 21 Zhou, W., Gao, X., Liu, D. & Chen, X. Gold Nanoparticles for In Vitro Diagnostics. *Chem Rev* **115**, 10575-10636, doi:10.1021/acs.chemrev.5b00100 (2015).

- 22 Grzelczak, M., Perez-Juste, J., Mulvaney, P. & Liz-Marzan, L. M. Shape control in gold nanoparticle synthesis. *Chem Soc Rev* **37**, 1783-1791, doi:10.1039/b711490g (2008).
- 23 Liebig, F., Sarhan, R. M., Prietzel, C., Reinecke, A. & Koetz, J. "Green" gold nanotriangles: synthesis, purification by polyelectrolyte/micelle depletion flocculation and performance in surface-enhanced Raman scattering. *Rsc Advances* **6**, 33561-33568, doi:10.1039/c6ra04808k (2016).
- 24 Pazos-Perez, N., Garcia de Abajo, F. J., Fery, A. & Alvarez-Puebla, R. A. From nano to micro: synthesis and optical properties of homogeneous spheroidal gold particles and their superlattices. *Langmuir* **28**, 8909-8914, doi:10.1021/la3002898 (2012).
- 25 Ye, X., Zheng, C., Chen, J., Gao, Y. & Murray, C. B. Using binary surfactant mixtures to simultaneously improve the dimensional tunability and monodispersity in the seeded growth of gold nanorods. *Nano Lett* **13**, 765-771, doi:10.1021/nl304478h (2013).
- 26 Sun, Y. & Xia, Y. Shape-controlled synthesis of gold and silver nanoparticles. *Science* **298**, 2176-2179, doi:10.1126/science.1077229 (2002).
- 27 Braeckmans, K., De Smedt, S. C., Leblans, M., Pauwels, R. & Demeester, J. Encoding microcarriers: present and future technologies. *Nat Rev Drug Discov* **1**, 447-456, doi:10.1038/nrd817 (2002).
- 28 Golightly, R. S., Doering, W. E. & Natan, M. J. Surface-enhanced Raman spectroscopy and homeland security: a perfect match? *Acs Nano* **3**, 2859-2869, doi:10.1021/nn9013593 (2009).
- 29 Cao, Y. C., Jin, R. & Mirkin, C. A. Nanoparticles with Raman spectroscopic fingerprints for DNA and RNA detection. *Science* **297**, 1536-1540, doi:10.1126/science.297.5586.1536 (2002).
- 30 Fernandez-Lopez, C. *et al.* Highly controlled silica coating of PEG-capped metal nanoparticles and preparation of SERS-encoded particles. *Langmuir* **25**, 13894-13899, doi:10.1021/la9016454 (2009).
- 31 Kustner, B. *et al.* SERS labels for red laser excitation: silica-encapsulated SAMs on tunable gold/silver nanoshells. *Angew Chem Int Ed Engl* **48**, 1950-1953, doi:10.1002/anie.200804518 (2009).
- 32 Wang, G., Park, H. Y., Lipert, R. J. & Porter, M. D. Mixed monolayers on gold nanoparticle labels for multiplexed surface-enhanced Raman scattering based immunoassays. *Anal Chem* **81**, 9643-9650, doi:10.1021/ac901711f (2009).
- 33 Guerrero-Martinez, A., Perez-Juste, J. & Liz-Marzan, L. M. Recent progress on silica coating of nanoparticles and related nanomaterials. *Adv Mater* **22**, 1182-1195, doi:10.1002/adma.200901263 (2010).
- 34 Alvarez-Puebla, R., Liz-Marzán, L. M. & García de Abajo, F. J. Light Concentration at the Nanometer Scale. *The Journal of Physical Chemistry Letters* **1**, 2428-2434, doi:10.1021/jz100820m (2010).
- 35 Brus, L. Noble Metal Nanocrystals: Plasmon Electron Transfer Photochemistry and Single-Molecule Raman Spectroscopy. *Accounts of Chemical Research* **41**, 1742-1749, doi:10.1021/ar800121r (2008).
- 36 Nelayah, J. *et al.* Mapping surface plasmons on a single metallic nanoparticle. *Nat Phys* **3**, 348-353, doi:http://www.nature.com/nphys/journal/v3/n5/supinfo/nphys575_S1.html (2007).
- 37 Rodriguez-Lorenzo, L. *et al.* Zeptomol detection through controlled ultrasensitive surface-enhanced Raman scattering. *J Am Chem Soc* **131**, 4616-4618, doi:10.1021/ja809418t (2009).
- 38 Rodriguez-Lorenzo, L. *et al.* Intracellular mapping with SERS-encoded gold nanostars. *Integr Biol (Camb)* **3**, 922-926, doi:10.1039/c1ib00029b (2011).
- 39 Yang, M. *et al.* SERS-active gold lace nanoshells with built-in hotspots. *Nano Lett* **10**, 4013-4019, doi:10.1021/nl101946c (2010).

- 40 Fresnais, J., Lavelle, C. & Berret, J. F. Nanoparticle Aggregation Controlled by Desalting Kinetics. *The Journal of Physical Chemistry C* **113**, 16371-16379, doi:10.1021/jp904665u (2009).
- 41 Moskovits, M. & Vlckova, B. Adsorbate-induced silver nanoparticle aggregation kinetics. *J Phys Chem B* **109**, 14755-14758, doi:10.1021/jp051177o (2005).
- 42 Su, X. *et al.* Composite organic-inorganic nanoparticles (COINs) with chemically encoded optical signatures. *Nano Lett* **5**, 49-54, doi:10.1021/nl0484088 (2005).
- 43 Lutz, B. R. *et al.* Spectral analysis of multiplex Raman probe signatures. *ACS Nano* **2**, 2306-2314, doi:10.1021/nn800243g (2008).
- 44 Sun, L. *et al.* Composite Organic-Inorganic Nanoparticles as Raman Labels for Tissue Analysis. *Nano Lett.* **7**, 351 (2007).
- 45 Brown, L. O. & Doorn, S. K. Optimization of the preparation of glass-coated, dye-tagged metal nanoparticles as SERS substrates. *Langmuir* **24**, 2178-2185, doi:10.1021/la703218f (2008).
- 46 Brown, L. O. & Doorn, S. K. A controlled and reproducible pathway to dye-tagged, encapsulated silver nanoparticles as substrates for SERS multiplexing. *Langmuir* **24**, 2277-2280, doi:10.1021/la703853e (2008).
- 47 Goddard, G. *et al.* High-Resolution Spectral Analysis of Individual SERS-Active Nanoparticles in Flow. *Journal of the American Chemical Society* **132**, 6081-6090, doi:10.1021/ja909850s (2010).
- 48 Chen, G. *et al.* Measuring ensemble-averaged surface-enhanced Raman scattering in the hotspots of colloidal nanoparticle dimers and trimers. *J Am Chem Soc* **132**, 3644-3645, doi:10.1021/ja9090885 (2010).
- 49 Jin, R. Nanoparticle clusters light up in SERS. *Angew Chem Int Ed Engl* **49**, 2826-2829, doi:10.1002/anie.200906462 (2010).
- 50 Li, S., Pedano, M. L., Chang, S. H., Mirkin, C. A. & Schatz, G. C. Gap structure effects on surface-enhanced Raman scattering intensities for gold gapped rods. *Nano Lett* **10**, 1722-1727, doi:10.1021/nl100099g (2010).
- 51 M Moskovits, G. B., SJ Lee, T Laurence, N Fera , L Fabris *et al.* Generalized approach to SERS-active nanomaterials via controlled nanoparticle linking, polymer encapsulation, and small-molecule infusion. *J.Phys. Chem. C.* **113**, 13622-13629 (2009).
- 52 Pallaoro, A., Braun, G. B., Reich, N. O. & Moskovits, M. Mapping local pH in live cells using encapsulated fluorescent SERS nanotags. *Small* **6**, 618-622, doi:10.1002/sml.200901893 (2010).
- 53 Rycenga, M., Camargo, P. H. C., Li, W., Moran, C. H. & Xia, Y. Understanding the SERS Effects of Single Silver Nanoparticles and Their Dimers, One at a Time. *The Journal of Physical Chemistry Letters* **1**, 696-703, doi:10.1021/jz900286a (2010).
- 54 Stoerzinger, K. A., Hasan, W., Lin, J. Y., Robles, A. & Odom, T. W. Screening Nanopyramid Assemblies to Optimize Surface Enhanced Raman Scattering. *The Journal of Physical Chemistry Letters* **1**, 1046-1050, doi:10.1021/jz100095b (2010).
- 55 Mir-Simon, B., Reche-Perez, I., Guerrini, L., Pazos-Perez, N. & Alvarez-Puebla, R. A. Universal One-Pot and Scalable Synthesis of SERS Encoded Nanoparticles. *Chem. Mater.* **27**, 950-958, doi:10.1021/cm504251h (2015).
- 56 Pazos-Perez, N. *et al.* Organized Plasmonic Clusters with High Coordination Number and Extraordinary Enhancement in Surface-Enhanced Raman Scattering (SERS). *Angew. Chem. Int. Ed.* **51**, 12688-12693, doi:10.1002/anie.201207019 (2012).
- 57 Guicheteau, J. *et al.* Bacillus spore classification via surface-enhanced Raman spectroscopy and principal component analysis. *Appl Spectrosc* **62**, 267-272, doi:10.1366/000370208783759623 (2008).
- 58 Jarvis, R. M. & Goodacre, R. Discrimination of bacteria using surface-enhanced Raman spectroscopy. *Anal Chem* **76**, 40-47, doi:10.1021/ac034689c (2004).

- 59 Jarvis, R. M. & Goodacre, R. Characterisation and identification of bacteria using SERS. *Chem Soc Rev* **37**, 931-936, doi:10.1039/b705973f (2008).
- 60 Muhamadali, H. *et al.* Rapid, accurate, and comparative differentiation of clinically and industrially relevant microorganisms via multiple vibrational spectroscopic fingerprinting. *Analyst* **141**, 5127-5136, doi:10.1039/c6an00883f (2016).
- 61 Zhang, L. *et al.* Multifunctional magnetic-plasmonic nanoparticles for fast concentration and sensitive detection of bacteria using SERS. *Biosens Bioelectron* **31**, 130-136, doi:10.1016/j.bios.2011.10.006 (2012).
- 62 Szymborski, T., Witkowska, E., Adamkiewicz, W., Waluk, J. & Kaminska, A. Electrospun polymer mat as a SERS platform for the immobilization and detection of bacteria from fluids. *Analyst* **139**, 5061-5064, doi:10.1039/c4an01137f (2014).
- 63 Liu, T. Y. *et al.* Functionalized arrays of Raman-enhancing nanoparticles for capture and culture-free analysis of bacteria in human blood. *Nat Commun* **2**, 538, doi:10.1038/ncomms1546 (2011).
- 64 Walter, A., Marz, A., Schumacher, W., Rosch, P. & Popp, J. Towards a fast, high specific and reliable discrimination of bacteria on strain level by means of SERS in a microfluidic device. *Lab Chip* **11**, 1013-1021, doi:10.1039/c0lc00536c (2011).
- 65 Cheng, I. F., Lin, C. C., Lin, D. Y. & Chang, H. C. A dielectrophoretic chip with a roughened metal surface for on-chip surface-enhanced Raman scattering analysis of bacteria. *Biomicrofluidics* **4**, doi:10.1063/1.3474638 (2010).
- 66 Sackmann, E. K., Fulton, A. L. & Beebe, D. J. The present and future role of microfluidics in biomedical research. *Nature* **507**, 181-189, doi:10.1038/nature13118 (2014).
- 67 Abalde-Cela, S., Abell, C., Alvarez-Puebla, R. A. & Liz-Marzán, L. M. Real Time Dual-Channel Multiplex SERS Ultradetection. *The Journal of Physical Chemistry Letters* **5**, 73-79, doi:10.1021/jz402419k (2014).
- 68 Fenniri, H. & Alvarez-Puebla, R. High-throughput screening flows along. *Nat Chem Biol* **3**, 247-249 (2007).
- 69 Mühlig, A. *et al.* LOC-SERS: A Promising Closed System for the Identification of Mycobacteria. *Analytical Chemistry* **88**, 7998-8004, doi:10.1021/acs.analchem.6b01152 (2016).
- 70 Cheng, I. F., Chang, H.-C., Chen, T.-Y., Hu, C. & Yang, F.-L. Rapid (<5 min) Identification of Pathogen in Human Blood by Electrokinetic Concentration and Surface-Enhanced Raman Spectroscopy. *Scientific Reports* **3**, 2365, doi:10.1038/srep02365 (2013).
- 71 Lin, H.-Y. *et al.* On-line SERS Detection of Single Bacterium Using Novel SERS Nanoprobes and A Microfluidic Dielectrophoresis Device. *Small* **10**, 4700-4710, doi:10.1002/smll.201401526 (2014).
- 72 Madiyar, F. R. *et al.* Integration of a nanostructured dielectrophoretic device and a surface-enhanced Raman probe for highly sensitive rapid bacteria detection. *Nanoscale* **7**, 3726-3736, doi:10.1039/c4nr07183b (2015).
- 73 Wang, C., Madiyar, F., Yu, C. & Li, J. Detection of extremely low concentration waterborne pathogen using a multiplexing self-referencing SERS microfluidic biosensor. *Journal of Biological Engineering* **11**, 9, doi:10.1186/s13036-017-0051-x (2017).
- 74 Pethig, R. Review Article—Dielectrophoresis: Status of the theory, technology, and applications. *Biomicrofluidics* **4**, 022811, doi:10.1063/1.3456626 (2010).
- 75 H.Telle, A. G. U. A. R. J. D. *Laser chemistry: Spectroscopy, dynamics and applications*. (John Willey & Sons, 2007).
- 76 K. Thyagarajan, A. G. *Lasers: Fundamentals and applications*. (Springer, 2010).
- 77 A.Requena, J. Z. *Espectroscopia*. (Pearson education, S.A., 2004).
- 78 Hollas, J. M. *Modern Spectroscopy*. (John Wiley & Sons, 2004).
- 79 Levine, I. N. *Fisicoquímica*. Vol. 2 (Mc Graw Hill, 2005).
- 80 Wolf, P. M. P. a. P. A. Vol. Solid State physics (Academic Press, New York, London, 1973).

- 81 Dressel, M. & Gruener, G. (AAPT, 2002).
- 82 Turkevich, J., Stevenson, P. C. & Hillier, J. A study of the nucleation and growth processes in the synthesis of colloidal gold. *Discussions of the Faraday Society* **11**, 55-75, doi:10.1039/df9511100055 (1951).
- 83 Gorman, C. B., Feldheim, D. L. & Fuierer, R. R. (Google Patents, 2009).
- 84 Link, S. & El-Sayed, M. A. Size and Temperature Dependence of the Plasmon Absorption of Colloidal Gold Nanoparticles. *The Journal of Physical Chemistry B* **103**, 4212-4217, doi:10.1021/jp984796o (1999).
- 85 Turkevich, J., Garton, G. & Stevenson, P. The color of colloidal gold. *Journal of Colloid Science* **9**, 26-35 (1954).
- 86 L.Mandelstam, G. L. a. *Eine Neue Erscheinung Bei Der Lichtzerstruung in Krystallen*. Vol. 16 557 (Naturwissenschaften, 1928).
- 87 V.Raman, D. S. k. a. C. A New Type of Secondary Radiation. *Nature* **121** (1928).
- 88 Adolf, S. Zur Quantentheorie der Dispersion. *Naturwissenschaften* **11**, 873-875 (1923).
- 89 Krishnan, R. S. & Shankar, R. K. Raman effect: History of the discovery. *Journal of Raman Spectroscopy* **10**, 1-8, doi:10.1002/jrs.1250100103 (1981).
- 90 Alvarez-Puebla, R. A. & Liz-Marzan, L. M. SERS detection of small inorganic molecules and ions. *Angew Chem Int Ed Engl* **51**, 11214-11223, doi:10.1002/anie.201204438 (2012).
- 91 Radziuk, D. & Moehwald, H. Prospects for plasmonic hot spots in single molecule SERS towards the chemical imaging of live cells. *Phys Chem Chem Phys* **17**, 21072-21093, doi:10.1039/c4cp04946b (2015).
- 92 Alvarez-Puebla, R. A. & Liz-Marzan, L. M. SERS-Based Diagnosis and Biodetection. *Small* **6**, 604-610, doi:10.1002/smll.200901820 (2010).
- 93 Sonntag, M. D. *et al.* Molecular plasmonics for nanoscale spectroscopy. *Chem Soc Rev* **43**, 1230-1247, doi:10.1039/c3cs60187k (2014).
- 94 Grésillon, S. *et al.* Experimental Observation of Localized Optical Excitations in Random Metal-Dielectric Films. *Physical Review Letters* **82**, 4520-4523 (1999).
- 95 Kim, W., Safonov, V., Shalaev, V. M. & Armstrong, R. Fractals in microcavities: Giant coupled, multiplicative enhancement of optical responses. *Physical Review Letters* **82**, 4811 (1999).
- 96 Markel, V. A. *et al.* Near-field optical spectroscopy of individual surface-plasmon modes in colloid clusters. *Physical Review B* **59**, 10903-10909 (1999).
- 97 Lee, S. J., Morrill, A. R. & Moskovits, M. Hot Spots in Silver Nanowire Bundles for Surface-Enhanced Raman Spectroscopy. *Journal of the American Chemical Society* **128**, 2200-2201, doi:10.1021/ja0578350 (2006).
- 98 Otto, A. What is observed in single molecule SERS, and why? *Journal of Raman Spectroscopy* **33**, 593-598, doi:10.1002/jrs.879 (2002).
- 99 Le Ru, E. C., Meyer, M., Blackie, E. & Etchegoin, P. G. Advanced aspects of electromagnetic SERS enhancement factors at a hot spot. *Journal of Raman Spectroscopy* **39**, 1127-1134, doi:10.1002/jrs.1945 (2008).
- 100 Sharma, B., Frontiera, R. R., Henry, A.-I., Ringe, E. & Van Duyne, R. P. SERS: Materials, applications, and the future. *Materials Today* **15**, 16-25, doi:[http://dx.doi.org/10.1016/S1369-7021\(12\)70017-2](http://dx.doi.org/10.1016/S1369-7021(12)70017-2) (2012).
- 101 Lin, X.-F., Ren, B. & Tian, Z.-Q. Electrochemical and Surface-Enhanced Raman Spectroscopic Studies on the Adsorption and Electrooxidation of C1 Molecules on a Roughened Rh Electrode. *The Journal of Physical Chemistry B* **108**, 981-986, doi:10.1021/jp035433d (2004).
- 102 Zheng, J.-Z., Ren, B., Wu, D.-Y. & Tian, Z.-Q. Thiourea adsorption on a Pt surface as detected by electrochemical methods and surface-enhanced Raman spectroscopy. *Journal of Electroanalytical Chemistry* **574**, 285-289, doi:<http://dx.doi.org/10.1016/j.jelechem.2004.08.009> (2005).

- 103 Ren, B., Lin, X.-f., Yan, J.-w., Mao, B.-w. & Tian, Z.-q. Electrochemically Roughened Rhodium Electrode as a Substrate for Surface-enhanced Raman Spectroscopy. *The Journal of Physical Chemistry B* **107**, 899-902, doi:10.1021/jp026862z (2003).
- 104 Muniz-Miranda, M. Surface Enhanced Raman Scattering of 4,4'-Bipyridine Adsorbed on Smooth Copper, Silver and Aluminium Surfaces Activated by Deposited Silver Particles. *Journal of Raman Spectroscopy* **27**, 435-437, doi:10.1002/(SICI)1097-4555(199605)27:5<435::AID-JRS990>3.0.CO;2-0 (1996).
- 105 Xu, W. *et al.* Surface enhanced Raman spectroscopy on a flat graphene surface. *Proceedings Of The National Academy Of Sciences* **109**, 9281-9286, doi:10.1073/pnas.1205478109 (2012).
- 106 Xu, W., Mao, N. & Zhang, J. Graphene: A Platform for Surface-Enhanced Raman Spectroscopy. *Small* **9**, 1206-1224, doi:10.1002/smll.201203097 (2013).
- 107 Musumeci, A. *et al.* SERS of Semiconducting Nanoparticles (TiO₂ Hybrid Composites). *Journal of the American Chemical Society* **131**, 6040-6041, doi:10.1021/ja808277u (2009).
- 108 Livingstone, R. *et al.* Surface Enhanced Raman Spectroscopy of Pyridine on CdSe/ZnBeSe Quantum Dots Grown by Molecular Beam Epitaxy. *The Journal of Physical Chemistry C* **114**, 17460-17464, doi:10.1021/jp105619m (2010).
- 109 Wang, Y. *et al.* Mercaptopyridine Surface-Functionalized CdTe Quantum Dots with Enhanced Raman Scattering Properties. *The Journal of Physical Chemistry C* **112**, 996-1000, doi:10.1021/jp077467h (2008).
- 110 Korte, K. E., Skrabalak, S. E. & Xia, Y. Rapid synthesis of silver nanowires through a CuCl- or CuCl₂-mediated polyol process. *Journal of Materials Chemistry* **18**, 437-441, doi:10.1039/b714072j (2008).
- 111 Tao, A., Sinsersuksakul, P. & Yang, P. Polyhedral Silver Nanocrystals with Distinct Scattering Signatures. *Angewandte Chemie International Edition* **45**, 4597-4601, doi:10.1002/anie.200601277 (2006).
- 112 Smith, E. & Dent, G. *Modern Raman spectroscopy: a practical approach*. (John Wiley & Sons, 2013).
- 113 Alvarez-Puebla, R. A. Effects of the Excitation Wavelength on the SERS Spectrum. *J Phys Chem Lett* **3**, 857-866, doi:10.1021/jz201625j (2012).
- 114 Weber, W. H. & Merlin, R. *Raman scattering in materials science*. Vol. 42 (Springer Science & Business Media, 2013).
- 115 Grubisha, D. S., Lipert, R. J., Park, H.-Y., Driskell, J. & Porter, M. D. Femtomolar Detection of Prostate-Specific Antigen: An Immunoassay Based on Surface-Enhanced Raman Scattering and Immunogold Labels. *Analytical Chemistry* **75**, 5936-5943, doi:10.1021/ac034356f (2003).
- 116 Alvarez-Puebla, R. A. *et al.* Gold nanorods 3D-supercrystals as surface enhanced Raman scattering spectroscopy substrates for the rapid detection of scrambled prions. *Proceedings Of The National Academy Of Sciences* **108**, 8157-8161, doi:10.1073/pnas.1016530108 (2011).
- 117 Neugebauer, U., Rösch, P. & Popp, J. Raman spectroscopy towards clinical application: drug monitoring and pathogen identification. *International Journal of Antimicrobial Agents* **46**, S35-S39, doi:10.1016/j.ijantimicag.2015.10.014.
- 118 Madigan, M. T., Martinko, J. M. & Parker, J. *Brock biology of microorganisms*. Vol. 11 (prentice hall Upper Saddle River, NJ, 1997).
- 119 Hausman, G. M. C. R. E. *The Cell : A molecular Approach 7th*. (Sinauer Associates, 2015).
- 120 Rogers, K. *Bacteria and Viruses*. (Britannica Educational Publishing, 2010).
- 121 Price, P. W., Denno, R. F., Eubanks, M. D., Finke, D. L. & Kaplan, I. *Insect ecology: behavior, populations and communities*. (Cambridge University Press, 2011).

- 122 Frey-Klett, P. *et al.* Bacterial-fungal interactions: hyphens between agricultural, clinical, environmental, and food microbiologists. *Microbiology and Molecular Biology Reviews* **75**, 583-609 (2011).
- 123 Meers, J. & Jannasch, H. Growth of bacteria in mixed cultures. *CRC Critical Reviews in Microbiology* **2**, 139-184 (1973).
- 124 Newell, D. G. *et al.* Food-borne diseases—the challenges of 20years ago still persist while new ones continue to emerge. *International journal of food microbiology* **139**, S3-S15 (2010).
- 125 Van Belkum, A. *et al.* Guidelines for the validation and application of typing methods for use in bacterial epidemiology. *Clinical Microbiology and Infection* **13**, 1-46 (2007).
- 126 Selye, H. *Stress in health and disease*. (Butterworth-Heinemann, 2013).
- 127 Engelkirk, P. G. & Duben-Engelkirk, J. L. *Laboratory diagnosis of infectious diseases: essentials of diagnostic microbiology*. (Lippincott Williams & Wilkins, 2008).
- 128 Murray, P. R., Rosenthal, K. S. & Pfaller, M. A. *Medical microbiology*. (Elsevier Health Sciences, 2015).
- 129 Tallawi, M., Opitz, M. & Lieleg, O. Modulation of the mechanical properties of bacterial biofilms in response to environmental challenges. *Biomaterials Science*, doi:10.1039/c6bm00832a (2017).
- 130 Microbial Biofilms. *Annual Review of Microbiology* **49**, 711-745, doi:10.1146/annurev.mi.49.100195.003431 (1995).
- 131 Gupta, P., Sarkar, S., Das, B., Bhattacharjee, S. & Tribedi, P. Biofilm, pathogenesis and prevention—a journey to break the wall: a review. *Archives of Microbiology* **198**, 1-15, doi:10.1007/s00203-015-1148-6 (2016).
- 132 Stoodley, P., Sauer, K., Davies, D. & Costerton, J. W. Biofilms as complex differentiated communities. *Annual Reviews in Microbiology* **56**, 187-209 (2002).
- 133 Cultivating the "Uncultivable". *Annual Review of Microbiology* **71**, null, doi:10.1146/annurev-micro-090816-093449 (2017).
- 134 Sanders, E. R. Aseptic Laboratory Techniques: Plating Methods. *Journal of Visualized Experiments : JoVE*, 3064, doi:10.3791/3064 (2012).
- 135 Madigan, M. T. *et al.* back cover, 27 (Pearson Education International, 2003).
- 136 Fuqua, W. C., Winans, S. C. & Greenberg, E. P. Quorum sensing in bacteria: the LuxR-LuxI family of cell density-responsive transcriptional regulators. *J Bacteriol* **176**, 269-275 (1994).
- 137 Wuster, A. & Babu, M. M. Conservation and evolutionary dynamics of the agr cell-to-cell communication system across firmicutes. *J Bacteriol* **190**, 743-746, doi:10.1128/jb.01135-07 (2008).
- 138 Gram, C. Vol. 2 185-189 (Fortschritte der Medicin, 1884).
- 139 Holt, J. *Description Bergey's Manual of Determinative Bacteriology*. 9th edn, (Springer,, 1993).
- 140 Lolis, E. & Bucala, R. Therapeutic approaches to innate immunity: severe sepsis and septic shock. *Nat Rev Drug Discov* **2**, 635-645, doi:10.1038/nrd1153 (2003).
- 141 Fair, R. J. & Tor, Y. Antibiotics and Bacterial Resistance in the 21st Century. *Perspect Medicin Chem* **6**, 25-64 (2014).
- 142 Davies, J. & Davies, D. Origins and Evolution of Antibiotic Resistance. *Microbiol Mol Biol Rev* **74**, 417-433 (2010).
- 143 Ventola, C. L. The Antibiotic Resistance Crisis: Part 1: Causes and Threats. *P T* **40**, 277-283 (2015).
- 144 Thomson, K. S. *et al.* A Novel Topical Combination Ointment with Antimicrobial Activity against Methicillin-Resistant *Streptococcus aureus*, Gram-Negative Superbugs, Yeasts, and Dermatophytic Fungi. *Curr Ther Res Clin Exp* **83**, 8-12, doi:10.1016/j.curtheres.2016.07.001 (2016).

- 145 Prescott, H. C., Langa, K. M., Liu, V., Escobar, G. J. & Iwashyna, T. J. Increased 1-year healthcare use in survivors of severe sepsis. *Am J Respir Crit Care Med* **190**, 62-69, doi:10.1164/rccm.201403-0471OC (2014).
- 146 Krumholz, H. M. Post-hospital syndrome--an acquired, transient condition of generalized risk. *N Engl J Med* **368**, 100-102, doi:10.1056/NEJMp1212324 (2013).
- 147 Iwashyna, T. J., Cooke, C. R., Wunsch, H. & Kahn, J. M. The Population Burden of Long-Term Survivorship after Severe Sepsis Among Older Americans. *J Am Geriatr Soc* **60**, 1070-1077 (2012).
- 148 Quartin, A. A., Schein, R. M., Kett, D. H. & Peduzzi, P. N. Magnitude and duration of the effect of sepsis on survival. Department of Veterans Affairs Systemic Sepsis Cooperative Studies Group. *JAMA* **277**, 1058-1063 (1997).
- 149 Stevenson, E. K., Rubenstein, A. R., Radin, G. T., Wiener, R. S. & Walkey, A. J. Two decades of mortality trends among patients with severe sepsis: a comparative meta-analysis*. *Crit Care Med* **42**, 625-631, doi:10.1097/ccm.000000000000026 (2014).
- 150 Singer, M. *et al.* The Third International Consensus Definitions for Sepsis and Septic Shock (Sepsis-3). *JAMA* **315**, 801-810, doi:10.1001/jama.2016.0287 (2016).
- 151 Ryan, K. J. & Ray, C. G. Medical microbiology. *McGraw Hill* **4**, 370 (2004).
- 152 Koenig, J. M. & Keenan, W. J. Group B streptococcus and early-onset sepsis in the era of maternal prophylaxis. *Pediatr Clin North Am* **56**, 689-708, Table of Contents, doi:10.1016/j.pcl.2009.04.003 (2009).
- 153 Parker, R. E. *et al.* Association between genotypic diversity and biofilm production in group B Streptococcus. *BMC Microbiol* **16**, 86, doi:10.1186/s12866-016-0704-9 (2016).
- 154 Glaser, P. *et al.* Genome sequence of Streptococcus agalactiae, a pathogen causing invasive neonatal disease. *Molecular Microbiology* **45**, 1499-1513 (2002).
- 155 Poyart, C. *et al.* Attenuated virulence of Streptococcus agalactiae deficient in D-alanyl-lipoteichoic acid is due to an increased susceptibility to defensins and phagocytic cells. *Molecular Microbiology* **49**, 1615-1625, doi:10.1046/j.1365-2958.2003.03655.x (2003).
- 156 Hulmani, M., Kakar, S. & Kumar, V. J. Methicillin-resistant Staphylococcus aureus menace: A dermatologist's perspective. *Clinical Dermatology Review* **1**, 4 (2017).
- 157 van Wamel, W. J. Staphylococcus aureus infections, some second thoughts. *Curr Opin Infect Dis*, doi:10.1097/qco.0000000000000366 (2017).
- 158 Becker, K., Heilmann, C. & Peters, G. Coagulase-Negative Staphylococci. *Clin Microbiol Rev* **27**, 870-926 (2014).
- 159 Rigby, K. M. & DeLeo, F. R. Neutrophils in innate host defense against Staphylococcus aureus infections. *Semin Immunopathol* **34**, 237-259 (2012).
- 160 Sande, M. & Wilson, W. *Current diagnosis & treatment in infectious diseases*. (McGraw-Hill Professional, 2001).
- 161 Vila, J. *et al.* Escherichia coli: an old friend with new tidings. *FEMS Microbiol Rev*, doi:10.1093/femsre/fuw005 (2016).
- 162 Tashiro, Y., Eida, H., Ishii, S., Futamata, H. & Okabe, S. Generation of Small Colony Variants in Biofilms by Escherichia coli Harboring a Conjugative F Plasmid. *Microbes Environ*, doi:10.1264/jsme2.ME16121 (2017).
- 163 Mulvey, M. A., Schilling, J. D., Martinez, J. J. & Hultgren, S. J. Bad bugs and beleaguered bladders: Interplay between uropathogenic Escherichia coli and innate host defenses. *Proceedings Of The National Academy Of Sciences* **97**, 8829-8835, doi:10.1073/pnas.97.16.8829 (2000).
- 164 Moradali, M. F., Ghods, S. & Rehm, B. H. A. Pseudomonas aeruginosa Lifestyle: A Paradigm for Adaptation, Survival, and Persistence. *Front Cell Infect Microbiol* **7** (2017).
- 165 BONTEN, M. J. M., BERGMANS, D. C. J. J., SPEIJER, H. & STOBBERINGH, E. E. Characteristics of Polyclonal Endemicity of Pseudomonas aeruginosa Colonization in Intensive Care Units.

- American Journal of Respiratory and Critical Care Medicine* **160**, 1212-1219, doi:10.1164/ajrccm.160.4.9809031 (1999).
- 166 Lee, K. & Yoon, S. S. Pseudomonas aeruginosa biofilm, a programmed bacterial life for fitness. *J Microbiol Biotechnol*, doi:10.4014/jmb.1611.11056 (2017).
- 167 Rada, B. Interactions between Neutrophils and Pseudomonas aeruginosa in Cystic Fibrosis. *Pathogens* **6**, 10 (2017).
- 168 Peleg, A. Y. & Hooper, D. C. Hospital-Acquired Infections Due to Gram-Negative Bacteria. *N Engl J Med* **362**, 1804-1813 (2010).
- 169 Hughes, J., Rees, S., Kalindjian, S. & Philpott, K. Principles of early drug discovery. *Br J Pharmacol* **162**, 1239-1249 (2011).
- 170 Sperling, R. A. & Parak, W. J. Surface modification, functionalization and bioconjugation of colloidal inorganic nanoparticles. *Philosophical Transactions of the Royal Society A: Mathematical, Physical and Engineering Sciences* **368**, 1333-1383, doi:10.1098/rsta.2009.0273 (2010).
- 171 Hermanson, G. T. *Bioconjugate techniques*. (Academic press, 2013).
- 172 Murphy, K. & Weaver, C. *Janeway's immunobiology*. (Garland Science, 2016).
- 173 Kausaite-Minkstimiene, A., Ramanaviciene, A., Kirlyte, J. & Ramanavicius, A. Comparative Study of Random and Oriented Antibody Immobilization Techniques on the Binding Capacity of Immunosensor. *Analytical Chemistry* **82**, 6401-6408, doi:10.1021/ac100468k (2010).
- 174 Guddat, L. W., Herron, J. N. & Edmundson, A. B. Three-dimensional structure of a human immunoglobulin with a hinge deletion. *Proc Natl Acad Sci U S A* **90**, 4271-4275 (1993).
- 175 Huber, R., Deisenhofer, J., Colman, P. M., Matsushima, M. & Palm, W. Crystallographic structure studies of an IgG molecule and an Fc fragment. *Nature* **264**, 415-420 (1976).
- 176 Amzel, L. M. & Poljak, R. J. Three-dimensional structure of immunoglobulins. *Annu Rev Biochem* **48**, 961-997, doi:10.1146/annurev.bi.48.070179.004525 (1979).
- 177 Schroeder, H. W. & Cavacini, L. Structure and Function of Immunoglobulins. *J Allergy Clin Immunol* **125**, S41-52 (2010).
- 178 Lu, B., Smyth, M. R. & O'Kennedy, R. Oriented immobilization of antibodies and its applications in immunoassays and immunosensors. *Analyst* **121**, 29R-32R (1996).
- 179 Weiping, Q. *et al.* Orientation of Antibodies on a 3-Aminopropyltriethoxysilane-Modified Silicon Wafer Surface. *Journal of inclusion phenomena and macrocyclic chemistry* **35**, 419-429, doi:10.1023/a:1008192209162 (1999).
- 180 Chames, P., Van Regenmortel, M., Weiss, E. & Baty, D. Therapeutic antibodies: successes, limitations and hopes for the future. *British Journal of Pharmacology* **157**, 220-233, doi:10.1111/j.1476-5381.2009.00190.x (2009).
- 181 Reichert, J. M., Rosensweig, C. J., Faden, L. B. & Dewitz, M. C. Monoclonal antibody successes in the clinic. *Nat Biotech* **23**, 1073-1078 (2005).
- 182 Ellington, A. D. & Szostak, J. W. In vitro selection of RNA molecules that bind specific ligands. *Nature* **346**, 818-822, doi:10.1038/346818a0 (1990).
- 183 Tuerk, C. & Gold, L. Systematic evolution of ligands by exponential enrichment: RNA ligands to bacteriophage T4 DNA polymerase. *Science* **249**, 505-510 (1990).
- 184 Jenison, R. D., Gill, S. C., Pardi, A. & Polisky, B. High-resolution molecular discrimination by RNA. *Science* **263**, 1425-1429 (1994).
- 185 Aquino-Jarquín, G. & Toscano-Garibay, J. D. RNA aptamer evolution: two decades of SELECTION. *Int J Mol Sci* **12**, 9155-9171, doi:10.3390/ijms12129155 (2011).
- 186 Sefah, K., Shangquan, D., Xiong, X., O'Donoghue, M. B. & Tan, W. Development of DNA aptamers using Cell-SELEX. *Nat Protoc* **5**, 1169-1185, doi:10.1038/nprot.2010.66 (2010).
- 187 Sharma, T. K. & Shukla, R. Nucleic acid aptamers as an emerging diagnostic tool for animal pathogens. *Advances in Animal and Veterinary Sciences* **2**, 50-55 (2014).

- 188 Adhikari, N. K., Fowler, R. A., Bhagwanjee, S. & Rubenfeld, G. D. Critical care and the global burden of critical illness in adults. *Lancet* **376**, 1339-1346, doi:10.1016/s0140-6736(10)60446-1 (2010).
- 189 Angus, D. C. & van der Poll, T. Severe sepsis and septic shock. *N Engl J Med* **369**, 2063, doi:10.1056/NEJMc1312359 (2013).
- 190 Cockerill, F. R. *et al.* Optimal Testing Parameters for Blood Cultures. *Clin. Infect. Dis.* **38**, 1724-1730, doi:10.1086/421087 (2004).
- 191 Fournier, P-E. *et al.* Modern clinical microbiology: new challenges and solutions. *Nat. Rev. Microbiol.* **11**, 574-585, doi:10.1038/nrmicro3068 (2013).
- 192 De Wildt, R. M. T., Mundy, C. R., Gorick, B. D. & Tomlinson, I. M. Antibody arrays for high-throughput screening of antibody-antigen interactions. *Nat. Biotechnol.* **18**, 989-994, doi:10.1038/79494 (2000).
- 193 Ottesen, E. A., Jong, W. H., Quake, S. R. & Leadbetter, J. R. Microfluidic digital PCR enables multigene analysis of individual environmental bacteria. *Science* **314**, 1464-1467, doi:10.1126/science.1131370 (2006).
- 194 Maier, T., Klepel, S., Renner, U. & Kostrzewa, M. Fast and reliable MALDI-TOF MS-based microorganism identification. *Nat. Methods* **3**, i-ii, doi:10.1038/nmeth870 (2006).
- 195 Zhang, Q. *et al.* Acceleration of Emergence of Bacterial Antibiotic Resistance in Connected Microenvironments. *Science* **333**, 1764-1767, doi:10.1126/science.1208747 (2011).
- 196 Perros, M. A sustainable model for antibiotics. *Science* **347**, 1062-1064, doi:10.1126/science.aaa3048 (2015).
- 197 Kanthor, R. Diagnostics: Detection drives defence. *Nature* **509**, S14-S15, doi:10.1038/509S14a (2014).
- 198 Zumla, A. *et al.* Rapid point of care diagnostic tests for viral and bacterial respiratory tract infections-needs, advances, and future prospects. *Lancet Infect. Dis.* **14**, 1123-1135, doi:10.1016/S1473-3099(14)70827-8 (2014).
- 199 Howes, P. D., Chandrawati, R. & Stevens, M. M. Colloidal nanoparticles as advanced biological sensors. *Science* **346**, doi:10.1126/science.1247390 (2014).
- 200 I-Fang, C., Chang, H.-C., Chen, T.-Y., Hu, C. & Yang, F.-L. Rapid (<5 min) Identification of Pathogen in Human Blood by Electrokinetic Concentration and Surface-Enhanced Raman Spectroscopy. *Scientific Reports* **3**, 2365, doi:10.1038/srep02365 (2013).
- 201 Pelaz, B. *et al.* The state of nanoparticle-based nanoscience and biotechnology: Progress, promises, and challenges. *Acs Nano* **6**, 8468-8483, doi:10.1021/nn303929a (2012).
- 202 Piorek, B. D. *et al.* Free-surface microfluidic control of surface-enhanced Raman spectroscopy for the optimized detection of airborne molecules. *Proc. Nat. Acad. Sci. Usa* **104**, 18898-18901, doi:10.1073/pnas.0708596104 (2007).
- 203 Rodrigo, D. *et al.* Mid-infrared plasmonic biosensing with graphene. *Science* **349**, 165-168, doi:10.1126/science.aab2051 (2015).
- 204 Hol, F. J. H. & Dekker, C. Zooming in to see the bigger picture: Microfluidic and nanofabrication tools to study bacteria. *Science* **346**, doi:10.1126/science.1251821 (2014).
- 205 Chen, W. *et al.* Identification of Bacteria in Water by a Fluorescent Array. *Angew. Chem. Int. Ed.* **53**, 13734-13739, doi:10.1002/anie.201407606 (2014).
- 206 Gracie, K. *et al.* Simultaneous detection and quantification of three bacterial meningitis pathogens by SERS. *Chem. Sci.* **5**, 1030-1040, doi:10.1039/c3sc52875h (2014).
- 207 Kang, D.-K. *et al.* Rapid detection of single bacteria in unprocessed blood using Integrated Comprehensive Droplet Digital Detection. *Nat. Commun.* **5**, 5427, doi:10.1038/ncomms6427 (2014).
- 208 Wang, H. *et al.* Simultaneous Capture, Detection, and Inactivation of Bacteria as Enabled by a Surface-Enhanced Raman Scattering Multifunctional Chip. *Angew. Chem. Int. Ed.* **54**, 5132-5136, doi:10.1002/anie.201412294 (2015).

- 209 Wang, Y., Yan, B. & Chen, L. SERS Tags: Novel Optical Nanoprobes for Bioanalysis. *Chem. Rev.* **113**, 1391-1428, doi:10.1021/cr300120g (2013).
- 210 Carregal-Romero, S. *et al.* Multiplexed sensing and imaging with colloidal nano- and microparticles. *Annu Rev Anal Chem (Palo Alto Calif)* **6**, 53-81, doi:10.1146/annurev-anchem-062012-092621 (2013).
- 211 Choi, S. W. *et al.* Rapid in vivo detection of isoniazid-sensitive Mycobacterium tuberculosis by breath test. *Nat. Commun.* **5**, 4989, doi:10.1038/ncomms5989 (2014).
- 212 Lee, P. C. & Meisel, D. Adsorption and surface-enhanced Raman of dyes on silver and gold sols. *J. Phys. Chem.* **86**, 3391-3395, doi:10.1021/j100214a025 (1982).
- 213 Li, H. *et al.* Synthesis of Monodisperse, Quasi-Spherical Silver Nanoparticles with Sizes Defined by the Nature of Silver Precursors. *Langmuir* **30**, 2498-2504, doi:10.1021/la4047148 (2014).
- 214 Li, H., Xia, H., Wang, D. & Tao, X. Simple Synthesis of Monodisperse, Quasi-spherical, Citrate-Stabilized Silver Nanocrystals in Water. *Langmuir* **29**, 5074-5079, doi:10.1021/la400214x (2013).
- 215 Paramelle, D. *et al.* A rapid method to estimate the concentration of citrate capped silver nanoparticles from UV-visible light spectra. *Analyst* **139**, 4855-4861, doi:10.1039/C4AN00978A (2014).
- 216 Balows, A., Hausler, W. J., Ohashi, M. & Turano, A. *Laboratory Diagnosis Of Infectious Diseases: Principles And Practice.* (1988).
- 217 Goldman, E. & Green, L. H. *Practical Handbook Of Microbiology.* (2008).
- 218 García de Abajo, F. J. Multiple scattering of radiation in clusters of dielectrics. *Physical Review B* **60**, 6086-6102 (1999).
- 219 García de Abajo, F. J. & Howie, A. Retarded field calculation of electron energy loss in inhomogeneous dielectrics. *Physical Review B* **65**, 115418 (2002).
- 220 Hudson, J. B. *Surface Science: an Introduction.* (Butterworth-Heinemann Limited, 1992).
- 221 Johnson, P. B. & Christy, R. W. Optical Constants of the Noble Metals. *Physical Review B* **6**, 4370-4379 (1972).
- 222 Zavaleta, C. L. *et al.* Multiplexed imaging of surface enhanced Raman scattering nanotags in living mice using noninvasive Raman spectroscopy. *Proceedings Of The National Academy Of Sciences* **106**, 13511-13516, doi:10.1073/pnas.0813327106 (2009).
- 223 Evans, J. W. Random and cooperative sequential adsorption. *Rev. Mod. Phys.* **65**, 1281-1329 (1993).
- 224 Cang, H. *et al.* Probing the electromagnetic field of a 15-nanometre hotspot by single molecule imaging. *Nature* **469**, 385-388, doi:<http://www.nature.com/nature/journal/v469/n7330/abs/10.1038-nature09698-unlocked.html#supplementary-information> (2011).
- 225 Liu, Z. *et al.* Revealing the molecular structure of single-molecule junctions in different conductance states by fishing-mode tip-enhanced Raman spectroscopy. *Nat. Commun.* **2**, doi:10.1038/ncomms1310 (2011).
- 226 Svedberg, F., Li, Z., Xu, H. & Käll, M. Creating Hot Nanoparticle Pairs for Surface-Enhanced Raman Spectroscopy through Optical Manipulation. *Nano Lett.* **6**, 2639-2641, doi:10.1021/nl062101m (2006).
- 227 Schlücker, S. Surface-Enhanced Raman Spectroscopy: Concepts and Chemical Applications. *Angew. Chem. Int. Ed.* **53**, 4756-4795, doi:10.1002/anie.201205748 (2014).
- 228 Singhal, A., Haynes, C. A. & Hansen, C. L. Microfluidic Measurement of Antibody-Antigen Binding Kinetics from Low-Abundance Samples and Single Cells. *Anal. Chem.* **82**, 8671-8679, doi:10.1021/ac101956e (2010).
- 229 Tong, S. Y. C., Davis, J. S., Eichenberger, E., Holland, T. L. & Fowler, V. G. *Staphylococcus aureus* Infections: Epidemiology, Pathophysiology, Clinical Manifestations, and Management. *Clin. Microbiol. Rev.* **28**, 603-661, doi:10.1128/cmr.00134-14 (2015).

- 230 Kaasch, A. J. *et al.* *Staphylococcus aureus* Bloodstream Infection: A Pooled Analysis of Five Prospective, Observational Studies. *J. Infection* **68**, 242-251, doi:<http://dx.doi.org/10.1016/j.jinf.2013.10.015> (2014).
- 231 van Hal, S. J. *et al.* Predictors of Mortality in *Staphylococcus aureus* Bacteremia. *Clin. Microbiol. Rev.* **25**, 362-386, doi:10.1128/cmr.05022-11 (2012).
- 232 Wang, J. *et al.* Magnetically Assisted Surface-Enhanced Raman Spectroscopy for the Detection of *Staphylococcus aureus* Based on Aptamer Recognition. *ACS Appl. Mater. Interfaces* **7**, 20919-20929, doi:10.1021/acsami.5b06446 (2015).
- 233 Lane, L. A., Qian, X. M. & Nie, S. M. SERS Nanoparticles in Medicine: From Label-Free Detection to Spectroscopic Tagging. *Chemical Reviews* **115**, 10489-10529, doi:10.1021/acs.chemrev.5b00265 (2015).
- 234 Lin, D., Qin, T., Wang, Y., Sun, X. & Chen, L. Graphene Oxide Wrapped SERS Tags: Multifunctional Platforms toward Optical Labeling, Photothermal Ablation of Bacteria, and the Monitoring of Killing Effect. *Acs Applied Materials & Interfaces* **6**, 1320-1329, doi:10.1021/am405396k (2014).
- 235 Huang, J. A., Zhang, Y. L., Ding, H. & Sun, H. B. SERS-Enabled Lab-on-a-Chip Systems. *Adv. Opt. Mater.* **3**, 618-633, doi:10.1002/adom.201400534 (2015).
- 236 Pallaoro, A., Hoonejani, M. R., Braun, G. B., Meinhart, C. D. & Moskovits, M. Rapid Identification by Surface-Enhanced Raman Spectroscopy of Cancer Cells at Low Concentrations Flowing in a Microfluidic Channel. *Acs Nano* **9**, 4328-4336, doi:10.1021/acsnano.5b00750 (2015).
- 237 White, I. M., Yazdi, S. H. & Yu, W. W. Optofluidic SERS: synergizing photonics and microfluidics for chemical and biological analysis. *Microfluid. Nanofluid.* **13**, 205-216, doi:10.1007/s10404-012-0962-2 (2012).
- 238 Pazos-Perez, N. *et al.* Ultrasensitive multiplex optical quantification of bacteria in large samples of biofluids. *Scientific Reports* **6**, 29014, doi:10.1038/srep29014 <http://www.nature.com/articles/srep29014#supplementary-information> (2016).
- 239 Bunka, D. H. J. & Stockley, P. G. Aptamers Come of Age – at Last. *Nature Rev. Microbiol.* **4**, 588-596 (2006).
- 240 Keefe, A. D., Pai, S. & Ellington, A. Aptamers as Therapeutics. *Nat. Rev. Drug. Discov.* **9**, 537-550 (2010).
- 241 Pfeiffer, C. *et al.* Interaction of colloidal nanoparticles with their local environment: the (ionic) nanoenvironment around nanoparticles is different from bulk and determines the physico-chemical properties of the nanoparticles. *Journal of the Royal Society Interface* **11**, doi:10.1098/rsif.2013.0931 (2014).
- 242 Maiolo, D., Del Pino, P., Metrangolo, P., Parak, W. J. & Baldelli Bombelli, F. Nanomedicine delivery: does protein corona route to the target or off road? *Nanomedicine (Lond)* **10**, 3231-3247, doi:10.2217/nnm.15.163 (2015).
- 243 Cao, X. *et al.* Combining Use of a Panel of ssDNA Aptamers in the Detection of *Staphylococcus aureus*. *Nucleic Acid Res.* **37**, 4621-4628, doi:10.1093/nar/gkp489 (2009).
- 244 Mir-Simon, B. *et al.* SERS Efficiencies of Micrometric Polystyrene Beads Coated with Gold and Silver Nanoparticles: the Effect of Nanoparticle Size. *J. Optics* **17**, 114012 doi:10.1088/2040-8978/17/11/114012 (2015).
- 245 Fabris, L. SERS Tags: The Next Promising Tool for Personalized Cancer Detection? *ChemNanoMat* **2**, 249-258, doi:10.1002/cnma.201500221 (2016).
- 246 Rodriguez-Lorenzo, L., Fabris, L. & Alvarez-Puebla, R. A. Multiplex optical sensing with surface-enhanced Raman scattering: A critical review. *Analytica Chimica Acta* **745**, 10-23, doi:10.1016/j.aca.2012.08.003 (2012).
- 247 Anker, J. N. *et al.* Biosensing with Plasmonic Nanosensors. *Nat. Mater.* **7**, 442-453 (2008).

- 248 Gordon, M. R. *et al.* Field Guide to Challenges and Opportunities in Antibody–Drug Conjugates for Chemists. *Bioconjugate Chem.* **26**, 2198-2215, doi:10.1021/acs.bioconjchem.5b00399 (2015).
- 249 Lee, J.-O. *et al.* Aptamers as Molecular Recognition Elements for Electrical Nanobiosensors. *Anal. Bioanal. Chem.* **390**, 1023-1032, doi:10.1007/s00216-007-1643-y (2008).
- 250 Lee, J. F., Stovall, G. M. & Ellington, A. D. Aptamer Therapeutics Advance. *Curr. Op. Chem. Biol.* **10**, 282-289, doi:<http://dx.doi.org/10.1016/j.cbpa.2006.03.015> (2006).
- 251 Yagupsky, P. & Nolte, F. S. Quantitative aspects of septicemia. *Clinical Microbiology Reviews* **3**, 269-279, doi:10.1128/cmr.3.3.269 (1990).

Appendix

Appendix I

LIST OF FIGURES

Figure 2.1.....10

Most prevalent pathogens in (A) community-acquired and (B) nosocomial infections. Viral agent in red.

Figure 2.2.....12

Some examples for the actual detection of microorganism in clinical diagnosis. (A) Cell culture, (B) Mass spectrometry of isolated pure colonies, (C) ELISA, (D) Lateral flow immunochromatography, and (E) PCR.

Figure 2.3.....16

TEM images of NPs with different shapes, sizes and composition; (A) Au nanospheres; (B) Au nanorods; (C) Ag nanoplates; (D) Au nanostars; (E) Ag nanobars; (F) Ag nanocubes.

Figure 2.4.....19

(A) Examples of encoded plasmonic nanostructures. (B) Encoded gold spheres and their plasmonic response. (C) SERS response of encoded gold spheres with four different SERS labels.

Figure 2.5.....20

(A) SEM image showing coverage of Ag NPs on *Bacillus atrophaeus* spores. (B) *Bacillus atrophaeus* spore spectra overlaid showing good signal reproducibility. (C) PCA plot showing discrimination between five *Bacillus* spore samples and *Pantoea agglomerans*.

Figure 2.6.....21

(A) Schematics of the condensation process of magnetic Au NPs and bacteria, together with a SEM image of the area of analysis. (B) Scheme of embedding bacteria on the SERS platform directly from the solution and SEM image.(C) Schematic diagram showing the cross-sectional view of a bacterium on a Van-coated substrate. SEM images of bacteria on the substrate.

Figure 2.7.....23

(A) Application of two-phase liquid/liquid segmented flow in a microfluidic chip for the acquisition of Raman spectra of the separation medium oil and SERS spectra. (B) Scheme of sample preparation.

Figure 2.8.....25

(A) Outline of the DEP capture of the bacteria coated with SERS-encoded NPs for the Raman detection. A representative TEM of *E. coli* DH α 5 bacterial cells attached with SERS-encoded NPs. (B) Optical microscope image (c) SERS intensity from the samples with the bacterial.

Figure 2.9.....27

Diagram showing the propagation of an electromagnetic wave.

Figure 2.10.....29

An illustration the excitation of dipole surface plasmon oscillations.

Figure 2.11.....29

Characteristic extinction spectra corresponding to spherical and rod shaped Au NPs.

Figure 2.12.....32

Schematic representation of the Rayleigh and Raman scattering.

Figure 2.13.....33

Raman active and IR active vibrations of carbon dioxide.

Figure 2.14.....33

Changes in the polarizability of the carbon dioxide molecule.

Figure 2.15.....35

Schematic configuration of a hot spot.

Figure 2.16.....36

Approximate wavelength ranges where Ag, Au, and Cu have been well characterized and are established to support SERS.

Figure 2.17.....37

Summary of shapes, LSPR absorption peaks, demonstrated applications, and methods for Synthesis of Ag NPs.

Figure 2.18.....39

Schematic representation of a dispersive Raman instrument coupled with a confocal microscope with a detailed description of a microscope objective.

Figure 2.19.....41

Universal phylogenetic tree. This tree is derived from comparative sequencing of ribosomal RNA.

Figure 2.20.....44

Clinical and diagnostic methods used for isolation and identification of infectious pathogens.

Figure 2.21.....46

Structural features of the cell wall that distinguishes the Gram+ from the Gram- bacteria.

Figure 2.22.....47

Summary of classes of antibiotics.

Figure 2.23.....54

Relative size of NPs and biomolecules, drawn to scale. Schematic representation of a NP with PEG, streptavidin, transferrin, Ab, albumin and ssDNA.

Figure 2.24.....55

Schematic representation of an antibody molecule and its fragments.

Figure 2.25	55
Schematic of a typical IgG.	
Figure 2.26	56
Selex method.	
Figure 3.1	69
Detailed schematics of the detection region in the millifluidic chipset.	
Figure 3.2	71
Electric field intensity enhancement generated by a dimer of Ag NPs embedded in water.	
Figure 3.3	72
SERS enhancement produced by Ag NP dimers in aqueous solution.	
Figure 3.4	73
SERS enhancement for Au and Ag dimers of different size.	
Figure 3.5	75
Near-field intensity in bacteria covered with nanoparticles.	
Figure 3.6	76
Simulated distribution of gap distances between NPs attached on the pathogen membrane at different normalized times.	
Figure 3.7	79
Conceptual view of the MODS and its relevant components.	
Figure 3.8	80
Encoded nanoparticles and their interaction with bacteria. (A) SERS spectra of the different coded particles. (B) TEM images of the targeted bacteria (<i>E. coli</i> , <i>P. aeruginosa</i> , <i>S. aureus</i> , and <i>S. agalactiae</i>) coated with their respective matching NPs.	

Figure 3.9	81
Optical extinction of functionalized Ag NPs in aqueous solution and representative TEM images of the encoded nanoparticles.	
Figure 3.10	82
Optimization of the concentration of encoded NPs for reduction of background noise from the codes of dispersed NPs against the signal of decorated pathogens in the measurement area of the millifluidic chipset.	
Figure 3.11	84
MODS performance for contaminated samples. (A) Correlation between temporal series. (B) Cellular cultures (24-48 hours). (C) Comparison of the bacteria concentrations as determined by MODS.	
Figure 3.12	85
Results for serum sample spiked with <i>E. coli</i> at different concentrations. (A) Cellular cultures. (B) Detection and quantification results obtained in our MODS device. (C) Statistical comparison of bacteria concentrations as determined by MODS versus traditional cultures.	
Figure 3.13	86
Same as Figure 3.12 for <i>P. aeruginosa</i> instead of <i>E. coli</i> .	
Figure 3.14	87
Same as Figure 3.12 for <i>S. aureus</i> instead of <i>E. coli</i>	
Figure 3.15	88
Same as Figure 3.12 for <i>S. agalactiae</i> instead of <i>E. coli</i> .	
Figure 3.16	89
Results for serum sample spiked with both <i>E. coli</i> and <i>S. aureus</i> . (A) Cellular cultures for each bacteria. (B) Detection and quantification results obtained with MODS. (C) Statistical comparison of bacteria concentrations as determined by MODS versus traditional cultures.	

Figure 3.17.....90

Blood sample spiked with *E. coli*, *S. agalactiae*, and *S. aureus*. (A) Cellular cultures for each bacteria (a volume 0.5 mL for each). (B) Detection and quantification results obtained in MODS.

Figure 3.18.....91

Biodiversity of *E. coli*. Left: TEM images of several single or clustered *E coli* CFU's coated with nanoparticles. Center: SERS detection results on the millifluidic MODS device. Right: Spectra corresponding to the events highlighted by circles in the previous plot.

Figure 3.19.....93

(A) Kinetics of NP aggregation as measured through the time-dependent SERS signal after adding *E. coli* to the mixture of coded NPs. (B) Simulation of the temporal evolution of Ag NP aggregation on the bacteria membrane produced by random NP-membrane encounters. (C) Near-electric-field intensity in a rod-like individual *E. coli* covered with Ag NPs and detail of the array revealing the formation of optical hotspots.

Figure 4.1.....105

Schematic representation of the nanoparticle SERS encoding and functionalization with antibodies and aptamers.

Figure 4.2.....107

(A) LSPR of MBA-encoded Ag NP before and after bioconjugation with Apt or Ab (B, C). Time-monitoring of the optical properties for SERS encoded nanoparticles, conjugated either with aptamers (B) or antibodies (C) in PBS.

Figure 4.3.....107

SERS response in suspension of MBA-encoded silver nanoparticles before (grey) and after bioconjugation with aptamers (yellow) or antibodies (blue).

Figure 4.4.....108

Representative TEM images of MBA-encoded Ag NPs before and after bioconjugation with Apt or Ab.

Figure 4.5.....108

Bacterial cultures of the *S.aureus* solution.

Figure 4.6.....109

Conceptual view of microfluidics-optical device for bacterial quantification and its relevant components. SERS encoded silver nanoparticles functionalized with *S.aureus* selective antibodies or aptamers are mixed with the infected fluids.

Figure 4.7.....109

Comparison of the SERS intensity of the band at 1078 cm^{-1} (ring breathing of MBA).

Figure 4.8.....110

TEM images of *S.aureus* as a function of the incubation time with the SERS encoded Ag NPs functionalized with either Apt or Ab.

Figure 4.9.....111

Quantification of *S. aureus* at different bacteria concentrations through (A) bacterial culture and (B) our microfluidic optical system. (C) Comparison of the bacteria concentrations as determined by traditional cultures and NPs with Apt.

Figure 4.10.....114

Quantification of *S. aureus* in different biofluids through (A) bacterial culture and (B) our microfluidic optical system. (C) Comparison of the bacteria concentrations as determined by traditional cultures and NPs with Apt.

Appendix II

LIST OF TABLES

Table 1	49
Sump up of microorganisms that acquired a special relevance or high incidence rates in hospitals.	
Table 2	50
Short characterization and description of <i>Streptococcus agalactiae</i> .	
Table 3	51
Short characterization and description of <i>Staphylococcus aureus</i> .	
Table 4	52
Short characterization and description of <i>Escherichia coli</i> .	
Table 5	53
Short characterization and description of <i>Pseudomona aeruginosa</i> .	
Table 6	60
Aptamers advantages vs antibodies.	

CARME CATALÀ GARCÍA, PhD



Highly motivated professional, excellent interpersonal skills, multi-tasker

PERSONAL INFORMATION

carmecatala@gmail.com

679446146

LANGUAGES

Spanish - Native language

Catalan - Native language

English - professional proficiency

TECHNICAL SKILLS

Organic chemistry

Optical microscopy

Microbiology

WORKING EXPERIENCE

Universitat Rovira i Virgili

ETSEQ (Escola tècnica superior d'Enginyeria Química)

Research in nanoscience in **Zeptonic group**

2013-2017

PhD in nanoscience, materials and microbiology .

Specific objectives:

- Synthesis and functionalization of plasmonic nanostructures with different Raman codes.

- Bio-functionalization of the encoded nanoparticles with different bio-recognition elements (antibodies or aptamers)

- Assays in saline medium and biological samples using the bio-functionalized encoded plasmonic nanostructures and the microorganisms.

Universitat Rovira i Virgili

CREPI (Chemical Reaction Engineering & Process Intensification Group)

2012

Master Thesis on sustainable production and environmental engineering.

Anaerobic pilot plant for the treatment of biological sludge: Homogenization, reduction and inertization of biological sludge.

Universitat Rovira i Virgili

Environmental Technician in **SRCIT** (Servei de recursos tècnics i tecnològics)

2011-2013

Collaboration in a project managed from "Generalitat de Catalunya" based on improving the protection of the

- promoting the minimisation of waste and their danger nurturing selective waste collection

- wasting evaluation

- refusing disposal

- recovering of spaces and soils deteriorated by the uncontrolled unloading of waste or by pollutants

Ingeme, S.L.

2009-2010

Responsible for managing the waste generated coming from animal breeding, agriculture and other temporal projects such as pneumatic tyre's recycling in order to find out second life mainly for roads' materials.

CEOP, Centre d'estudis i orientació professional

2009-2011

Teacher

Academic support focused on high-school, university and other

EDUCATION AND TRAINING

Universitat Rovira i Virgili - Tarragona ETSEQ (Escola tècnica superior d'Enginyeria Química) 2017	PhD in nanoscience, materials and microbiology
Universitat Rovira i Virgili - Tarragona 2012	Master on sustainable production and environmental engineering
Universidad de Navarra 2010	Bachelor Degree in Biochemistry
Universidad de Navarra 2009	Bachelor Degree in Biology

GRANTS & AWARDS

Ministerio de Economía y Competitividad

2015 -2017

Methodology for the recognition and biodetection of new pathogen agents with optical methods:

The example of Dawasaki disease

Principal Researcher: Ramón Álvarez Puebla

Agència de Gestió d'Ajuts Universitaris i de Recerca (AGAUR), Generalitat de Catalunya

2014-2016

Reference group in Catalunya RS reactive Strips

Principal Researcher: Ramón Álvarez Puebla

CTQC- Centre Tecnològic de la Química de Catalunya

2014-2017

Development of new optical sensors for diagnosis and biosensing

Principal Researcher: Ramón Álvarez Puebla

PATENTS

Inventors: Nicolás Pazos-Perez, Elena Pazos, Carme Català, Bernat Mir-Simon, Sara Gomez-de Pedro, Juan Sagalés, Carlos Villanueva, Ramón A. Álvarez-Puebla

Title: A method for detection of presence or absence of analytes in fluids and an optical detection system for carrying out the method.

Request number: PCT/EP2015/067717

Priority country: Europa

Date: 31/07/2015

Entity: Medcom Advance SA

PUBLICATIONS

C. Catala, B. Mir-Simon, X. Feng, C. Cardozo, N. Pazos-Perez, E. Pazos, S. Gómez-de Pedro, L. Guerrini, A. Soriano, J. Vila, F. Marco, E. Garcia-Rico, R.A. Alvarez-Puebla,^{1,9*} A. R.A. Alvarez-Puebla,* Online SERS quantification of Staphylococcus aureus and the application to diagnostics in human fluids Advanced Materials Technologies (2016) (DOI: 10.1002/admt.201600163)

N. Pazos-Perez, E. Pazos, **C. Catala**, B. Mir-Simon, S. Gomez-de-Pedro, J. Sagales, C. Villanueva, J. Vila, A. Soriano, F. J. García de Abajo,* R. A. Alvarez-Puebla* Ultrasensitive multiplex optical quantification of bacteria in large samples of biofluids Scientific Reports (2016) 6:29014 (DOI: 10.1038/srep29014)

C. Catala, N. Pazos-Perez, L. Guerrini, R.A. Alvarez-Puebla* SERS methods for diagnosis of infectious diseases in Nanotechnologies in Preventive and Regenerative Medicine (V. Uskokovic Ed.) Elsevier (2017-accepted) Chapter (ISBN: 9780323480635) Invited Book Chapter.Hardcover ISBN: 9780323480635

